

2. Automotive Metals

A. Processing and Manufacturability - Oak Ridge National Laboratory

Field Technical Monitor: C. D. Warren
Oak Ridge National Laboratory
1 Bethel Valley Road, Oak Ridge, TN 37831
(865) 574-9693; e-mail: warrencd@ornl.gov

Technology Area Development Manager: William Joost
U.S. Department of Energy
1000 Independence Ave., S.W.; Washington, DC 20585
(202) 287-6020; e-mail: william.joost@ee.doe.gov

Contractor: Oak Ridge National Laboratory (ORNL)
Contract No.: DE-AC05-00OR22725

Executive Summary

The low density of magnesium (Mg) alloys makes them good candidates for lightweight construction of components in the automotive industry. However, they exhibit much more complex mechanical behavior than other more commonly used automotive materials. Among certain Mg alloys, preliminary tests also indicate significant strain rate sensitivity, dependent on loading mode, that is coupled with internal damage accumulation. Very limited test data is available, which combined with an insufficient understanding of the underlying loading-induced property degradation mechanisms in Mg alloys, adds to the reservations for their use as structural materials.

Metals make up about 80% of all the materials used for light vehicle construction, and by a wide margin, the largest fraction of the metals is steels (Schnatterly, 2007; Schultz, 2007). Various steels represent about 62% of average vehicle weight. Of the various steel mill products used for auto construction, about 70% of the total, or 839 kg of the average light vehicle weight of 1,970 kg, is supplied as flat-rolled carbon steel for chassis parts and body panels.

The traditional sheet steels used for chassis and body constructions are the so-called “mild” steels. The combined interests of improving crash worthiness and reducing vehicle weights were at least partially responsible for the development of the first generation (Gen I) of advanced high-strength steels (AHSSs). This effort is aimed at developing the fundamental understanding that will allow the development of a third generation (Gen III) of AHSSs.

This project consists of two separate tasks. The first is an effort to characterize the high strain rate response of automotive grade Mg alloys. The second is focused on developing a fundamental understanding of the austenite-ferrite transformation in steels, which will be necessary to develop the next generation of AHSSs that will overcome difficulties in use associated with the second generation AHSSs.

Activity and Developments

High Strain Rate Characterization of Magnesium Alloys

Principal Investigator: Srdjan Simunovic, ORNL
(865) 241-3863; e-mail: simunovics@ornl.gov

Principal Investigator: J. Michael Starbuck, ORNL
(865) 576-3633; e-mail: starbuckjm@ornl.gov

Principal Investigator: Don Erdman, ORNL
(865) 576-4069; e-mail: erdmandl@ornl.gov

Accomplishments

- Developed shear specimen in tensile test configuration for high speed testing of Mg alloys and conducted strain rate tests for two Mg alloys.
- Developed a new method for controlling applied strain for high-speed tensile tests. The method allows for investigation of material internal state as a function of strain rate.
- Measured internal damage of Mg AM60B alloy as a function of strain and strain rate using optical microscopy.
- Developed constitutive models for tested Mg alloys based on high strain rate tensile experiments.
- Transferred technology by publishing project's data and findings on the World Wide Web.

Future Direction

- Optimize methods for strain control at high strain rates.
- Develop methods for measurement of mechanical property degradation in Mg alloys by mechanical tests.
- Measure property degradation using mechanical tests for Mg alloys.
- Develop strain rate dependent constitutive models for Mg alloys based on internal damage measurements using optical microscopy and mechanical tests.

Technology Assessment

- Target: Develop new test methods, material data (material property databases), and analytical tools for design and analysis of vehicle structural components with Mg alloys. The material information includes mechanical properties, characterization of internal degradation processes, and failure characterization under low and high rates of deformation that is required for structural analysis and design.
- Gap: A lack of material characterization technologies and mechanical property data for automotive Mg alloys. New test techniques are needed to develop microstructure-property relations and to investigate underlying deformation and damage mechanisms under vehicle in-service conditions.

Introduction

The low density of Mg alloys makes them good candidates for lighter weight construction of components in the automotive industry. Mg alloys, however, exhibit much more complex mechanical behavior than conventional automotive materials. The mechanical response of Mg alloys involves anisotropy, nonisotropic hardening, yield asymmetry, lower ductility, and significant degradation of effective properties due to the formation and growth of micro-defects under in-service loading. Under crash conditions, Mg alloys exhibit a strong tendency for fracturing in contrast to the large plastic deformation of conventional materials. The plastic deformations are exploited for crash energy dissipation in current designs. Accordingly, the material characterization procedures and constitutive models should be much more complex than the commonly used uniaxial tests and isotropic plasticity material models for steel. Another issue of concern for automotive designers is the strain rate sensitivity of Mg alloys. However, the lack of strain rate sensitivity information, experimental methods, and understanding of loading-induced property degradation add to the uncertainty, overdesign, and reservations about wider use of Mg alloys.

We are developing methods that enable characterization of the material internal state and its evolution under impact. The new information and models that result from this research will reduce uncertainties in component design thereby reducing the overdesign and vehicle weight.

Approach

The objective of this research is to determine strain rate dependent mechanical properties of automotive Mg alloys under different loading conditions. The experiments were conducted under various strain rates ranging from quasi-static up to 1,000/s. This range of strain rates (termed intermediate strain rate regime) is essential to automotive design because it corresponds to the strain rates that are experienced during high-speed forming and vehicle crash.

Measurement of mechanical properties in the intermediate strain rate regime is inherently difficult because of the strong wave reflections and difficulty in establishing dynamic equilibrium in the samples and sensors. Test methods in this range have not been standardized and the area is a subject of intensive research and development. In addition, the deformation of Mg alloys is accompanied by significant internal damage (void nucleation, growth, coalescence, failure) as a result of the complex deformation mechanisms inherent in the Mg crystal structure (hexagonal close packed). As the response of the material notably changes with the change in strain rates, it is important to investigate and understand how the underlying kinematic mechanisms change as well.

The main scientific and technical goals of this research project are (1) development of detailed information about Mg alloy mechanical properties in the intermediate strain rate regime, (2) characterization of corresponding property degradation by the control of imparted strain during the tests, (3) development of test methods and procedures that can be standardized for widespread use, and (4) development of material models and properties for automotive design.

Results and Discussion

Developed test methods, test data, and material data from the tests conducted so far on the project are available on the World Wide Web (http://thyme.ornl.gov/Mg_new). The web interface is used for technology transfer and communication of the results to the research community. The web page is included in the main newsletter for the crash simulation community (FEA Information Engineering Journal, <http://www.feainformation.com>).

We have developed new techniques to generate reliable tensile stress-strain data within the intermediate strain rate regime for the sheet form of Mg alloys and used them in tests on Mg alloys AZ31 and AM60B. The tests are conducted on a custom-designed high-speed servohydraulic machine combined with three-dimensional (3D) digital image correlation method (DICM). The specimen displacement is resolved accurately using 3D DICM correlation instead of actuator motion. Stresses are calculated based on the elastic strains in the tab of a dog-bone-shaped specimen. Using this technique, the stresses measured at strain rates of 100 s^{-1} and lower show little or no noise compared to load cell signals. When the strain rates are higher than 250 s^{-1} , the noise and oscillations in the stress measurements are significantly decreased (from $\sim 250 \text{ MPa}$ to

~50 MPa). For both materials, the yield strength and ultimate tensile strength were found to increase slightly when the strain rate was increased from 1 s^{-1} to $1,000 \text{ s}^{-1}$ (shown in Figure 1). AZ31 showed consistent elongation of 20% minimum for all tested specimens. For AM60B, the specimen elongation ranged from 10% to 20% for the tested strain rates. The new method is described in a journal article by Wang et al. (Wang et al., 2011).

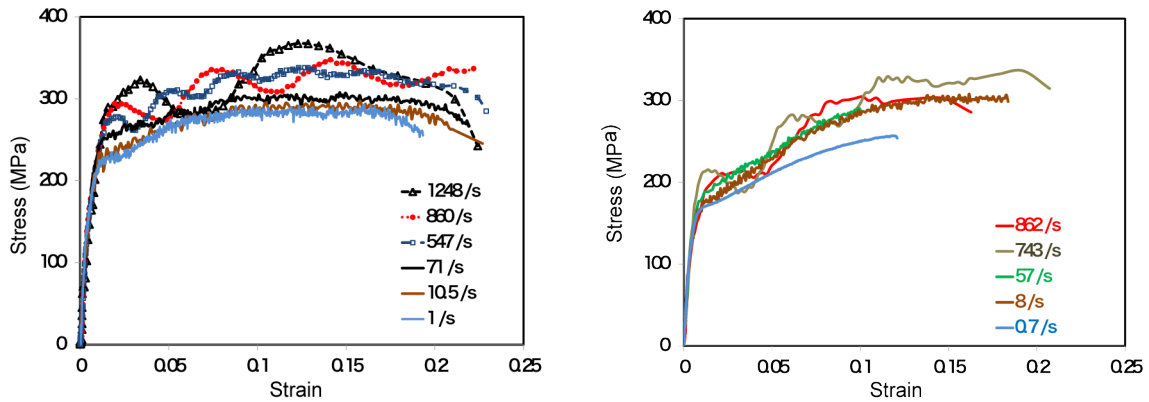


Figure 1. Strain rate effect on Mg alloy (a) AZ31 and (b) AM60B.

Quasi-static shear strength of the sheet materials is usually determined using a tensile testing apparatus by introducing two offset slots with a certain angle to create a shear alignment in the testing piece (ASTM standard ASTM B831-15). In this research, we have developed a new specimen design based on a paper by Lademo (Lademo et al., 2009). The design allows us to achieve constraint shear strain within the shear ligament illustrated in Figure 2. The test is extended to an intermediate speed testing regime for Mg alloys AZ31 and AM60B. The shear strain in the specimen was measured using 3D DICM. At higher testing speed, the load is resolved using the measurement of strains in the area of the specimen that undergoes uniform elastic elongation. Both tested Mg alloys showed very small strain rate sensitivity in shear (Figure 3). The shear strength for AZ31 is in the range of ~183 MPa to 200 MPa for the tested strain rates of 1 s^{-1} to 167.5 s^{-1} . AM60B shows lower shear strength than AZ31 with values of ~160 MPa to 180 MPa for the tested strain rates. In addition, observations of the specimens during tests show that AZ31 fractured in a shear mode; however, in contrast, most of the AM60B specimens fractured in a “cup” mode indicating significant growth of internal damage. The tearing off of the cup for AM60B explains the load bearing phenomena after maximum load on the stress-strain curves.

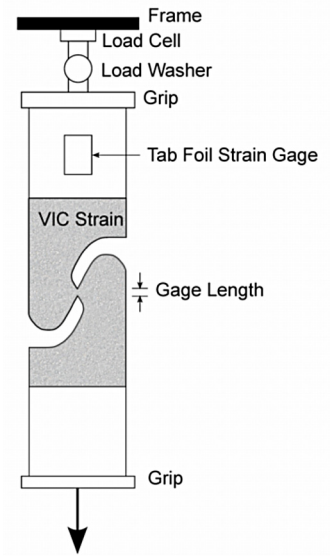


Figure 2. Specimen geometry for shear testing of Mg alloys.

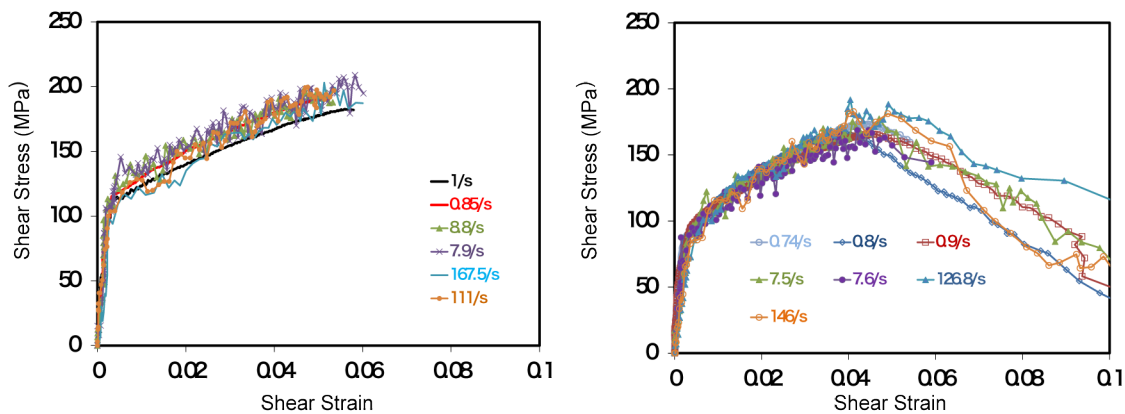


Figure 3. Strain rate effect on shear properties of Mg alloy (a) AZ31 and (b) AM60B.

Material mechanical response and microstructure changes such as microstructure defect evolution are often dependent on the levels of imparted strains and strain rates. For standard dog-bone tensile specimen geometry, to characterize the evolution of the internal state of a material at different strain levels, it must be possible to instantly stop (interrupt) the deformation. This load interruption is possible at very low loading rates, but at the velocities necessary to generate strain rates of 1/s and higher, the inertia of the loading equipment and control system make this task impractical. In this research, we have developed a technique that enables measurement of material behavior under multiple strain rates and prescribed strains using a single specimen design. The method combines specially tapered shaped specimens as shown in Figure 4. The shapes are determined using analytical models and finite element simulations in order to impart the desired strain and strain rate. Three-dimensional DICM is used for the measurement of the strain field across the entire gage to measure and verify the test conditions.

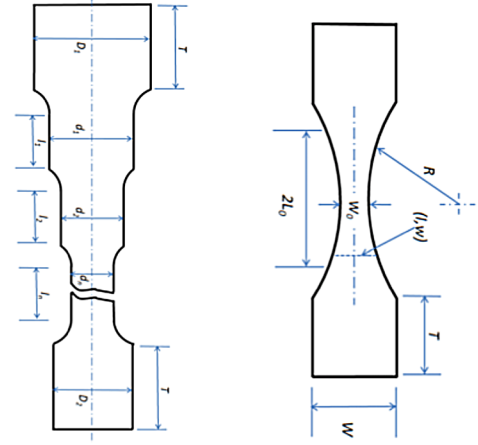


Figure 4. Test specimens used for the application of prescribed strain under high strain rates. The narrowest section acts as a mechanical fuse for cut-off strain.

Figure 5 shows the application of this technique to Mg alloy AM60B top hats with radii of 5.05 in. and 1.3 in. that were tested at 500 in./s. Different levels of strain were achieved across the specimen length within one specimen. The location-specific strain rates were also achieved by changes in the specimen curvature. This new specimen design and testing procedure can produce continuously varying levels of plastic strain achieved at various locations in the specimen and at different strain rates. This specimen design also reduces the size of conventional test matrices and overall testing time and permits more focus on test analysis and modeling. The method is currently under U.S. patent application.

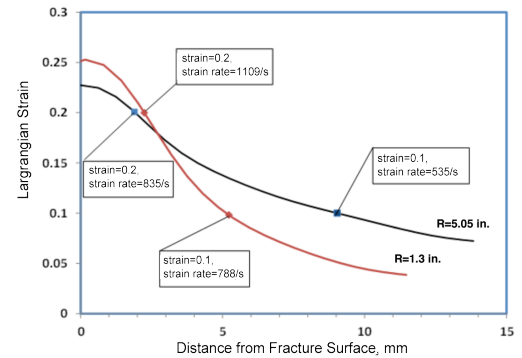


Figure 5. Strain distribution of AM60B specimens with two different radii. Tests were conducted at nominal speed of 500 in./s.

We have developed procedures for quantification of evolving stages of damage based on image processing and mechanical tests with the controlled strain application. Porosity is often used in the constitutive models of porous plasticity that are based on void formation and growth. Figure 6 shows the effect of strain rate on void growth. It shows not only that the void growth is dependent on the applied strain but also that it is dependent on the strain rate.

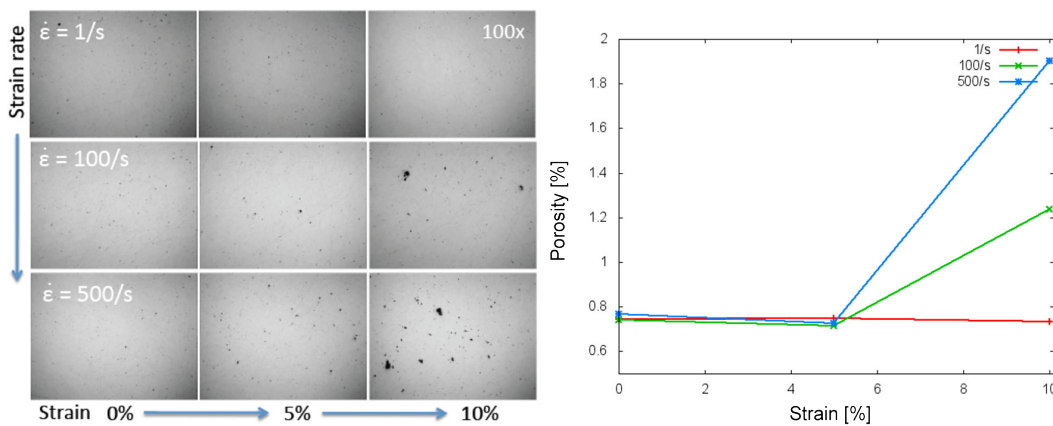


Figure 6. Material porosity as a function of strain and strain rate for AM60B alloy.

Conclusions

We have developed new methods for characterization of Mg alloys under intermediate (automotive) strain rates of loading. When fully developed, the tests will provide needed data for more effective design with Mg alloys and lightweight automotive designs. The output from this project is available at http://thyme.ornl.gov/Mg_new.

R&D Fundamental Study of the Relationship of Austenite-Ferrite Transformation Details to Austenite Retention in Carbon Steels

Principal Investigator: Michael Santella, ORNL
(865) 574-4805; e-mail: santellaml@ornl.gov

Accomplishments

- Variations in heat treating conditions and surface coatings on DP780 were evaluated by synchrotron diffractions for their effect on ferrite stability during intercritical annealing at 800°C.
- Hot-roll bonding was used to produce steel strip containing approximately equal fractions of ferrite and austenite.

Future Directions

- Rolling and heat treating experiments will be used to produce steel strips containing more than 10% austenite.
- Alloy compositions that promote higher amounts of retained austenite will be identified for preparation of laboratory-scale heats.

Technology Assessment

- Target: Enable the development of more ductile AHSSs (Gen III) by developing an understanding of the austenite-ferrite transformation.
- Gap: Steels showing the effects of transformation-induced plasticity (TRIP) are higher strength but not sufficiently ductile for many automotive applications.
- Gap: An understanding of mechanisms that could be used to increase AHSS ductility is not fully developed.

Introduction

Metals make up about 80% of all the materials used for light vehicle construction and, by a wide margin, the largest fraction of the metals is steels (Schnatterly, 2007; Schultz, 2007). Steels represent about 62% of average vehicle weight. Of the various steel mill products used for auto construction, about 70% of the total, or 839 kg of the average light vehicle weight of 1,970 kg, is supplied as flat-rolled carbon steel for chassis parts and body panels.

The traditional sheet steels used for chassis and body constructions are the so-called “mild” steels. The combined interests of improving crash worthiness and reducing vehicle weights were at least partially responsible for the development of Gen I AHSSs. What is now desired is Gen III AHSSs that borrow from previous alloy development efforts to achieve intermediate strengths and ductilities but at costs that would make their acceptance for automotive construction feasible. Controlling cost will likely require that Gen III AHSSs be no more than modestly alloyed compared to Gen I AHSSs and capable of being produced within existing steel mill infrastructures.

Approach

It is well known that retaining austenite in automotive sheet steels can markedly improve ductility at high strength through the TRIP effect. Until recently in FY 2011, this project emphasized better fundamental understanding of austenite-ferrite transformations to enable a more scientific approach to improving properties through novel processing compatible with existing mill infrastructures.

Technical issues addressed include the following.

- Making direct in situ observations of the time dependence of austenite-ferrite transformation behavior at elevated temperatures during rapid heating/cooling and during low temperature treatments designed to maximize retained austenite
- Measuring partitioning of carbon between austenite and ferrite during processing
- Understanding effects of critical alloying elements such as carbon, manganese, and silicon on transformation behavior and retention of austenite

Complications associated with using the synchrotron facilities shifted project activities to alternate approaches of investigating ways to promote or increase austenite/ferrite ratios in flat-rolled steels.

Materials and Experimental Details

Most of the synchrotron experiments were conducted with the uncoated dual phased steel, DP780 (ArcelorMittal). Diffraction experiments were done on the UNICAT X-33 bending magnet beam line at the Advanced Photon Source (Argonne National Laboratory, Argonne, Illinois).

Experiments to produce a laminated steel of approximately equal parts ferrite and austenite were conducted by a series of cold and hot rolling trials.

Results and Discussion

Initial results showed that during diffraction at 800°C there was a significant and continuous decrease of austenite fraction from about 66% to 44%. Thermodynamic equilibrium calculations suggested that DP780 should be 75%–80% austenite at 800°C, and this amount was verified by independent heat treating experiments. The inconsistency between phase fractions determined by synchrotron diffraction and those measured in independent experiments and predicted by thermodynamic analysis continued to be the project focus. Failure to resolve the inconsistency would indicate that the current approach to determining phase fractions is inappropriate and that an alternate method is needed to continue this type of phase transformation analysis. Possible causes of the inconsistent behavior are as follows.

- Equilibrium is not being achieved in 120 s at 800°C.
- Decarburization is occurring during diffraction. This will locally decrease the carbon concentration which has a significant effect on phase fractions.
- Some step in the data analysis is not being handled accurately. Data analysis routines are being reexamined and validated.
- Other experimental issues related to the heating stage are also being reevaluated.

These issues were systematically addressed with experiments aimed at better controlling the atmosphere used during diffraction experiments and the surface condition of the specimens. **Figure 7** shows results from three experiments where austenitizing was done for either 2 minutes or 20 minutes at 970°C and intercritical holding at 800°C was done for either 2 or 20 minutes. The austenitizing conditions were chosen to promote homogenization of the austenite before the transformation at 800°C. Regardless of austenitizing time, the ferrite volume fraction increases with intercritical holding time, even when held for 20 minutes. The increase of ferrite amount and its failure to stabilize can reasonably be explained by decarburization.

Specimens of the DP780 were vapor coated with platinum and silica in an attempt to suppress carbon loss from the specimen surfaces while allowing diffraction from the ferrite and austenite to be detected. Results from one of these experiments are shown in Figure 8. Neither coating suppressed the apparent carbon loss as evidenced by the continuously increasing ferrite fraction during holding at 800°C. Additionally, both types of coating preferentially attenuated diffracted intensity due to the ferrite.

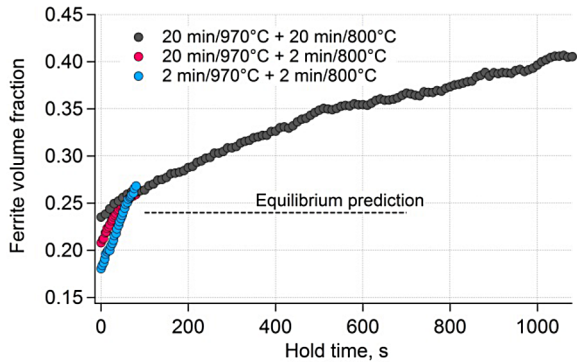


Figure 7. Variation of ferrite fraction with intercritical holding of DP780 at 800°C for austenitizing at 970°C for either 2 or 20 minutes.

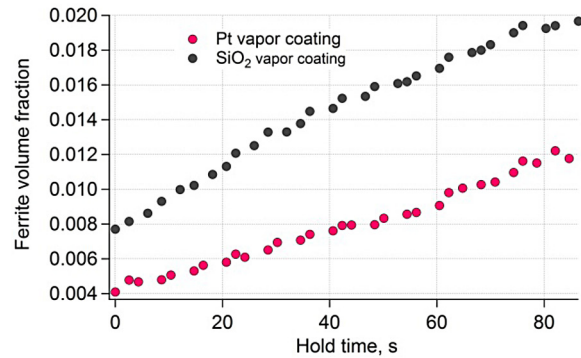


Figure 8. Variation of ferrite fraction with intercritical holding of DP780 at 800°C. Specimens were coated with either Pt or SiO₂.

Several trials were conducted to investigate the potential of using rolling to produce microstructures of about equal parts ferrite and austenite. Initial attempts relied on cold rolling using procedures described in published works, but acceptable results were never obtained. Eventually, hot rolling proved effective for producing laminated structures such as the one shown in Figure 9. This strip was produced by first hot-roll-bonding 6 mm thick plates of A36 carbon steel and Type 304 austenitic stainless steel. After three iterations of rolling with 50% reduction, the strip consisted of four layers of the A36 alternating with four of the 304. For the fourth rolling iteration, the carbon steel surfaces were mated together so that the external surfaces consisted of the austenitic steel. After the final roll bonding pass, the strip was reheated and further hot rolled to a thickness of 3.5 mm. This strip will be used to start verifying the property benefits predicted for such microstructures.

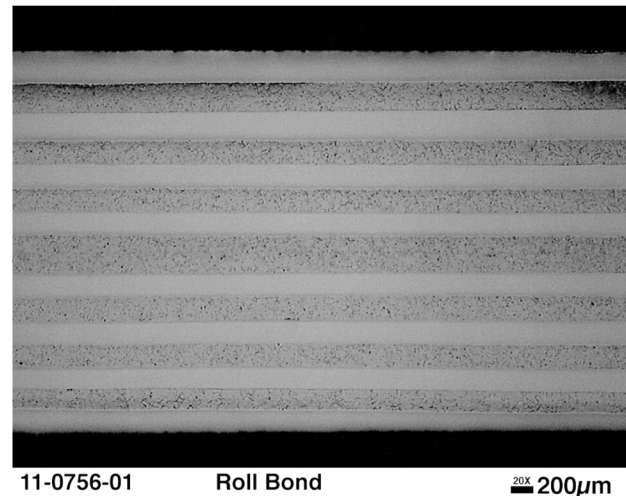


Figure 9. Cross-section view of laminated carbon and stainless steel produced by hot-roll bonding. Upper and lower surface layers are stainless steel.

Conclusions

Initial synchrotron diffraction experiments demonstrated that phase fractions and lattice parameters could be continuously measured during heat treatments similar to those used in processing automotive sheet steels. However, inconsistencies were observed between phase fractions determined by diffraction and those measured by independent experiments. Subsequent diffraction experiments and related analyses attributed the inconsistencies to decarburization. Modification of the diffraction apparatus to control carbon loss is beyond the project scope so the synchrotron experiments will not continue.

Rolling trials were used to produce steel strip with about equal fractions of austenite and ferrite. The strip will be used to verify predictions of the potential benefits of such microstructures on strength and ductility. Microstructures consisting of ferrite + austenite or martensite + austenite are predicted to meet Gen III steel targets.

Conclusions

New methods for characterization of Mg alloys under intermediate strain rates have been developed. The data are useful for vehicle structural designs with Mg and are available on the Internet to potential users.

Synchrotron diffraction experiments demonstrated that phase fractions and lattice parameters could be measured during heat treatment of carbon steels, but inconsistencies were noted between phase fractions determined by independent experiments. Rolling trials produced steel strip with equal fractions of austenite and ferrite. Those strips will be used to verify predictions and demonstrate benefits on strength and ductility. It is predicted that microstructures of ferrite + austenite and martensite + austenite will meet Gen III program targets for a more ductile AHSS.

Presentations/Publications/Patents

Bow, A.; Cline, F.; Davis, C.; Erdman, D.; Wang, Y. High Speed Tensile Test of AZ31 Magnesium Alloy, ORNL student intern poster presented at ORNL, August 2011.

Simunovic, S.; Wang, Y.; Erdman, D.; Kunc, V.; Starbuck, J. M. High Strain Rate Characterization of Magnesium Alloys, invited talk presented at Materials Science and Technology (MS&T) 2011 Conference and Exhibition, Columbus, Ohio, October 16–20, 2011.

Wang, Y.; Erdman, D. L.; Kunc, V.; Simunovic, S. Material Mechanical Characterization Method for Multiple Strains and Strain Rates, U.S. Patent Pending, 61/485, 163, May 12, 2011.

Wang, Y.; Xu, H.; Erdman, D. L.; Starbuck, M. J.; Simunovic, S. Characterization of High Strain Rate Mechanical Behavior of AZ31 Magnesium Alloy Using 3D Digital Image Correlation. *Adv. Eng. Mater.* [Online early access]. DOI: 10.1002/adem.201100048. First published online May 17, 2011.

Wang, Y.; Xu, H.; Erdman, D. L.; Starbuck, M. J.; Simunovic, S. Characterization of High Strain Rate Mechanical Behavior of AZ31 Magnesium Alloy Using 3D Digital Image Correlation. In preparation; to be submitted for publication.

West, N.; Wang, Y.; Erdman, D. L.; Xu, H.; Simunovic, S. High Speed Testing of Notched Aluminum 7075-T6 with 3D Image Correlation, poster presented at the ORNL Science Undergraduate Laboratory Internship program review, ORNL, August 2010.

References

Lademo, O.-G.; Engler, O.; Keller, S.; Berstad, T.; Pedersen, K. O.; Hopperstad, O. S. Identification and Validation of Constitutive Model and Fracture Criterion for AlMgSi Alloy with Application to Sheet Forming. *Mater. Des.* 2009, 30, 3005–3019.

Nyberg, E. A.; Luo, A. A.; Sadayappan, K.; Shi, W. Magnesium for Future Autos. *Adv. Mater. Processes* 2008, 166 (10), 35–37.

Schnatterly, J. Steel Content of North American Vehicles. Presented at the Great Designs in Steel seminar, 2007 (<http://members.steel.org/AM/Template.cfm?Section=GDIS&CONTENTID=24666&TEMPLATE=/CM/HTMLDisplay.cfm>).

Schultz, R. A. Metallic Material Trends for North American Light Vehicles. Presented at the Great Designs in Steel seminar, 2007 (<http://members.steel.org/AM/Template.cfm?Section=GDIS&CONTENTID=24666&TEMPLATE=/CM/HTMLDisplay.cfm>).

Wang, Y.; Xu, H.; Erdman, D. L.; Starbuck, M. J.; Simunovic, S. Characterization of High Strain Rate Mechanical Behavior of AZ31 Magnesium Alloy Using 3D Digital Image Correlation. *Adv. Eng. Mater.* [Online early access]. DOI: 10.1002/adem.201100048. First published online May 17, 2011.

B. Processing and Manufacturability

Pacific Northwest National Laboratory

Field Technical Monitor: Dean Paxton
Pacific Northwest National Laboratory
902 Battelle Boulevard; P.O. Box 999; Richland, WA 99352
(509)375-2620; e-mail: dean.paxton@pnl.gov

Technology Area Development Manager: William Joost
U.S. Department of Energy
1000 Independence Ave., S.W.; Washington, DC 20585
(202) 287-6020; e-mail: william.joost@ee.doe.gov

Contractor: Pacific Northwest National Laboratory (PNNL)
Contract No.: DE-AC05-00OR22725 & DE-AC06-76RLO1830

Executive Summary

The Processing & Manufacturability project consists of six tasks focused on research and development (R&D) activities advancing the basic mechanical properties, manufacturability, and cost of lightweight materials towards the levels needed for increased implementation in automotive applications. These tasks include the following:

- First Generation Advanced High-Strength Steels (AHSS) Deformation Fundamentals
- Aerodynamic Lightweight Cab Structures
- Non-Rare Earth (RE) High-Performance Wrought Magnesium (Mg) Alloys
- Pulse Pressure Forming of Lightweight Materials
- Ultrafine Grain Foils and Sheet by Large Strain Extrusion Machining (LSEM)
- Mg Research and Technology Development.

The following sections outline specific task work conducted at PNNL in the area of processing and manufacturability of lightweight metals. Each task supports one or more goals within the Processing & Manufacturability Agreement as outlined below.

Activity and Developments

First Generation Advanced High-Strength Steels Deformation Fundamentals

Principal Investigator: Xin Sun, PNNL
(509) 372-6489; e-mail: xin.sun@pnnl.gov

Industry Partners:
Donald L. Jordan, Ford Motor Company
(313) 805-4829; e-mail: djorda19@ford.com

Paul J. Belanger, General Motors
(586) 209-1224; e-mail: paul.belanger@gm.com

Dajun Zhou, Chrysler Corporation
(248) 944-1197; e-mail: djz13@chrysler.com

Accomplishments

- Performed various analyses and experiments (i.e., chemical composition analysis, static tensile test, channel forming test, hole expansion test) on eight DP980 steels from different suppliers.
- Performed metallographic analyses on the DP980 steels and obtained three-dimensional microstructure books.
- Performed image analyses on the scanning electron microscope (SEM) pictures to quantify the microstructural features of the steels. Examined the obtained quantities of the microstructural features with respect to the macroscopic deformation features.

Future Directions

- Perform nano-indentation test to quantify the strength disparity between the ferrite and martensite phase of the DP980 steels.
- Perform microstructural analysis for wider areas to examine the martensite distribution features.
- Perform microstructure-based finite element (FE) analysis for the DP980 steels to gain fundamental understandings on the failure driving forces.

Technology Assessment

- Target: Develop the fundamental understandings on key mechanical properties and microstructural features influencing the local formability of AHSS.
- Gap: In addition to the microstructural features investigated in this project, the strength disparity between the constituent phases needs to be quantified to examine its influence on the macroscopic deformation features.

Introduction

AHSS are being increasingly used by the automotive industry to cost effectively reduce vehicle weight. However, a noticeable degree of inconsistent forming behaviors has been observed for the first generation AHSS in production and they appear to be associated with the inherent microstructure-level inhomogeneities for various AHSS. This indicates the basic material property requirements and screening methods currently used by the automotive industry for the mild steel and high-strength low alloys are no longer sufficient for qualifying today's AHSS used in vehicle manufacturing applications.

This project is focused on developing fundamental understandings on key mechanical properties and microstructure features influencing the local formability of AHSS. Only after these fundamental understandings are established can a set of more relevant material acceptance criteria and the associated screening methods be developed to address the local formability of the first generation AHSS. The ultimate goal of this project is to reduce launch time and promote wider applications of AHSS in vehicle bodies.

Approach

Project members started with DP980 as model steels and were able to acquire eight different types of DP980 sheet steels with thickness ranging from 1 to 2 mm from various steel suppliers, including both domestic and foreign producers. Project members labeled these different steels with generic designations (A to H) for the purpose of this project. In fiscal year (FY) 2011, chemical composition analyses were performed on all eight different DP980 materials to have information on the additional elements of interest, using Inductively Coupled Plasma-Atomic Emission Spectroscopy following the American Society for Testing and Materials (ASTM) E 1019-08 standard. Static tensile tests ($\dot{\epsilon} = 10^{-4}$ / sec) have been completed on all the obtained materials using subsized ASTM E8 samples along the rolling and transverse directions for both the center and edge areas of the sheets. Channel forming tests and hole expansion tests have also been performed to find the differences in each material's localized deformation capacity.

Microstructure analyses have been performed on all the obtained DP980 materials using SEM. For this purpose, SEM pictures of in-plane/through-thickness microstructures were obtained from both of the surface and midthickness regions along the rolling and transverse directions for both the center and edge areas of all DP980 materials. Image processing tools were then adopted to mathematically quantify the microstructural features (i.e., volume fraction, grain size, grain orientation, etc.) of these different materials. The information obtained from the microstructure image analysis is expected to correlate the macroscopic deformation features observed in various experiments and can then be used to determine the key factors influencing the local formability of these materials.

Technology Transfer Path

This task is mainly focused on the development of fundamental understandings on key mechanical properties and microstructure features influencing the local formability of AHSS. This project has active industrial participation from automotive original equipment manufactures (OEM) and various domestic and international steel suppliers. The results have been transferred to industry participants through periodic project review meetings as well as project reports. The team plans to present and publish their findings in conferences and peer-reviewed journals to enable dissemination to a broader engineering community.

Results and Discussion

Through chemical analyses, we found that all the materials have similar and relatively high carbon and manganese contents, and they also have similar aluminum (Al) contents. Other alloying elements— such as chromium, copper, molybdenum, and silicon (Si)—are generally different in content for different materials as they have their own roles in achieving the required DP980 properties through different thermal mechanical processes. **Figure 1** shows the examples of stress-strain curves and ultimate tensile strengths obtained from the tests for DP980 steels. **Figure 1a** shows four stress-strain curves of DP980 C for the center and edge areas along the rolling and transverse directions. Most of the DP980 steels exhibit different stress-strain behaviors depending on the sample locations and loading directions as shown in **Figure 1a**. These differences are possibly due to relatively banded microstructures along the rolling directions and the slightly different microstructural features between the center and edge areas (i.e., edge effect). **Figure 1b** compares the stress-strain curves of the DP980 steels for the center area along the rolling direction. As shown in the figure, DP980 steels show large discrepancies in their performance such that they have different initial yield strength, ultimate tensile strengths, total elongation, hardening rate, and other parameters. This discrepancy is believed to be caused by the different microstructural features between the steels as mentioned for the case in **Figure 1a**. Microstructural features from SEM analyses are expected to explain these different macroscopic behaviors. **Figure 2** shows some sample pictures of channel forming test and hole expansion test.

Only materials C, D, F, G, and H are selected for the forming test due to the allowable thickness limit of the forming die. In the forming test, materials C and D show good localized formability (Figure 2a), whereas materials F and G show fracture during the forming process (Figure 2b). Based on the channel forming test results, the materials' localized formability can be ranked in decreasing order as C, D, H, G, and F. Note the materials with high-uniform ductility/elongation (F and G) do not necessarily show good localized formability. Hole expansion tests are also being performed as shown in Figure 2 to establish the difference in localized stretchability between the materials. Samples were prepared using two different hole-cutting methods (i.e., electron discharge machining and punching) to examine the influence of edge preparation on materials' stretchability. The hole expansion test results will be summarized and analyzed in the near future. Figure 3 shows some sample three-dimensional microstructure books for the DP980 steels investigated, composed by stitching the two-dimensional SEM pictures along rolling, transverse, and in-plane directions. As shown in the figure, the materials exhibit different microstructure features.

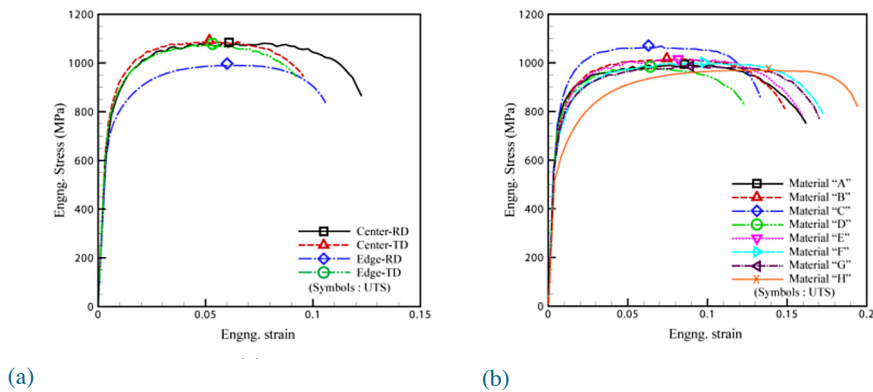


Figure 1. Stress-strain curves for (a) DP980 C and (b) eight different DP980 steels

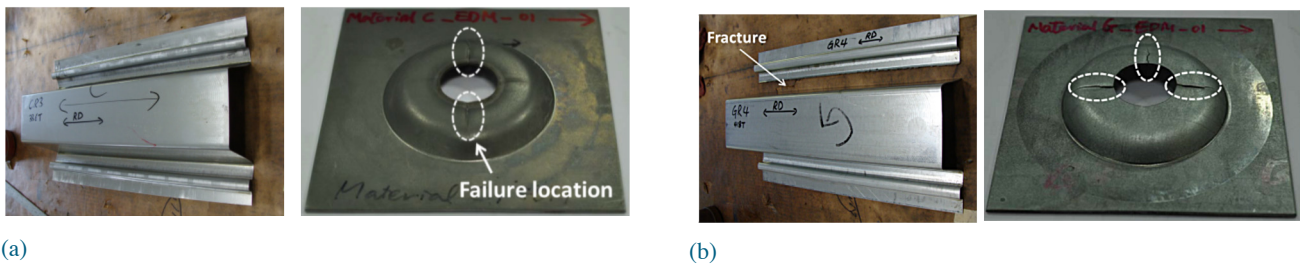


Figure 2. Examples of forming test and hole expansion test results for DP980 (a) C and (b) G

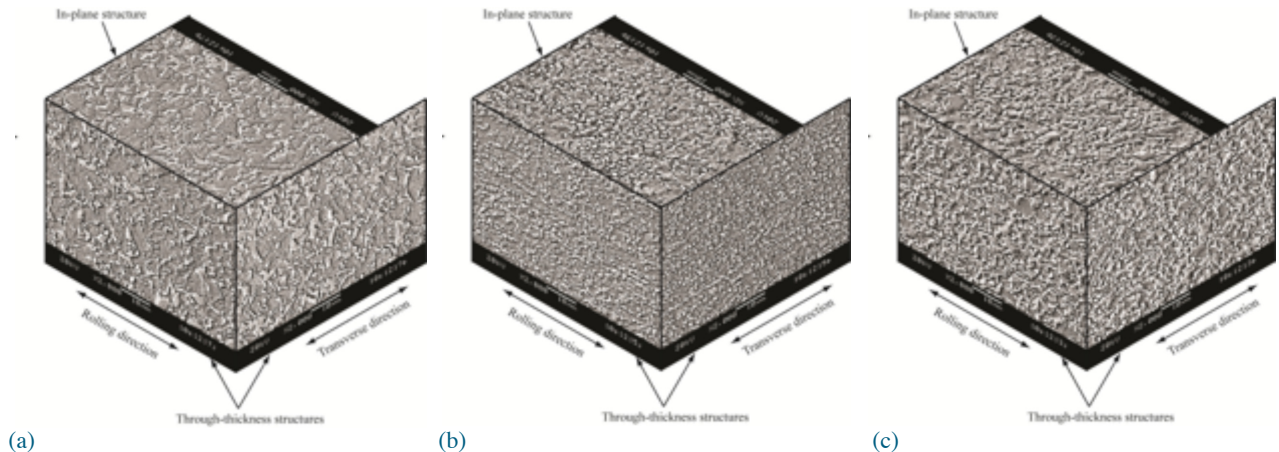


Figure 3. Possible three-dimensional microstructures for DP980 (a) D, (b) H, and (c) G

For example, material D has relatively large and sharp-edged martensite grains homogeneously distributed in the ferrite matrix, whereas material H has small martensite grains with clear banded structures. These different microstructural features are expected to induce different local formability. Next, numerical image processing was performed on the obtained SEM pictures to quantify the microstructural features of the eight DP980 steels. Figure 4 shows some sample results of the image analyses. Figure 5 shows the correlations between martensite volume fraction and aspect ratio with the material macroscopic

formability ranking. The results in Figure 5 indicate that no clear trend on macroscopic formability can be established with the microstructure features alone. Similar attempts at correlating microstructure features alone with ultimate ductility yield similar results. These results indicate the strength disparity between the ferrite and martensite phases of the different DP steels may have more significant effects on their macroscopic deformation capacities. As a next step, the project team will use nano-indentation tests to quantify the strength disparity of the two phases and then to investigate its effects on the macroscopic properties.

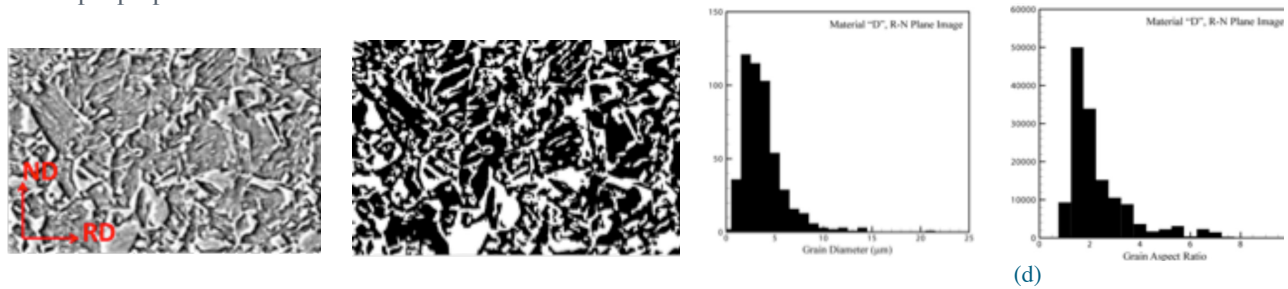


Figure 4. Examples of image process of microstructure: (a) an actual microstructure of DP980 D; (b) final binary image after process; (c) and (d) are histograms for martensite grain-size and aspect ratio

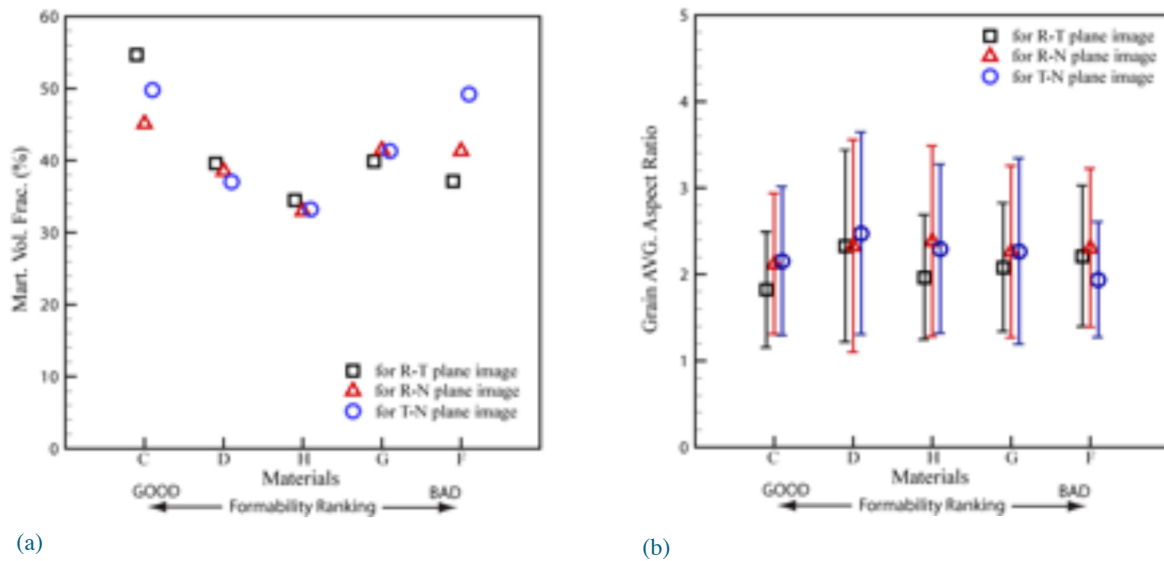


Figure 5. Example plots of microstructural features of DP980 steels as functions of their formability ranking: (a) martensite volume fractions versus formability ranking; (b) average martensite aspect ratio versus formability ranking

Conclusions

Eight different DP980 steels were acquired from different suppliers and various tests have been performed for different locations and directions to establish the fundamental understandings on key mechanical properties and the microstructure features influencing the local formability of AHSS. It was observed from the test results that all DP980 steels show large discrepancies in their performance, which is possibly due to their different microstructural features. Results to date indicate microstructural features alone are not responsible for the drastically different macroscopic deformation behaviors. As the strength disparity between the constituent phases may also have significant effects on the behaviors of multi-phase steels, nano-indentation test is being planned to measure the strength disparity. Larger-area microscopes are also considered to examine the martensite distribution features in details.

Aerodynamic Lightweight Cab Structure Components

Principal Investigator: Mark T. Smith, PNNL
(509) 375-4478; e-mail: mark.smith@pnnl.gov

Investigator: Nona Larson, PACCAR Technical Center
(360) 757-5365; e-mail: nona.larson@paccar.com

Accomplishments

- Completed simulated Al sheet forming sequences using tensile specimen-based tests. Simulated forming included maximum hot tensile ductility, hot forming followed by cold forming steps, and cold forming combined with hot forming steps. Results for the simulated hot tensile forming/cold forming sequence indicated that significant increases in overall material elongation are possible.
- Design for a prototypical cab “A-pillar” tool was completed and a subcontract for tooling fabrication placed. The tooling will allow Al sheet materials to be hot preformed and cold finish formed to simulate an actual component forming manufacturing process.

Future Directions

- Complete fabrication of hot preforming and cold finish forming tool sets and perform simulated biaxial forming of prototype “A-pillar” components.
- Conduct material property and finish system characterization of formed “A-pillar” components to confirm the ability to meet PACCAR materials and manufacturing specifications.
- Engage Magna Cosma International in evaluation of potential hot and cold forming process sequences to establish manufacturing feasibility.

Technology Assessment

- Target: Develop elevated temperature hot forming process, combined with cold finish forming that can increase the useable elongation and formability to over 40% for a 6000-series Al sheet alloy. Room temperature forming limits for current generation automotive grade 6000-series alloys are generally limited to the equivalent of 18 to 20% tensile elongations, depending on component geometry and part complexity.
- Target: Demonstrate the feasibility of hot forming complex Al sheet components requiring overall formability levels of up to 40% equivalent tensile elongation, while meeting mechanical property and finish requirements for exterior cab component applications.
- Gap: Current 6000-series Al sheet alloys have desirable strength levels and surface finish characteristics, but lack sufficient formability (>18-20% tensile elongation) to allow their use in the manufacture of many aerodynamic cab components and structures.
- Gap: Existing Al hot forming processes result in formed sheet tensile properties that are typically below 100 MPa yield strength levels. This limits the use of hot-formed Al sheet in applications that require higher strengths (150 MPa) for long-term fatigue and dent resistance.

Introduction

The objective of this project is to demonstrate lightweight materials manufacturing methods that will increase the efficiency of Class 8 trucks by enabling more widespread use of mass-saving Al and enabling aerodynamic styling through the use of a new approach to Al sheet forming. The project will develop forming technology that will enable Al sheet to replace sheet steel and molded fiber reinforced glass composite panels and components, providing individual panel and component weight savings of approximately 40%.

Approach

- The project will use an elevated temperature forming process, to be developed at PNNL, to demonstrate enhanced ductility in 6000-series Al alloy sheet. The high-ductility forming process will enable PACCAR member companies to design prototype cab components with aerodynamic features that would otherwise not be feasible for manufacturing. PNNL will develop and optimize a hot form + cold forming process using sheet tensile specimens and the PACCAR Technical Center will evaluate surface conditions and corrosion behavior for formed specimens. Based on the selected process parameters, PNNL and the PACCAR Technical Center will design and build a prototype component for laboratory testing at the technical center. The technology for the process developed at PNNL will be transferred to a tier 1 supplier and project partner, Magna Cosma International, who will build full-scale prototype components for the PACCAR Technical Center, who will then finish the parts and perform durability testing including fatigue and corrosion testing. Planned technical steps and milestones include conducting elevated temperature tensile tests at various strain rates on the alloy provided by the PACCAR Technical Center to develop a constitutive materials relation for use in forming analysis. These data will provide a basis for selection of the temperature and strain rates for subsequent forming trials.
- PNNL will study the microstructural evolution and hardening mechanisms to provide a basic understanding of the alloy behavior and how that can impact future component design to reduce mass and improve aerodynamic styling.
- Assuming a process route can be established, the full-scale component will be modeled at PNNL to determine the optimum forming process cycle.
- Depending on component size and forming requirements, a prototype die will be constructed and parts will be fabricated at either PNNL or Magna Cosma International.
- Given the high-temperature processing involved in the proposed forming approach, the PACCAR Technical Center will perform surface-oxide characterization and support the e-coat process development to assure good adherence through optimized parameters.
- Several prototype panels will be made and the PACCAR Technical Center will process the parts through the cab assembly and coating process and perform component testing. Component testing will include a durability test (possibly on a Cab shake system); corrosion testing; and mechanical properties testing, including tension and fatigue testing.

Technology Transfer Path

This task is primarily focused on demonstration of the development of a thermomechanical forming process that can achieve significantly enhanced levels of formability in Al sheet materials. PACCAR and its two truck companies have multiple applications where high formability and good post formed properties of the Al sheet would allow them to replace low-strength glass fiber composites in highly shaped aerodynamic panels and components. The project includes participation by Magna Cosma International, who is a major supplier of truck cab structures and components, and will facilitate transfer of the technology to a Tier 1 supplier.

Results and Discussion

The first phase of this project has evaluated a series of hot and cold forming steps using superplastic forming (SPF) type tensile specimens for the evaluations. Several combinations of hot straining to various strain levels followed by cold straining of approximately 5% were evaluated, and in all cases the specimens were then heat treated to simulate the vehicle paint bake cycle (180°C for 20 minutes) and tensile tested at room temperature. Room temperature tensile test results were then compared to baseline sheet properties, including yield stress, ultimate tensile stress, and elongation. Novelis Aluminum supplied two groups of materials for the evaluation, both being a 6000-series Al sheet alloy developed specifically for PACCAR cab structure applications. All materials were delivered in the solution-treated condition (-T4), and as such were tested within 3 months of delivery to ensure minimum effects of natural aging. Table 1 summarizes the tensile test results for the as-received materials, designated as 6XXX-1 and 6XXX-2 for the two material batches. Table 1 includes the as-received -T4 properties, as well as properties for the paint baked (PB) and 5% cold strain + PB. All values shown are the average of a minimum of three separate test specimens.

Table 1. Baseline 6000 sheet tensile properties

Material ID	Condition	0.2% Yield Strength (MPa)	Ultimate Tensile Strength (MPa)	Elongation (%)
6XXX-1	As-Received (AR)	120	210	22.1
6XXX-1	AR + PB	165	241	18.7
6XXX-1	AR + 5%CF + PB	207	255	20.9
6XXX-2	As-Received (AR)	135	228	23.6
6XXX-2	AR+PB	184	260	21.2
6XXX-2	AR + 5%CF + PB	230	274	27.1

AR = As received (-T4); PB = Paint bake (180°C, 20 minutes); CF = Cold form (room temperature strain)

The property results for the as-received material with 5% cold strain + PB represent the properties expected in design of cab structures and components, and therefore this condition best represents the baseline sheet properties. While the tensile elongations of the baseline condition are quite good for a 6000-series sheet alloy, suppliers have identified a number of cab components where ductility that exceeds 30% (as measured by tensile ductility) would allow 6000-series Al to replace sheet steel and fiber reinforced glass composites.

To investigate forming approaches and sequences that could result in increased ductility, PNNL used an SPF-style shoulder-loaded tensile specimen that allowed for controlled strains to be applied at elevated temperatures as well as room temperature.

The primary test variables selected for evaluation were test temperature and the amount of strain applied in each simulated forming step. After evaluation of hot forming (straining), this step was followed by cold forming. The reverse sequence: cold forming followed by hot forming was also investigated. Due to manufacturing considerations and favorable paint bake response, further testing efforts focused on the hot forming/cold forming sequence. In either forming sequence, the hot forming step allows an increased amount of tensile deformation (elongation) without the localization of strain that leads to necking failure.

The most likely explanation for the results is related to the development of the intermetallic precipitates that strengthen the alloy. In order to develop the maximum properties, the alloy must be heated to a temperature where all constituents are in a solid solution and rapidly quenched in water to maximize the alloying content of the metastable solution (-T4 solution heat treatment). Upon aging (precipitating from the metastable solution), the precipitates nucleate uniformly and homogeneously from an ideal solution heat treatment. This precipitate structure provides the maximum volume fraction of precipitates, which maximizes strength and provides the optimum combination of strength and ductility. The 6000-series alloy tested here is a compositionally lean alloy, and optimum heat treat is accomplished by combining cold work with solution heat treat to maximize precipitate nucleation (i.e. at dislocation tangles). In addition, the strain energy associated with the cold work increases the kinetics of the precipitation resulting in a better response at the low temperature, 20 minute, paint bake aging

conditions. Therefore, it would be expected that hot work, at or near the solutionizing temperature (approximately 540°C), followed by a rapid quench step (water or air quench) combined with cold work prior to paint bake should produce the best strength and ductility.

Table 2 contains a summary of the various hot forming/cold forming (straining) sequence steps along with the final tensile test properties and elongations. Note the total elongation is the sum of the simulated forming step strains plus the final elongation to failure.

Table 2. Summary of simulated forming test results for hot and cold strained specimens. Results for Novelis 6XXX-2 sheet.

Specimen Group	Forming Condition	Temp. (C)	Hot Strain (%)	Cold Strain (%)	0.2% Yield Strength (MPa)	Ultimate Tensile Strength (MPa)	Total Elongation (%)
29	HF/CF	450/RT	19.89	4.17	141.9	184.4	37.89
26	HF/CF	500/RT WQ	20.11	4.06	179.2	239.7	41.76
31	HF/CF	540/RT AC	29.38	4.36	201.0	249.0	45.91
30	HF/CF	540/RT WQ	28.92	4.27	223.1	262.4	45.80

HF/CF = Hot form then cold form; WQ = Water quench (from HF step); AC = Air cool (from HF step). All specimens received standard paint bake (180° C/20 minutes) prior to room temperature tensile test.

Results from Table 2 indicate that hot forming in the 450 to 540°C range with either air or water quench, followed by some level of cold strain and paint bake, can achieve total elongations in excess of 40%. In addition, strength levels that meet requirements for a minimum 150 MPa yield strength appear to be achievable.

In addition, increasing the hot strain portion of the simulated forming process resulted in significantly higher total elongations. Specimen dimensions were measured after the hot strain step and the specimen gage sections showed little or no strain localization. The temperature range between 450 and 540°C, and the combination of either air cool or water quench appears to offer considerable process flexibility, although straining at 540°C followed by water quench routinely provides the highest combination of strength and total elongation.

During the reporting period, the design of a three-dimensional representative component was completed. This component incorporates dimensional features that require material strains that greatly exceed the room temperature forming limits of 6000-series Al alloys. Figure 6 shows a view of the prototype component. Tooling for the prototype component has been designed and is currently being fabricated.

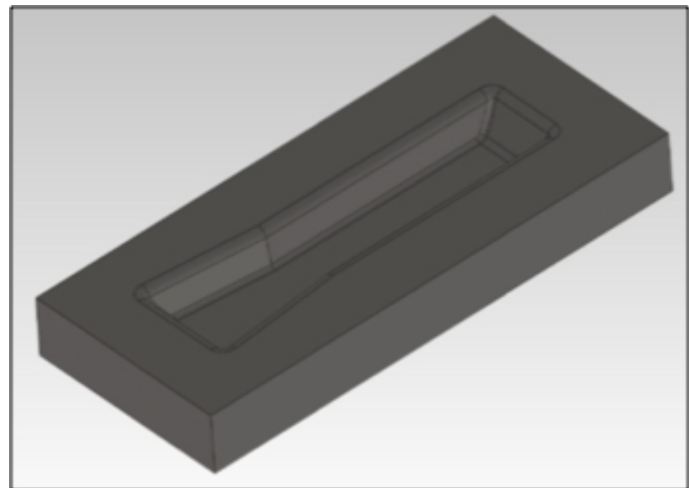


Figure 6. Three-dimensional prototype component die design

Conclusions

The first phase of this project has evaluated combinations of hot and cold forming steps for the 6000 series Al sheet alloy with the objective of demonstrating enhanced tensile ductility. Results indicate that high temperature hot forming (approaching the solutionizing temperature), followed by a cold forming step results in a useful increase in total tensile elongation. The forming sequence of hot forming into a preform shape, followed by cold forming or stamping is compatible with the cab structure and component manufacturing process as the final cold forming step ensures dimensional requirements are met. The next phase of the project will demonstrate the hot and cold forming process for a prototype three-dimensional component that will allow further validation of process steps and resulting material properties and surface characteristics.

Non-Rare Earth High-Performance Wrought Magnesium Alloys

Principal Investigator: Curtis A. Lavender, PNNL
(509) 372-6770; email: curt.lavender@pnnl.gov

Tim Skszek, Magna Cosma International
(248) 689-5512; email: tim.skszek@cosmaeng.com

Accomplishments

- Rapidly solidified materials from three Mg alloys were prepared and characterized to understand basic features of the microstructure of a known high-performance Mg alloy.
- Characterization of the high-performance Mg alloy indicates the RE element addition is acting as a nucleation site, producing fine-grain size and a finely distributed Mg-Zinc (Zn) precipitate. The combination of fine-grain size and precipitate size are likely combining to produce the exceptional strengths and anisotropy observed in the RE containing alloys.
- A simulated energy absorption test and sample has been designed that will use a small tubular sample that will be crushed at a crosshead velocity to produce a uniform initial strain rate of $1 \times 10^{-3} \text{ s}^{-1}$. This test and sample will be used to compare the energy absorption capability of the high-performance Mg alloys to 6061-T6 Al.
- Microstructure-based FE analysis has been initiated to understand the role of grain size, precipitate distribution, and dispersions on the alloy strength. This model will serve as a guide for the non-RE alloy development phase of the project.

Future Directions

- Consolidate the rapidly solidified materials by warm extrusion using a newly designed and fabricated 200-ton extrusion system at PNNL.
- Perform energy absorption testing by high-strain rate testing of a tubular product made from the extrusion.
- Produce a Zr-containing alloy that has an equivalent volume fraction of dispersion to the RE containing alloys.
- Produce at least three additional alloys based on the microstructural modeling to demonstrate the predictability of the performance and microstructure relationship.

Technology Assessment

- Target: Develop high-energy absorption Mg alloys that do not contain RE elements that can replace Al extrusions at a mass savings of 25% (based on density).
- Target: Use inverse process modeling to develop a low-cost process to produce microstructures required for high performance at a low cost, making Mg extrusion viable for automotive applications.

- Gap: Currently produced Mg alloys that possess high strength and ductility (energy absorption) use RE elements that increase cost and are of limited supply resulting in a reluctance of the automotive industry to use Mg extrusions.
- Gap: The cost to produce high-performance Mg extrusion has prevented use in automotive applications.

Introduction

The use of Mg in automotive applications where extrusions would be preferred has been limited by the cost and energy absorption capacity of Mg. Applications like bumper beams, crush tips, intrusion beams, and shotgun tubes (among others) comprise a significant vehicle mass savings opportunity if they could be fabricated from Mg. In the past, there have been projects where Mg has been processed for use in applications requiring energy absorption like that of Al. This was primarily accomplished by the use of very slow extrusion rates (raising cost) or by powder metallurgy processes requiring rapid solidification and RE alloying additions.

The purpose of this project is to develop and demonstrate low-cost wrought Mg alloys that do not rely on RE alloying elements for their strength, ductility, and energy absorption properties. A novel low-cost processing method, in conjunction with Mg alloys containing RE substitutes, will be developed to produce the microstructure and properties needed for the automotive applications in a cost-effective manner.

Technical Approach

The project will be performed in three phases: phases will start by the project team producing high-performance alloys using RE additions to develop high-energy absorbing microstructures that will be used as model systems for non-RE alloys. The second phase of the project will develop the microstructure found in phase 1 to develop high-performance alloys without RE additions. During the second phase, at least one alloy will be selected and processed for evaluation by Magna Cosma International for use in automotive applications that require additional formability such as bending or hydroforming. The third phase of the project will use an inverse process modeling method to develop a cost effective processing approach to produce the alloy with the energy absorbing properties.

The following technical steps are planned:

- Produce RE-Mg alloy extrusions and perform mechanical tests comparing quasi-static tension and compression results to the Al alloy 6061 and the conventional Mg alloy AZ31.
- Evaluate energy absorption capability of the RE-Mg via impact tests and compare to 6061 and AZ31.
- Evaluate—experimentally—the deformation mechanisms of the RE alloys using interrupted strain tests in tension and compression at room temperature.
- Develop a continuum level model to predict microstructure evolution and mechanical deformation behavior of Mg alloys during processing. Validate using experimental data.
- Downselect up to three alloys from the previous task, consolidate the materials by extrusion, and evaluate the non-RE alloys for strength and energy absorption characterization at both quasi-static and elevated strain-rate tension tests.
- Produce sufficient material to provide partner Magna Cosma International with tubular extrusions that can be formed into shapes such as crush tips, roof structural support beams, etc. for testing and comparison to conventional materials.
- Develop the “Model Alloy” by implementing statistical continuum mechanics model embedded with crystal plasticity. Use the model to predict grain size, dispersion, and textural effects.
- Use experimental data, crystal plasticity, inverse process path modeling, and laboratory demonstrations to develop the necessary process that will create the desired microstructure using an optimum low-cost, high shear, liquid-to-shape processing route.

- Prototype and demonstrate a small system to produce extruded shapes from direct liquid to solid processing. Although the system design will be driven by the modeling, it is anticipated the system will use pressurized liquid metal to fill a cavity that houses a series of high shear mixers. The liquid will be solidified during the mixing process, fracturing the coarse intermetallics, and produce the strain needed for the fine-grain size (as predicted by the inverse modeling) and provide the driving force for the subsequent extrusion.
- Magna Cosma International will evaluate extrusions produced by the system for formability. Billets produced by the process will be rolled at PNNL and subjected to formability tests using limited dome height and warm gas-pressure forming.
- The prototypic system and design methodology will be provided to Magnesium Elektron North America (MENA), who will perform cost analysis and scale the process for production of large quantities of material.

Technology Transfer Path

The technology transfer for this project will occur late in phase 2 and during phase 3. The initial phase will be focused on laboratory development and understanding the Mg alloys from a mechanistic standpoint. After the alloy is understood, the technology transfer will occur in two ways: 1) produce and deliver tubes to Magna Cosma for evaluation; and 2) transfer process knowledge to Transmet Inc. and MENA. In addition, MENA has contributed alloy feedstock for the early rapid solidification processing and has played an active role in alloy selection.

Magna Cosma and MENA are cost sharing partners in the project and Georgia Institute of Technology and Transmet are subcontractors and are or will be engaged in the project at the appropriate phases.

Results and Discussion

The initial phase of this effort was to determine the microstructural characteristics of a rapidly solidified high-performance, RE containing Mg alloy and compare that to conventional alloys with similar processing. High-performance Mg alloys exhibit yield strengths in excess of 500 MPa in both tension and compression, unlike conventional alloys where the compressive yield strength is 0.6 to 0.7 of the tensile yield strength. This behavior has been attributed to the fine-grain size and the contribution of twinning relative to the strengthening associated with grain boundaries where the reduction in strength associated with twinning is offset by the strengthening associated with the grain boundaries.

To investigate the effect of alloying on the microstructure, three alloys were processed. Each alloy contained approximately 6% weight Zn, alloy 2 contained 0.5% weight zirconium (Zr) and alloy 3 contained 3% weight RE and 2% weight aluminum (Al). The alloys were named: alloy 1 MgZnAl; alloy 2 MgZnZr; and alloy 3 MgZnAlRE. Alloys 2 and 3 were chosen for the availability of low solubility dispersions from Zr and RE, respectively, where alloy 3 had approximately six times that of alloy 2. The resulting microstructure can be seen in Figure 7 where alloy 1 (a) had a grain size in excess of 10 μ m, alloy 2 (b) was 2 to 4 μ m, and alloy 3 (c) was approximately 1 μ m.

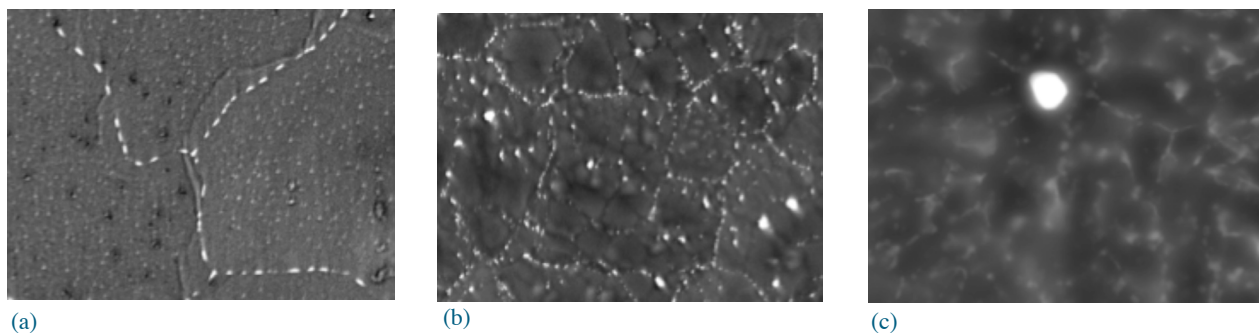


Figure 7. Scanning electron images of the alloys alloy 1 (a), MgZnZr (b), and MgAlZnAlRE (c) showing this difference in grain size associated with the as-solidified alloys

In all cases, the grain boundaries were lined with MgZn precipitates that became progressively finer with decreasing grain size. Alloys 2 and 3 contained Zr and RE, respectively, that formed intermetallic dispersions shown as larger white spots in figure 7b and 7c. The MgZr dispersions in alloy 2 were found within the grains and were approximately 0.2 μm in diameter, and in alloy 3 the MgRE intermetallic was found in two distinct sizes, 1 to 3 μm similar to the white spot in Figure 7c, and the very fine round particles (both light and dark) approximately 0.2 μm as observed in Figure 8.

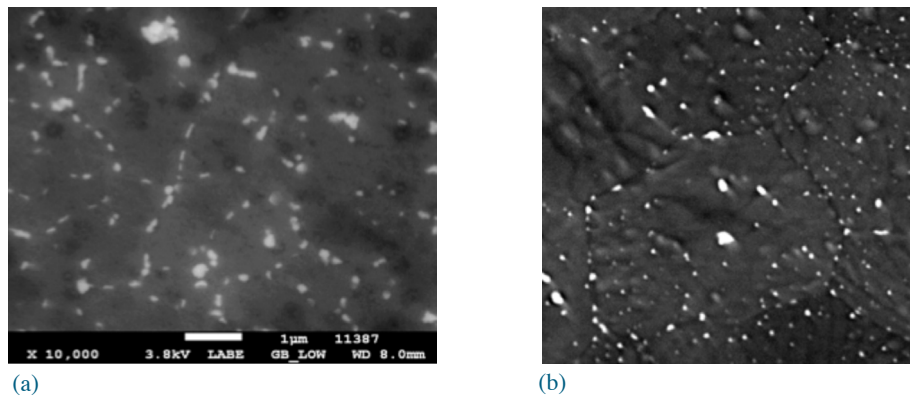


Figure 8. Scanning electron images of alloy 3 (a) and alloy 2 (b) showing the presence of MgRE (light and dark round particles) and MgZr (white globular particles) intermetallics. Most MgRE and MgZr particle were found within the grain whereas the particles found along the grain boundaries were predominately MgZn.

The dispersions Mg Zr and MgRE observed in alloys 2 and alloy 3, respectively, were predominately found within the grain and not at the boundaries, indicating dispersions were involved in the nucleation of the grain. Alloy 1, which had no low solubility dispersion with former and few nuclei, had a large-grain size; alloy 2, which had less nuclei than alloy 3, formed a grain size much finer than alloy 1 but larger than alloy 3. We theorize that alloy 3, which contained six times the dispersion-forming element by weight when compared to alloy 2, nucleated many more grains resulting in a finer-grain size. It is likely Zr is behaving similarly to the RE and that increased additions of Zr may reduce the grain size similarly to that of the RE.

Future tests will be performed with higher levels of Zr, although the increased addition of Zr is challenging due to the increase in liquidus and the challenges that presents for melting Mg alloys. Other dispersion formers will be investigated, such as ternary alloys that produce intermetallic compounds like MnAl_x, which are known to form during solidification and may be manipulated to produce fine-grain sizes.

Performance of the alloys will be evaluated using a tubular compression sample with a slenderness ratio that will result in buckling, similar to that observed in crush tube applications. The MgRE alloy, AZ31 and 6061-T6, will be tested for comparison of the ability of the sample to absorb energy; output of the test will be the area under the curve of the load displacement plot up to a displacement that is to be determined from the 6061-T6 test. Both ends of the tube will be unconstrained and will be pressed against hardened steel platens. The tube will be speckle patterned and tested with a crosshead velocity that would result in an initial strain rate of approximately $1 \times 10^{-3} \text{ s}^{-1}$ after which the strain rate will be determined from digital images taken by high-speed cameras. The outside diameter of the sample will be 10 mm with an overall length of 50 mm. The inside diameter will be varied to produce samples with equivalent mass for the Al and Mg, and a second set will be tested with an inside diameter that produces an equivalent load at yield (to be estimated prior to testing). The two test types were designed to determine if the absorbed energy is a function of geometry (equivalent mass) or strength (equivalent load).

Microstructure-based FE modeling was initiated and the first step was developing statistical stable microstructure information for FE analysis based on microstructural characterization from scanning electron microscopy and other chemical imaging facility. To simulate the microstructure, Voronoi tessellation was used based on the weight fraction of dispersion nuclei and the approximate size distribution. Alloys 2 and 3 were analyzed and the output grain size and simulated microstructure with similar particle distribution is provided in Figure 9. The microstructure predicted from the Voronoi tessellation correlated reasonably well with the grain size observed in the samples. This technique will be very useful in alloy development and prediction but most importantly can be used to input microstructure into the FE models from which strength, stress-strain behavior may be calculated.

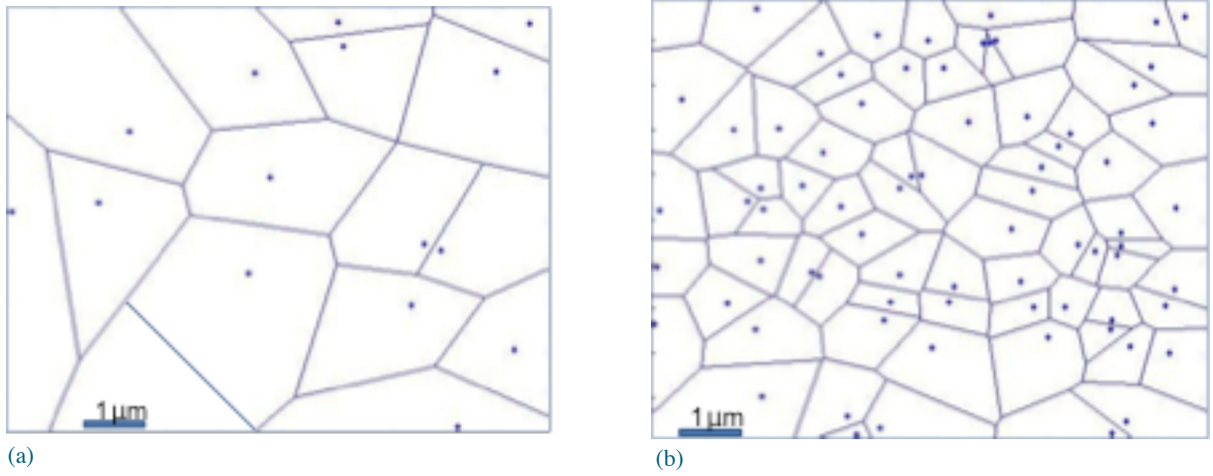


Figure 9. Voronoi tessellation simulation of the microstructure of alloy 2 (a) and alloy 3 (b) showing a correlation between number of dispersions and expected grain size

The correlation of grain size determined by the Voronoi tessellation and the scanning electron images may also support the theory that dispersions in the alloy control the grain size through nucleation. The mathematical theory behind the Voronoi tessellation is similar to the crystal growth expected with simultaneous nucleation from discrete particles.

Conclusions

The fine-grain size that is expected to produce high-energy absorbing Mg alloys is largely controlled by the presence of fine dispersions acting as nuclei.

Based on observed microstructure and the Voronoi tessellation, the nucleation may be independent of chemistry and a function of dispersion size and volume fraction. This indicates that a high performance, non-RE alloy may be feasible provided that dispersions can be developed in the microstructure from non-RE elements. Zr is a good candidate but increased levels of Zr create challenges for alloy processing; further work will be performed to evaluate the Zr addition.

Pulse Pressure Forming of Lightweight Materials

Principal Investigator: Richard W. Davies, PNNL
(509) 375-6474; e-mail: rich.davies@pnnl.gov

Principal Investigator: Aashish Rohatgi, PNNL
(509) 372-6047; e-mail: aashish.rohatgi@pnnl.gov

Principal Investigator: Mark T. Smith, PNNL
(509) 375-4478; e-mail: mark.smith@pnnl.gov

Accomplishments

- High-strain rate forming, using a Pulse Pressure Forming (PPF) technique, was demonstrated to enhance the room-temperature formability of 5182-O Al to levels that are typically expected during warm forming. The quantification of deformation history associated with this formability enhancement was made possible by a novel measurement technique developed at PNNL.
- Tensile stress-strain responses of AZ31B-O Mg, 5182-O Al, and DP600 steel sheets were determined at quasi-static and Hopkinson bar strain rates. The Johnson-Cook equation was used to describe the constitutive behavior of the test materials and to model sheet deformation behavior during PPF.

Future Directions

- The project ended in September 2011 but discussions with automotive OEMs will continue beyond the project end date to assist manufacturers in evaluating and commercializing PPF processes for enabling greater usage of lightweighting metals.
- Results of this project will be disseminated via publications in peer-reviewed journals and conference presentations.

Technology Assessment

- Target: Use high-rate forming to demonstrate enhanced room-temperature formability in sheet metals beyond what is achievable by room-temperature quasi-static forming. Concurrently, quantify the deformation history beyond what is obtainable by conventional post-deformation strain measurements.
- Target: Develop numerical model(s) to describe sheet metal behavior during PPF.
- Gap: Experimental techniques to quantify strain, strain rate, and strain path experienced by sheet metals during forming at high-strain rates do not exist. Instead, existing techniques are primarily limited to post-deformation strain measurements and in some cases, displacement/velocity measurements.
- Gap: Lack of quantitative data of sheet deformation history during high-rate forming has prevented validation of numerical models that describe the forming process.

Introduction

The ultimate goal of this project is to extend the formability of high-strength, lightweight metals (e.g., Al and Mg) and AHSS using PPF techniques such as electrohydraulic forming (EHF). PPF techniques have the potential to enhance formability of difficult to form metals, minimize or eliminate springback after forming, and use less expensive single-sided tooling. However, researchers lack understanding of practical forming limits in PPF processes and its dependence upon process parameters and tooling design. This project will quantify the deformation behavior of sheet metals during the EHF process and develop validated constitutive relations and numerical models to enhance our understanding of EHF and the sheet metal formability achievable through EHF.

Approach

High-rate deformation behavior of AZ31B-O Mg (1 mm), 5182-O Al (1 mm) and DP600 steel (1 mm) sheets during EHF was quantified using a novel technique comprising high-speed imaging and digital image correlation (Rohatgi et al. 2011). The “safe” strains and “incipient failure” strains on electro-hydraulically formed Al were quantified and compared against its quasi-static forming limits. AZ31B-O Mg sheets were subjected to quasi-static forming and EHF to determine the formability of Mg as a function of strain rate. Room-temperature tensile stress-strain behavior of all the test materials was determined at quasi-static (10^{-3} – 10^{-1} /s) and Hopkinson bar (1000 - \sim 2400 /s) strain rates. Sheet deformation during EHF was modeled in Abaqus using three-dimensional and axi-symmetric two dimensional models with numerical pressure pulse profiles and employing the Johnson-Cook equation to describe the material’s constitutive behavior.

Technology Transfer Path

Extension of this work to 6xxx and 7xxx series Al alloys is being discussed with the OEMs. Success in enhancing formability of these higher strength alloys (relative to 5xxx series) will make them a suitable alternative to steel currently used in closure and structural components.

Results and Discussion

Figure 10a shows the quasi-static forming-limit diagram (FLD) for 5182-O Al together with the major and minor strains of Al sheets that were free-formed or formed inside a conical die using EHF. The peak strain-rate at the apex was measured to be \sim 3900 /s and \sim 1700 /s, respectively, for free-formed and conical die-formed Al sheets. Figure 10b shows the EHF free-formed Al sample and the predicted strains.

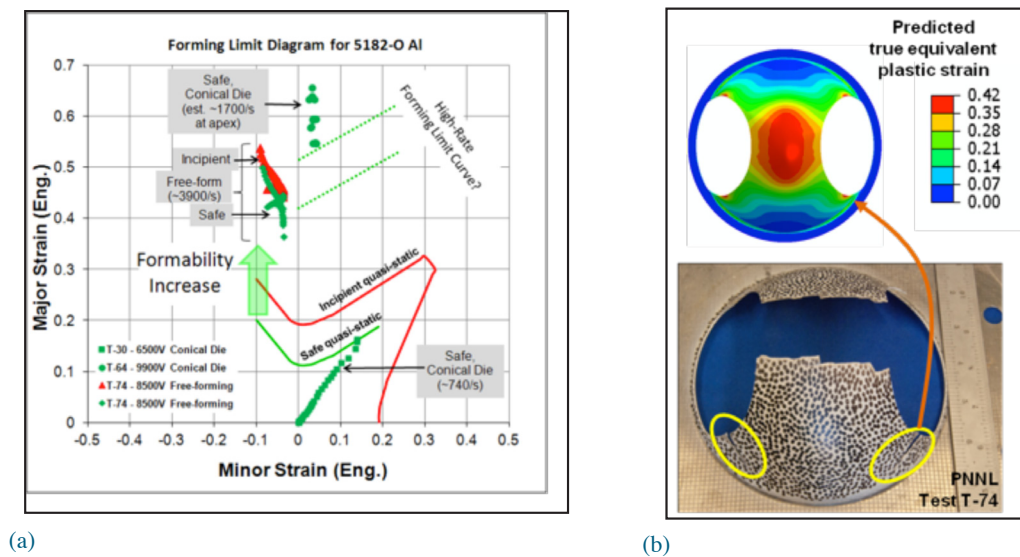


Figure 10. (a) Comparison of quasi-static FLD for Al and “safe” strains and “incipient failure” strains measured on EHF Al domes; (b) images of the Al test specimen (free-formed to failure by EHF) and the corresponding numerically predicted strains

A comparison of the quasi-static and EHF forming data in Figure 10a shows that the formability of 5182-O Al during EHF, and under conditions close to plane-strain, increased by \sim 2.5x relative to the corresponding safe forming limits under quasi-static forming. The peak strain-rate at the apex of the resulting Al dome was measured to be \sim 3900 /s. When the EHF process was performed inside a conical die, the plane-strain formability increased by \sim 6x relative to the corresponding safe forming limits under quasi-static forming. The peak strain-rate on the conical die-formed dome was measured to be \sim 1700 /s while the strain-rate near the locations of enhanced formability was estimated to be \sim 5000 /s. Note that enhanced

formability in Al, demonstrated at room-temperature through high strain-rate forming (Figure 10a), is generally seen at warm forming temperatures (Li and Ghosh 2004). Formability investigations to date have typically relied only on post-mortem strain measurements to quantify forming behavior (e.g., Balanethiram and Daehn 1992; Imbert et al. 2005) and as such, are unable to clarify the mechanism(s) behind enhanced formability.

However, PNNL's unique approach of combining high-speed imaging with the digital image correlation technique has enabled quantification of the deformation history (Rohatgi et al. 2011), which can help clarify the role of deformation parameters, such as strain path (Figure 11) and strain-rate, in influencing the formability.

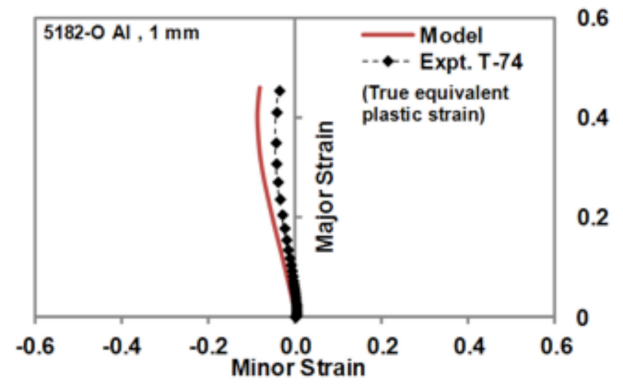


Figure 11. Simulated and experimentally measured strain-path at the apex of EHF free formed Al

Figure 12 shows the tensile stress-strain behavior of Mg, Al and steel sheet materials tested in the rolling direction. The results show that the flow stress of AZ31B-O and DP600 steel shows positive strain-rate sensitivity. However, 5182-O Al has relatively low strain-rate sensitivity but shows an apparent increase in strain-to-failure at higher strain-rates. Although the positive strain-rate sensitivity in Mg indicates the potential for enhancing its formability through high strain-rate forming (as demonstrated for Al in Figure 10a), only marginal improvement was observed during EHF. This marginal improvement was most likely caused by premature failure of the sheet around the tool radius. Therefore, improved tool design and further investigation is needed to ascertain the true influence of high strain-rates on the formability of Mg.

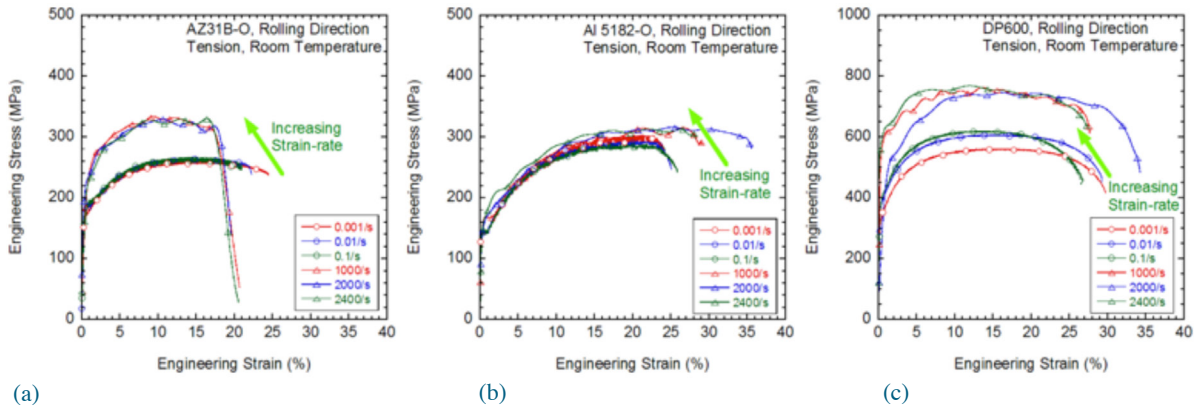


Figure 12. Tensile stress-strain curves for (a) AZ31B-O Mg, (b) 5182-O Al, and (c) DP600 steel at quasi-static and Hopkinson bar strain-rates (note different scaling on y-axis for DP600 steel)

The Johnson-Cook equation was used to describe the constitutive behavior of Mg, Al, and steel and is expressed in Equation 1

$$\sigma = (A + B\epsilon_p^n)(1 + C \ln \dot{\epsilon}_p)(1 - T^{*m}) \quad (1)$$

where σ is the flow stress, ϵ_p is the equivalent plastic strain, $\dot{\epsilon}_p = \dot{\epsilon}_p / \dot{\epsilon}_0$ is the dimensionless plastic strain-rate and $T^{*m} = (T - T_{room}) / (T_{melt} - T_{room})$ is the homologous temperature. T_{melt} is melting point, T_{room} is the room temperature and T is the temperature of a material element (all temperatures in Kelvin). The model parameters for AZ31B-O Mg, 5182-O Al, and DP600 steel are listed in Table 3.

Table 3. Johnson-Cook model parameters calibrated for AZ31B-O Mg, 5182-O Al and DP600

Material	A (MPa)	B (MPa)	C	n	m	T_{melt} (K)
AZ31B-O Mg	224	380	0.012	0.76	1.55	890
5182-O Al	106	569	0.001	0.4	3.2	900
DP600	590	980	0.01	0.25	3.0	1700

The Johnson-Cook equation (Equation 1) was successfully used to model the deformation behavior of sheet metals during EHF, as exemplified by the good correlation between the predicted and experimentally measured strain path in Al (Figure 11).

Conclusions

Relative to its room temperature formability at quasi-static strain-rates, the room temperature high-rate formability of 5182-O Al alloy increases by $\sim 2.5x$ and $\sim 6x$ during free-forming and inside a conical die, respectively, via EHF technique. Greater formability enhancement associated with forming inside a conical die suggests the importance of sheet-die interactions, in addition to the high strain-rates, in enhancing the formability of Al.

PNNL has developed a unique measurement capability that can quantify the deformation history (e.g., strain-rate, strain path, velocity, etc.) of sheet metals subjected to high-rate forming processes, such as EHF. This ability to quantify the deformation history will be crucial in clarifying the fundamental mechanism(s) that lead to enhanced formability and in designing commercial PPF processes.

Using tensile stress-strain data from room-temperature quasi-static and Hopkinson bar tests, the constitutive behavior of AZ31B-O Mg, 5182-O Al, and DP600 steel was described using the Johnson Cook equation. These data were successfully used to model the sheet deformation behavior during EHF and showed good agreement with experimental measurements.

Ultrafine Grain Foils and Sheet by Large Strain Extrusion Machining

Principal Investigator: Srinivasan Chandrasekar, School of Industrial Engineering, Purdue University
(765) 494-3623; e-mail: chandy@ecn.purdue.edu

Kevin Trumble, School of Materials Engineering, Purdue University
(765) 494-4114; e-mail: driscoll@ecn.purdue.edu

Mark T. Smith, PNNL
(509) 375-4478; e-mail: mark.smith@pnnl.gov

Accomplishments

- Mg AZ31B strip 2-mm thick by 25-mm wide was produced directly from wrought Mg feedstock using the LSEM process. Resulting properties met or exceeded wrought Mg sheet properties.
- Mg AZ31B strip 2-mm thick by 15-mm wide was produced directly from cast Mg feedstock using the LSEM process, with the resulting microstructure showing wrought-like grain structure and refinement.

Future Directions

- With remaining funding, the project will focus on refinement of the LSEM process parameters to produce submicron microstructures in thicker (1-2 mm) Mg strip. The submicron grain size would produce Mg strip having enhanced room temperature strength and forming properties.

Technology Assessment

- Target: Demonstrate the ability to make sheet-thickness Mg strip directly from wrought and cast Mg feedstock materials using the LSEM process.
- Gap: Current methods for producing Mg wrought sheet products require extensive thermomechanical processing steps, which result in high material cost. Alternate continuous casting technology has limited ability to process the range of Mg alloys and results in less than optimum sheet microstructures.

Introduction

PNNL and Purdue University are collaborating on a solution to overcome the cost barrier of implementing sheet Mg alloys in automotive applications. LSEM, under development by the Purdue University group, is a hybrid cutting-extrusion process in which sheet metals can be produced in a single-stage deformation process. The initial phase of the work has established the feasibility of producing nominal 2-mm thick sheet of Mg AZ31B using the LSEM process.

Approach

A rotary LSEM configuration, as implemented on a lathe, is shown schematically in Figure 13a. In the LSEM process, a constraining edge is used in addition to a cutting edge to impose large shear strains while controlling the product thickness. The chip thickness ratio, $\lambda = t_c/t$, and cutting tool rake angle (α) determine strain and strain path in the deformation zone. In Phase 1 of this project, LSEM trials were conducted under systematically varying conditions to establish the feasibility of producing 2-mm thick sheets from extruded Mg AZ31B billets. The main experiments were designed to establish the interactive effects of hydrostatic pressure and deformation zone temperature on the ability to suppress segmentation and produce continuous sheet. Figure 13b shows a key result based on the Phase 1 work—a 2-mm thick, continuous Mg AZ31B strip produced in LSEM by preheating the work piece (250°C) and controlling the hydrostatic pressure ($p/2k = 1.4$). The experiment shows LSEM can be tailored to produce large sections of sheet material, and at the limit of the current experimental tooling, can reach the nominal 2-mm thickness goal.

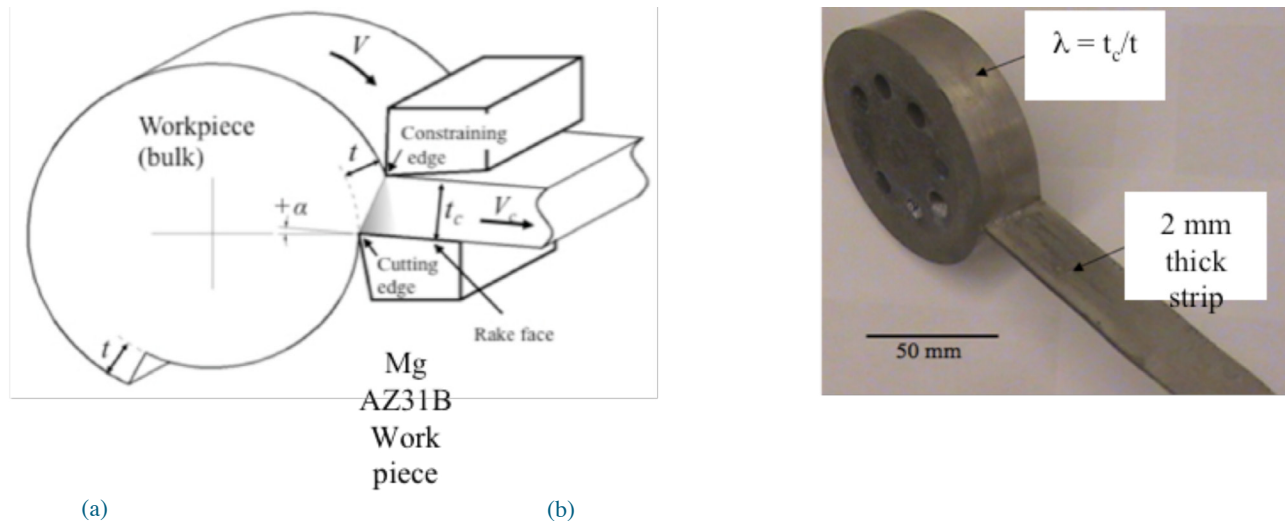


Figure 13. (a) LSEM in rotary configuration and λ is the chip thickness ratio; (b) the 2-mm thick, continuous MgAZ31B strip produced in LSEM

The LSEM process also results in grain refinement. Phase 2 work extended the range of deformation and temperature conditions to map the resulting grain size as a function of processing conditions. In addition, an initial study of crystallographic texture development in LSEM was also conducted. Pole figures were measured using an area detector X-ray diffractometer (GADDS, Bruker AXS) and a Rietveld refinement program called Materials Analysis Using Diffraction (MAUD). Preliminary results demonstrating continuous Mg AZ-31B strip production directly from as-cast ingot are also reported.

Technology Transfer Path

This task is primarily focused on demonstration of the LSEM process concept and scaling up of equipment to produce a suitable wide strip. If scale-up is successful, results will be presented to a number of materials and metals product suppliers in an attempt to transfer technology into the automotive materials supplier base.

Results and Discussion

The starting wrought MgAZ31B tooling plate stock (ThyssenKrupp, NA Inc.) exhibited a grain size of $16 \pm 2 \mu\text{m}$, as shown in Figure 14. The expected strong basal texture in the rolled plate is revealed by electron backscatter diffraction, as shown in Figure 14b.

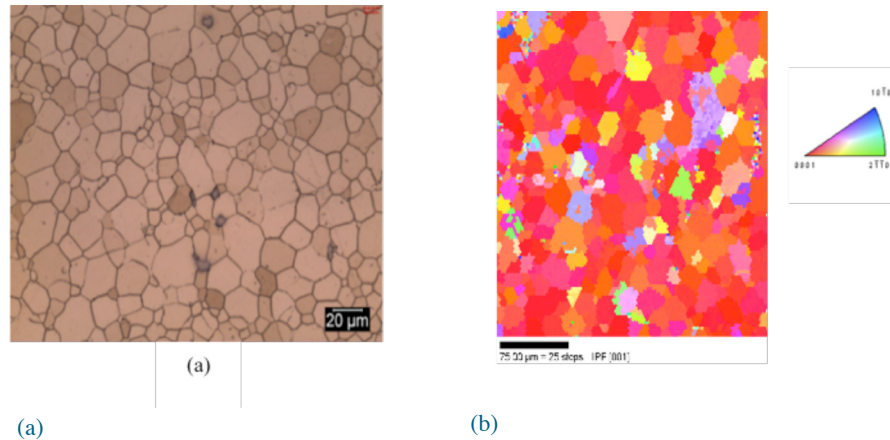


Figure 14. Wrought Mg AZ-31B tooling plate starting stock; (a) optical micrograph and (b) electron backscatter diffraction image showing strong basal texture

Grain refinement by LSEM was investigated for cutting ratios $\lambda = 0.5, 0.7$ and 1.0 and varying deformation temperature, controlled by preheating and/or cutting velocity. For temperatures above $\sim 220^\circ\text{C}$ and lower strains, a uniform recrystallized grain structure is achieved, with average grain size of $7 \mu\text{m}$ (Figure 15a). By decreasing the temperature and/or increasing strain, a grain size of $\sim 2 \mu\text{m}$ can be achieved, which is nearly a 10-fold reduction from the starting condition (Figure 15b).

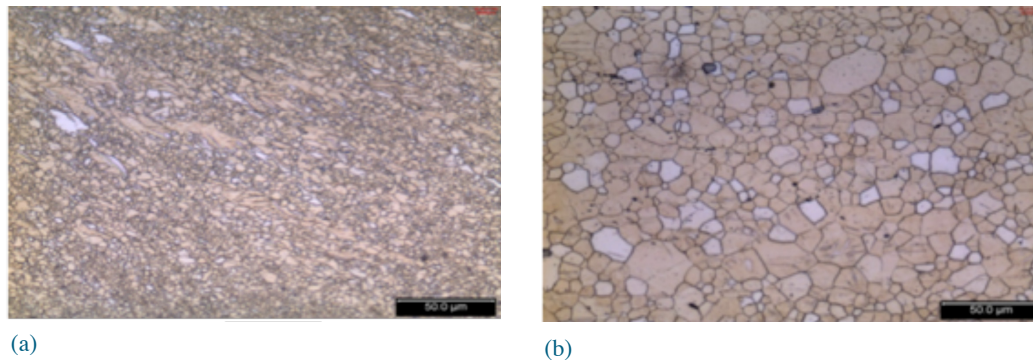


Figure 15. Optical micrographs showing grain refinement by LSEM; (a) higher temperature/lower strain (GS $\sim 7 \mu\text{m}$) and (b) lower temperature/higher strain (GS $\sim 2 \mu\text{m}$).

Grain size reduction to $\sim 2 \mu\text{m}$ is currently limited to strip thicknesses greater than $\sim 0.5 \text{ mm}$ due to experimental tooling constraints. At lower thicknesses, continuous strips can be produced at near ambient temperatures and higher strains. Figure 16 shows a thinner strip ($\sim 0.1 \text{ mm}$) produced under such conditions. The grain structure is not resolvable in the optical micrograph, indicating it is ultrafine. The hardness of this strip measured 110 kg/mm^2 , which is nearly twice that of the starting stock ($\sim 58 \text{ kg/mm}^2$). Recent transmission electron microscopy has confirmed the grain size is $\sim 200 \text{ nm}$. Further research is needed, but this result clearly shows LSEM is capable of producing true ultrafine grained MgAZ31B.

Pole figures for the starting bulk tooling plate and LSEM strip produced at near ambient temperature and $\lambda = 1.0$ are compared in Figure 17. The tooling plate exhibits the characteristic rolling texture of Mg alloys with the basal planes strongly oriented perpendicular to the broad faces of the plate. The LSEM strip, in contrast, exhibits a distinctive shear texture, with the basal poles tilted forward at an angle to the normal direction and cutting direction. Further experiments have shown that by controlling the deformation conditions in LSEM, it is possible to produce controlled mixtures of these textures.

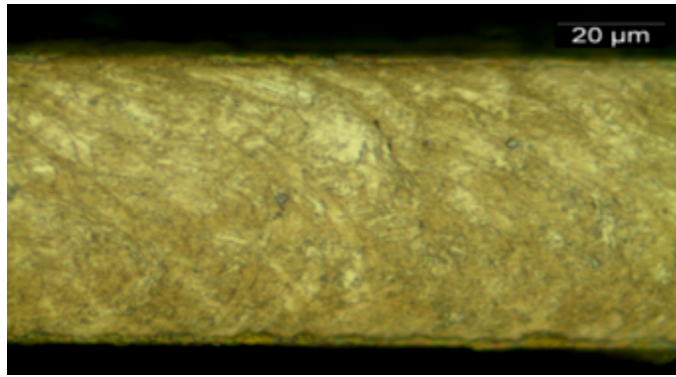


Figure 16. Optical micrograph showing unresolvable grain structure in LSEM strip produced at high strains

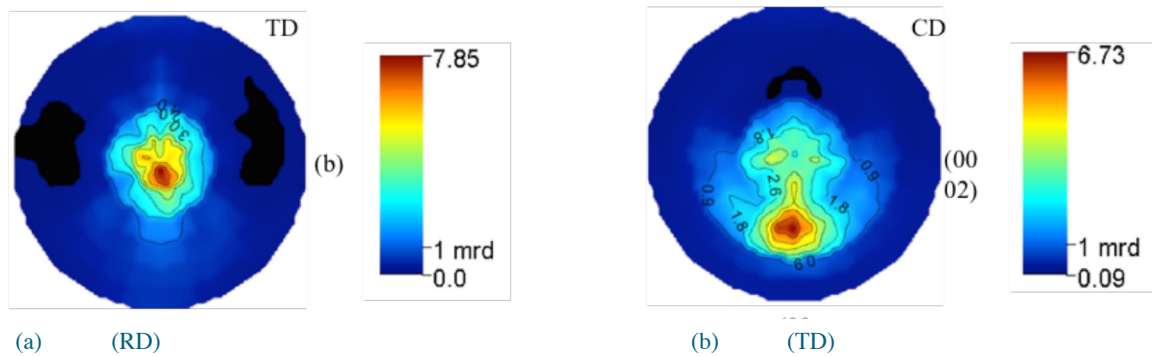


Figure 17. Pole figures (0002) showing (a) strong basal texture in MgAZ31B bulk tooling plate with basal poles normal to the rolling direction (RD), and (b) strong shear texture in LSEM strip with basal poles tilted in the cutting direction (CD)

Initial experiments have demonstrated that LSEM is capable of producing continuous strip directly for as cast MgAZ31B ingot, as shown in Figure 18. Microstructural characterization is continuing but early observations indicate that grain refinement similar to that observed in wrought stock is possible in the cast ingot, which may offer further scope for cost reduction in producing sheets using the LSEM process.



Figure 18. MgAZ31B strip produced directly from cast ingot by LSEM

Conclusions

Continuous sheets of MgAZ31B at thicknesses up to ~2 mm have been produced directly from wrought billet in the single-stage LSEM process. The process takes advantage of its ability to produce relatively high hydrostatic pressures and local deformation heating and is characterized by a critical temperature for continuous sheet formation that decreases with increased hydrostatic pressure and increases with increased sheet thickness. Through systematic experiments and modeling of the deformation field, the controlling ranges of these parameters have been elucidated. The process is capable of producing homogeneous microstructures showing grain refinement down to ~200 nm. Texture analysis shows that LSEM imparts distinctive shear textures, which may have important implications for sheet formability. Continuous MgAZ31B strips also can be produced directly from cast ingot, with grain refinement capabilities similar to those observed in LSEM of wrought stock.

Magnesium Research and Technology Development

Principal Investigator: Eric A. Nyberg, PNNL
(509) 375-2103; e-mail: Eric.Nyberg@pnl.gov

Accomplishments

- Organized the October 2010 Magnesium Front End Research and Development (MFERD) Annual Meeting in Ann Arbor, Michigan.
- Co-chaired the National Science Foundation (NSF)/DOE-sponsored workshop on Magnesium Science and Technology: Fundamental Research Issues.
- Updated the Magnesium Research & Development bibliographic database at <http://magnesium.pnnl.gov/>.
- Participated as Chairman of the poster and presentation sessions at the The Minerals, Metals, and Materials Society 2011 Annual Meeting & Exhibition, Magnesium Technology in San Diego, California, February 27–March 3, 2011.
- Presented “In-Plane Compressive Testing of Mg Alloy Sheet” as an invited keynote speaker at the 5th International Light Metals Technology Conference 2011 in Luneburg, Germany, July 19–22, 2011.
- Mentored a summer intern at PNNL who was funded as part of the Student Undergraduate Laboratory Internships (SULI) program. The intern, with assistance from a post-Master’s student, evaluated a method for compression testing Mg sheet and characterized die-cast alloys.
- Co-authored featured article in the TMS Journal of Metals entitled, “The TMS Magnesium Committee: Committed to the Advancement of Global Magnesium Technology.”
- Reviewed proposals and papers on various state-of-the-art Mg R&D.

Future Directions

- Continue to support DOE as the U.S. Project Technical Committee (PTC) Chairman by participating and reporting on relevant MFERD project activities in collaboration with China and Canada.
- Collect and assess state-of-the-art R&D on Mg alloys and various technologies that support the increased use of Mg in transportation applications (<http://magnesium.pnnl.gov/>).
- Participate in national and international technical conferences where the latest research is presented.

Introduction

A significant amount of R&D is being conducted around Mg alloys, Mg processing methods, and Mg applications. In addition to established die casting processing of Mg alloys, there has been considerable recent attention focused on wrought Mg processing and high-integrity casting technologies. Along with alloy and processing research, the international community is performing extensive property and applications development. Based on the evaluation of critical Mg research and technology developments, this project will result in recommended critical-path focus topics.

Approach

Maintain an active involvement on the national and international level as it relates to the broad study of Mg for transportation-related applications. This involves active participation as the Technical Chairman on the MFERD Program, continued involvement with the leading national research conferences (TMS Magnesium Technology), and, upon request, reviewing state of the art R&D proposals. Striving to build international collaboration with experts in the field of Mg is also an important approach to successfully maintaining an active role in state of the art research.

Results and Discussion

Organized the MFERD Annual Meeting

The project team organized the MFERD Annual meeting in October 2010, Ann Arbor, Michigan. This task involved reviewing, selecting, and contracting a meeting and hotel venue. The venue was at the Ross School of Business at the University of Michigan and was selected because it was within driving distance of the U.S. automaker team members to maximize meeting attendance. A registration website was created that allowed participants to conveniently register for the meeting online. Organizing the meeting also included editing and publishing the 529-page 2010 Annual Report. Included were the translated U.S. technical reports, along with similar input from the Canadian and Chinese PTC members.

There were 74 participants (16 from China, 18 from Canada, and 40 from the United States) (see [Figure 19](#)). There were 3 days of task level meetings where the task leaders summarized their recent work with each other and planned for their future work. The Project Steering Committee and PTC met to discuss management issues and progress. In addition, general sessions were held where the task leaders presented to the Project Steering Committee /PTC members current progress and plans. The 2010 Annual Report details the progress presented. The next MFERD Annual Meeting is scheduled for April or May 2012 in Xi'an, China.



Figure 19. MFERD 2010 Annual Meeting, University of Michigan

Co-organized the NSF/DOE Workshop on Magnesium Science and Technology: Fundamental Research Issues

This 2-day workshop was held May 19–20, 2011, in Arlington, Virginia, and brought together a diverse group of 52 scientists and engineers from academia, government laboratories, industry, and funding agencies to 1) identify the outstanding fundamental science issues that inhibit broader application of Mg alloys in structural (including biomedical) applications; and 2) to recommend research directions to address the outstanding issues.

Twelve invited speakers presented 11 lectures designed to set the tone for the smaller group discussions. Speakers represented a broad cross section of industry, academics, and national laboratories worldwide. They described recent advances and highlighted remaining gaps in understanding and opportunities for scientific impact, given new advanced experimental techniques and computational methods. The breakout discussion sessions addressed three strategic areas (Table 4):

Table 4. Discussions for NSF/DOE workshop on Magnesium Science and Technology: Fundamental Research Issues

<i>Alloy Design, Characterization, & Computational Tools</i>	<i>Processing & Manufacturing</i>	<i>Performance & Durability</i>
<i>CALPHAD, clustering</i>	<i>Primary, recycling, life cycle, etc.</i>	<i>Dynamic properties</i>
<i>Ab initio, MD, etc.</i>	<i>Casting, extrusion, rolling</i>	<i>Fatigue, fracture</i>
<i>ICME</i>	<i>Joining, welding, fastening</i>	<i>Multi-material solutions</i>
<i>Dislocations, twinning</i>	<i>Formability</i>	<i>Biomedical applications</i>
<i>High-resolution probes</i>	<i>Flammability</i>	<i>Coatings and corrosion</i>
<i>CALPHAD = Computer Coupling of Phase Diagrams and Thermochemistry; ICME = Institute for Computational & Mathematical Engineering</i>		

Some of the significant outcomes and topic areas of the workshop are listed below. Details of other topics were delivered in a report to NSF and the DOE-VTP authored by Dr. Agnew and reviewed by Mr. Nyberg and other members of the steering committee. Topics identified from the workshop included the following:

- Developing a better ability to predict macro/microstructure that results from the die casting processes would improve properties and foundry yields. This would enable the foundries to improve their margins or lower the price for the end user or consumer.
- Exploring low cost methods of primary conversion; e.g., strip casting of Mg alloy sheet is also fruitful, particularly if it can be partnered with low cost methods of sheet forming.
- Alloy development strategies targeting improved extrusion rates.
- Improved coatings, corrosion prevention, fatigue life, and understanding of fracture mechanism will all have a strong impact upon the long term cost of use.

Conclusions

This project is unique in that it does not have a finite end-point or conclusion. However, the international collaboration of the MFERD program will continue for 3 more years. Mr. Nyberg has been involved with the program since its planning stage. The benefit to DOE VTP in having an expert familiar with the latest activities in Mg R&D as it may be related to transportation should be recognized. This is further evidenced by the fact that Mr. Nyberg has been invited to participate in international program reviews, publication reviews, and workshops that help define the future direction and needs for research and technology development of Mg. Mr. Nyberg will continue to strive to provide the DOE VTP with key information that will be helpful in determining where and if funding is required to meet the challenge of reducing greenhouse gas emissions through light-weighting techniques realized when Mg is used in automotive and other transportation applications.

Conclusions

The Processing & Manufacturability project is focused on research and development (R&D) activities advancing the basic mechanical properties, manufacturability, and cost of lightweight materials towards the levels needed for increased implementation in automotive applications. This project includes 6 different tasks and Principal Investigator that each address an aspect of this materials challenge and seek to fill technical gaps that limit implementation of lightweight materials solutions in current or planned automotive applications. The following highlights summarize the accomplishments of the tasks in this project.

The *First Generation Advanced High-Strength Steels Deformation Fundamentals* task is developing the fundamental understandings on key mechanical properties and microstructural features influencing the local formability of AHSS.

- Performed various analyses and experiments (i.e., chemical composition analysis, static tensile test, channel forming test, hole expansion test) on eight DP980 steels from different suppliers.
- Performed image analyses on the SEM pictures to quantify the microstructural features of the steels. Examined the obtained quantities of the microstructural features with respect to the macroscopic deformation features.

The *Aerodynamic Lightweight Cab Structures* task is developing and will demonstrate an elevated temperature hot forming process, combined with cold finish forming that can increase the useable elongation and formability to over 40% for a 6000-series Al sheet alloy.

- Completed simulated Al sheet forming sequences using tensile specimen-based tests. Simulated forming included maximum hot tensile ductility, hot forming followed by cold forming steps, and cold forming combined with hot forming steps. Results for the simulated hot tensile forming/cold forming sequence indicated that significant increases in overall material elongation are possible.

The *Non-Rare Earth High-Performance Wrought Magnesium Alloys* task aims to develop high-energy absorption Mg alloys that do not contain RE elements that can replace Al extrusions at a mass savings of 25% (based on density).

- Rapidly solidified materials from three Mg alloys were prepared and characterized to understand basic features of the microstructure of a known high-performance Mg alloy.
- Characterization of the high-performance Mg alloy indicates the RE element addition is acting as a nucleation site, producing fine-grain size and a finely distributed MgZn precipitate. The combination of fine-grain size and precipitate size are likely combining to produce the exceptional strengths and anisotropy observed in the RE containing alloys.

The *Pulse Pressure Forming of Lightweight Materials* task uses high-rate forming to demonstrate enhanced room-temperature formability in sheet metals beyond what is achievable by room-temperature quasi-static forming. Concurrently, quantify the deformation history beyond what is obtainable by conventional post-deformation strain measurements.

- High-strain rate forming, using a Pulse Pressure Forming (PPF) technique, was demonstrated to enhance the room-temperature formability of 5182-O Al to levels that are typically expected during warm forming. The quantification of deformation history associated with this formability enhancement was made possible by a novel measurement technique developed at PNNL.
- Tensile stress-strain responses of AZ31B-O Mg, 5182-O Al, and DP600 steel sheets were determined at quasi-static and Hopkinson bar strain rates. The Johnson-Cook equation was used to describe the constitutive behavior of the test materials and to model sheet deformation behavior during PPF.

The *Ultrafine Grain Foils and Sheet by Large Strain Extrusion Machining* task's goal is to demonstrate the ability to make sheet-thickness Mg strip directly from wrought and cast Mg feedstock materials using the LSEM process. Current methods for producing Mg wrought sheet products require extensive thermomechanical processing steps, which result in high material cost.

- Mg AZ31B strip 2-mm thick by 25-mm wide was produced directly from wrought Mg feedstock using the LSEM process. Resulting properties met or exceeded wrought Mg sheet properties.

- Mg AZ31B strip 2-mm thick by 15-mm wide was produced directly from cast Mg feedstock using the LSEM process, with the resulting microstructure showing wrought-like grain structure and refinement.

The *Magnesium Research & Technology Development* task provides technical and administrative leadership on the topic of Mg materials research, specifically as the Technical Committee Chair-person for the US-Canada-China collaborative MFERD project.

- Organized the October 2010 MFERD Annual Meeting in Ann Arbor, Michigan and produced the 2010 Annual Report.
- Co-chaired the NSF/DOE-sponsored workshop on Magnesium Science and Technology: Fundamental Research Issues.

Presentations/Publications/Patents

Agnew, S.; Nyberg E.A.; Pollock, T.; Wagoner, R.; Powell, B.; Decker, R.; Shih, D. Final Report: Mg Science & Technology Workshop - Fundamental Research Issues. National Science Foundation and U.S. Department of Energy-Vehicle Technologies, Washington, D.C., 2011.

Choi, K.S.; Soulami, A.; Liu, W.N.; Sun, X.; Khaleel, M.A. Influence of Various Material Design Parameters on Deformation Behaviors of TRIP steels. *Computational Materials Science* 2010, 50, pp 720-730.

Choi, K.S.; Soulami, A.; Liu, W.N.; Sun, X.; Khaleel, M.A. Loading Path Dependence of Forming Limit Diagram of a TRIP800 Steel. *SAE International Journal of Materials and Manufacturing* 2011, 4, pp 75-83.

Choi, K.S.; Soulami, A.; Liu, W.N.; Sun, X.; Khaleel, M.A. Effects of Retained Austenite Stability and Volume Fraction on Deformation Behaviors of TRIP Steels. In *Proceedings of Materials Science and Technology 2010 Conference and Exhibition*; American Ceramic Society: Washington, D.C., 2010.

Davies, R.W. and Rohatgi, A. Pulse-Pressure Forming (PPF) of Lightweight Materials. Presented at the 2011 DOE Vehicle Technologies Program Review, May 10-13, 2011, Arlington, Virginia.

Davies, R.W.; Rohatgi, A.; Stephens, E.V.; Soulami, A.; Smith, M.T.; VanArsdale, G. Pulse Pressure Forming of Aluminum Alloys to Achieve Enhanced Formability at High Strain Rates. Presented at the International Symposium on Plasticity and its Current Applications, January 3-8, 2011, Puerto Vallarta, Mexico.

Maupin, H.; Nyberg E.A.; Mathaudhu, S. Magnesium Alloys in Army Applications: Past, Current and Future Solution. Presented at Federal Aviation Administration's Sixth Triennial International Fire & Cabin Safety Research Conference, October 25-28, 2010, Atlantic City, New Jersey.

Nyberg E.A.; Lavender, C.A.; Stephens, E.V.; Klingensmith, R.D.; Joshi, V.V. Edge-Wise Determination of Compression Strength in Magnesium Alloy Sheet. Poster presented at TMS Annual Meeting, February 27, 2011, San Diego, California. PNNL-SA-77934.

Nyberg E.A.; Joshi, V.V.; Edwards, D.J.; Soulami, A.; Chua, A.Z. In-Plane Compressive Testing of Magnesium Alloy Sheet. Presented at Light Metals Technology Conference, July 19, 2011, Luneburg, Germany. PNNL-SA-81322.

Rohatgi, A.; Stephens, E.V.; Soulami, A.; Davies, R.W.; Smith, M.T. Experimental Characterization of Sheet Metal Deformation During Electro-Hydraulic Forming. *J. Mater. Process. Technol.* 2011, 211, pp 1824-1833.

Rohatgi, A.; Stephens, E.V.; Davies, R.W.; Smith, M.T.; Soulami, A.; Ahzi, S. Electro-Hydraulic Forming of Sheet Metals: Free-forming vs. Conical-die Forming. In review. *J. Mater. Process. Technol.*

Sillekens W.H.; Nyberg E.A. The TMS Magnesium Committee: Committed to the Advancement of Global Magnesium Technology. *JOM*, 2011, 63, pp 9.

Soulami, A.; Choi, K.S.; Shen, Y.; Liu, W.N.; Sun, X.; Khaleel, M.A. On Deformation Twinning in a 17.5%Mn-TWIP Steel: A Physically-Based Phenomenological Model. *Materials Science and Engineering A*, 2011, 528, pp 1402-1408.

Sun, X.; Shen, Y.; Zbib, H.; Askari, H.; Choi, K.S.; Soulami, A.; Wang, C.M.; Khaleel, M.A. Origin of High Strength in Advanced High Strength Steels (AHSS). Presented in The 17th International Symposium on Plasticity & Its Current Applications, International Journal of Plasticity, 2011.

Sun, X.; Soulami, A.; Choi, K.S.; Chen, W. Effects of Loading Rate and Sample Geometry on Tensile Ductility of TRIP800 Steel. Materials Science and Engineering A, 2011, submitted for publication.

References

Balanethiram, V.S.; Daehn, G.S. Enhanced Formability of Interstitial Free Iron at High-Strain Rates. Scripta Metall. Mater. 1992, 27, pp 1783–1788.

Imbert, J.; Worswick, M.; Winkler, S.; Golovashchenko, S.; Dmitriev, V. Analysis of the Increased Formability of Aluminum Alloy Sheet Formed Using Electromagnetic Forming. SAE World Congress 2005, Paper 2005-01-0082, SAE International, Detroit, Michigan.

Li, D.; Ghosh, A.K. Biaxial Warm Forming Behavior of Aluminum Sheet Alloys. J. Mater. Process. Technol. 2004, 145, pp 281-293.

Rohatgi, A.; Stephens, E.V.; Soulami, A.; Davies, R.W.; Smith, M.T. Experimental Characterization of Sheet Metal Deformation During Electro-Hydraulic Forming. J. Mater. Process. Technol. 2011, 211, pp 1824-1833.

C. Production of Primary Magnesium - Solid Oxide Membrane Electrolysis of Magnesium: Scale-Up Research and Engineering for Light-Weight Vehicles - Metal Oxygen Separation Technologies, Inc.

Principal Investigator: Adam Powell, IV
Metal Oxygen Separation Technologies, Inc.
11 Michigan Drive; Natick, MA 01760-1334
e-mail: apowell@moxst.com

Technology Area Development Manager: William Joost
U.S. Department of Energy
1000 Independence Ave., S.W.; Washington, DC 20585
(202) 287-6020; e-mail: william.joost@ee.doe.gov

Contractor: Metal Oxygen Separation Technologies, Inc. (MOxST)
Contract No.:

Executive Summary

MOxST presents this project report on scale-up research and engineering of Solid Oxide Membrane (SOM) Electrolysis for magnesium (Mg) production. MOxST is pleased to report completion of all tasks.

Activity and Developments

Production of Primary Magnesium - Solid Oxide Membrane Electrolysis of Magnesium: Scale-Up Research and Engineering for Light-Weight Vehicles

Principal Investigator: Adam Powell, IV
e-mail: apowell@moxst.com

Accomplishments

- MOxST completed electrolysis experiments of 50 and 100 hour duration, and a static zirconia exposure test lasting 500 hours, with several tests incorporating MgO impurities, building our understanding of the long-term robustness of the yttria-stabilized zirconia (YSZ) tubes.
- A new heat transfer model has facilitated liquid condenser design and shown that a thick anode actually helps the process; that model and a model of flow and heat and mass transport in the molten salt electrolyte are helping MOxST to design the first self-heated SOM Electrolysis cell.
- Deep-immersion three-tube experiments ran at up to 205 A total current, with 100 A in one of the tubes. Both results are several times higher current than any previous work on this process.

- MOxST's liquid Mg condenser should release enough heat to calcine low-cost $\text{Mg}(\text{OH})_2$ for a large fraction of its feedstock.
- A new quantitative impurities mass balance analysis gives the cathode by-product mass and composition and molten salt drain rate as functions of raw material composition.

Future Direction

The next steps in the development of this process will be to scale its production as informed by this project's results. Such scale-up activities may consist of:

- Designing and building larger-scale electrolysis cells;
- Expanding on the development of zirconia as a solid electrolyte for metal production began during this project;
- Further developing mathematical models as tools for design of larger electrolysis cells;
- Tests of magnesium (Mg) product for composition, mechanical properties, and other fitness requirements for automotive use;
- Site selection studies for a future Mg production plant using this technology.

Technology Assessment

- Target: Mg is a promising material for motor vehicle weight reduction, with numerous benefits for vehicle application as outlined below. SOM Electrolysis is a promising new process for primary production of Mg (making the metal from naturally-occurring raw material such as its oxide or chloride).
- Gap: Current technologies for primary Mg production do not exhibit satisfactory price, price stability, or environmental impacts for very large scale adoption industry-wide to take advantage of its properties. The SOM Electrolysis process for primary Mg production has been under development in laboratories since 1996, but production has yet to proceed beyond laboratory scale, so it has yet to live up to its promise. This project's goal was to perform sufficient research to enable rapid scale-up of the process.

Introduction

Mg is the least dense engineering metal, with the highest stiffness-to-weight ratio. It is also potentially the most easily recycled of the proposed light weight vehicle materials, which include polymers and composites. Further Mg benefits include lower manufacturing cost and reduced noise, vibration, and harshness. For these reasons, U.S. auto makers would like to replace 640 lbs. of steel and aluminum (Al) alloy parts per vehicle with 350 lbs. of Mg equivalents by the year 2020, improving fleet fuel economy by about 1.5 mpg and reducing petroleum demand by over \$20 billion per year, as described in the USAMP report Magnesium Vision 2020 (USAMP 2006). This is of near-term importance to the auto industry because of new mandates for fuel efficiency and greenhouse emissions.

Unfortunately, between 2005 when that report was written and 2008, China used its market dominance in primary Mg production to turn export subsidies into export taxes, more than doubling the price, and dampening auto makers' enthusiasm for the metal. Furthermore, with very little environmental regulation, Chinese Mg producers emit large quantities of soot, greenhouse gases, and other pollutants. Primary production is lightly mentioned in Magnesium Vision 2020, but it has become a very significant barrier to widespread structural automotive use of Mg.

An environmentally clean and low-cost domestic source of Mg will not only directly create jobs in primary Mg production, but also build a Mg economy of die-casting companies and automotive parts suppliers. China has several research centers

focused on Mg technology, including one with 324 employees on a 700-acre campus (Peng 2009), and is rapidly moving up the value chain to advanced alloys, casting technologies, and deformation processes. Without U.S. domestic primary production, China will almost certainly become the undisputed world leader in all aspects of Mg technology, leaving many U.S. industries at a strategic disadvantage.

SOM Electrolysis

Fortunately, a new, low-cost, zero-emission process is ready for scale-up from laboratory to pilot- and full-scale production over the coming years. SOM Electrolysis, shown schematically in Figure 1 with the research cell in Figure 2, was originally developed by Uday Pal at Boston University (BU) with Department of Energy (DOE) funding (Contract No. C407200-AN8). It was continued under DOE's hydrogen program for primary Mg production for hydrogen storage (Award No. DE-FC36-04GO14011). Mg is clearly a strategic metal for energy efficiency and renewable energy.

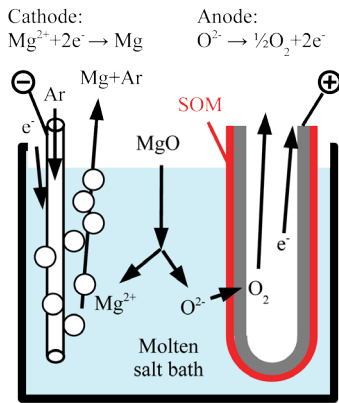


Figure 1. SOM Mg process schematic.

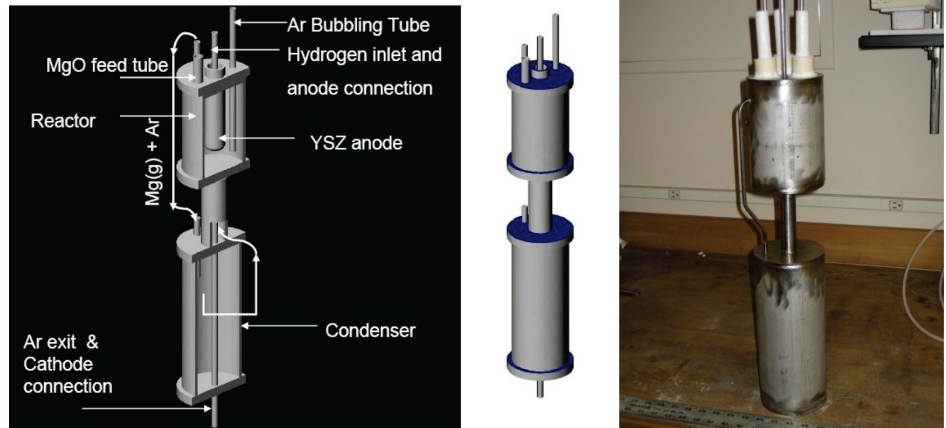


Figure 2. Experimental SOM Mg Diagrams and Photograph

The SOM process continuously feeds Mg oxide into a molten salt bath, where electricity splits it into Mg metal vapor and oxygen gas. Because of its simplicity and efficiency, the SOM process is the lowest-cost method proposed for producing Mg, as shown in Figure 3, with cost estimated at 62¢/lb (Das 2008). The SOM process also emits minimal waste and can operate in modular electrolysis cells, enabling small production facilities at very low capital cost to minimize startup risks.

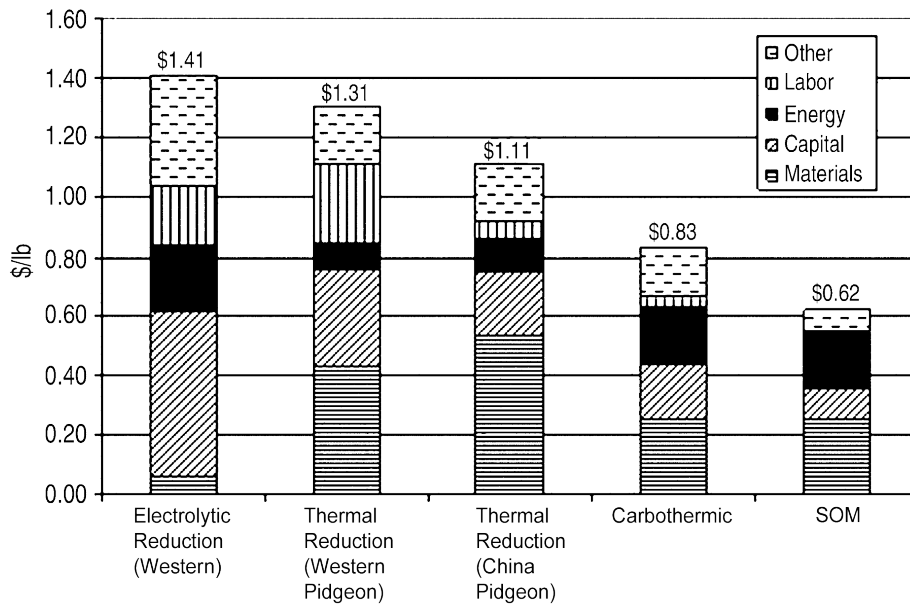


Figure 3. Cost per pound of Mg extraction using three existing and two new processes, from Sujit Das 2008.

The SOM conducts oxygen ions and blocks other elements, such as chlorine or fluorine, so the oxygen by-product is very pure. It is the only commercially viable anode for oxygen production in metal extraction: precious metal anodes in some experimental processes are not commercially viable and the graphite anode for Hall-Héroult Cell Al production reacts with oxygen and emits CO₂. Experimental nickel ferrite inert anodes for Al extraction produce contaminated oxygen, whereas the SOM Electrolysis oxygen byproduct is very pure.

The Mg metal vapor generated at the cathode exits the cell and goes to a condenser, which produces liquid Mg. Argon gas mixed with the Mg vapor prevents it from reducing the SOM and can be recycled back into the process. More electronegative impurity metals, e.g. Al, iron, nickel, etc., either stick to the cathode tube or collect in the bottom of the reactor and less electronegative elements such as calcium remain in ionic form in the molten salt bath. As a result, the Mg product is very pure, even when using inexpensive 98% pure Mg oxide. This sets this process apart from the Hall-Héroult Cell, which must begin with high-purity alumina from the Bayer process and results in much lower energy use, process wastes, and greenhouse emissions than for Al. That said, the presence of impurities in the raw material requires their removal from the reactor, which this proposal will address below.

Based on the experience of MOxST CTO Adam Powell with SOM Electrolysis over eight years, the MOxST NSF SBIR, MOxST's exclusive worldwide license option on the foundation SOM Electrolysis patents, and a growing portfolio of new patent applications, MOxST is uniquely able to conduct a scale-up project for SOM Electrolysis of Mg.

Process Cost, Energy Use, and Environmental Impact

SOM Electrolysis runs at 5 - 6.5V, and its energy consumption is given by:

$$5V = 5 \frac{J}{Coul} \times \frac{96540 \frac{J}{Coul} \times 2 \frac{mol e^-}{mol Mg} \times 454 \frac{g}{lb}}{3.6 \times 10^6 \frac{J}{kWh} \times 24.3 \frac{g}{mol Mg}} = 5.01 \frac{kWh}{lb Mg}$$

Therefore, each volt corresponds to 1 kWh/lb of electrical energy, divided by the current efficiency, which has been above 90%. Based on 5 kWh/lb of Mg product, an energy cost of 4¢/kWh arrives at 20¢/lb. Mg oxide costs about \$3000/T, or 15¢/lb, which is about 25¢ per pound of Mg product. If half of that price pays for energy, that translates to another 2.5 kWh/lb of Mg product, for a total of 7-8 kWh/lb. In contrast, the combined Bayer and Hall-Héroult processes consume about 18 kWh/lb. Using this process means that substituting Mg for Al can thus reduce the energy consumption and greenhouse emissions for primary processing by a factor of 2 or more on a per-pound basis. And Mg parts are 10-40% lighter than their Al counterparts, depending on whether strength or stiffness is the primary design consideration.

Labor costs are minimal because the process operates continuously and unattended for weeks or months at a time. There is no chlorine anywhere in the process, nor any water usage, and with renewable electricity, the entire process is carbon-free.

Approach

MOxST evaluated two types of zirconia SOM tubes for the electrolysis process: yttria-stabilized zirconia (YSZ) and magnesia-stabilized zirconia (MSZ). We characterized SOM durability utilizing two techniques. The first consisted of electrochemical measurements during electrolysis experiments such as potentiodynamic scans, impedance spectroscopy scan, and potentiostatic holds (monitoring the current during electrolysis). The second method was examining the polished cross section of the SOM after each experiment. This section also presents work on metallic Mg solubility in the molten salt.

Results and Discussion

Electrolysis Experiments

MOxST conducted 15 electrolysis experiments for the purpose of understanding SOM-flux interactions. Each one exposed the SOM to the Mg-electrolysis environment with varying salt composition. After the electrolysis experiment, we sectioned and polished the SOM tube and analyzed it using scanning electron microscopy.

The last three experiments were long-duration electrolysis runs, of at least 34 hours duration each. The major goals were to perform unattended SOM electrolysis and evaluate the durability of SOM after exposing it to molten salt under Mg-electrolysis. The last and longest of these started April 5, 2011 and ran for more than 80 hours. Figure 4 shows the current during that experiment's longest electrolysis run and the resulting Mg deposit.

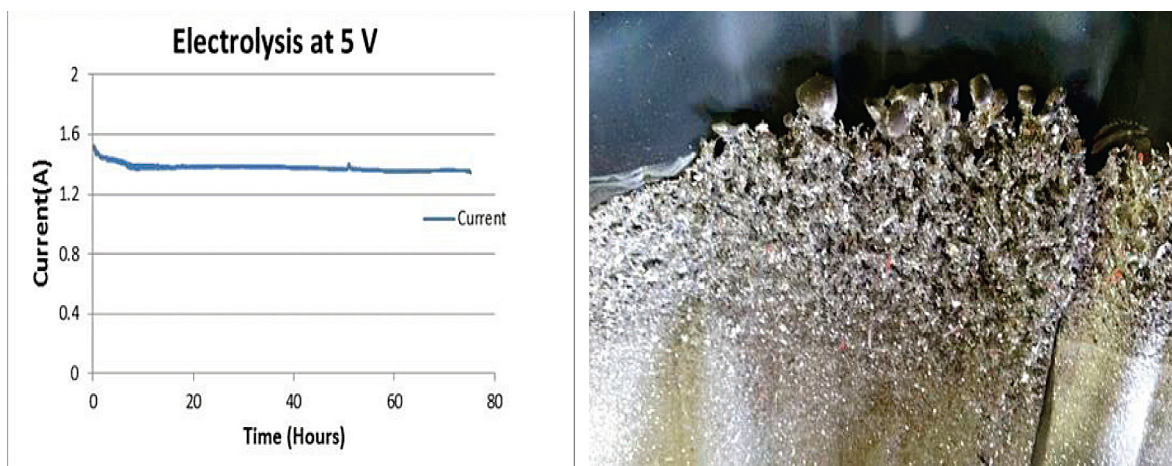


Figure 4. Current-time scan (left) during the longest electrolysis run of the April 5 experiment. Metal deposit on stainless shim from that experiment (right).

This experiment's current was low in comparison to previous experiments due to the use of a high-resistance current collector comprised of a 3 cm lanthanum strontium manganite (LSM) rod connected to a thin nickel wire. Though its resistance is high, this type of current collector has had the best long-duration performance. This experiment deposited approximately 12 g of Mg at a current efficiency of 40%.

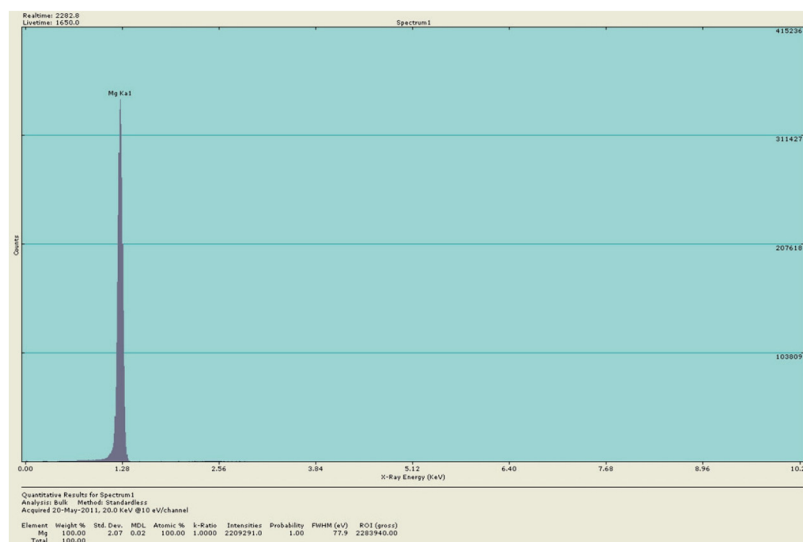


Figure 5 shows the energy dispersive X-ray (EDAX) spectrum of the Mg deposit from this experiment. EDAX can detect elements at 0.1% concentration, so the spectrum and analysis indicate that this magnesium is at least 99.9% pure.

Static Flux Exposure Experiments

To further analyze the SOM degradation mechanism of SOM, MOxST performed static exposure experiments, which exposed the SOM to molten salt at standard operating temperature with no current. A comparison of the yttrium composition at SOM/molten salt interface shows that the composition profile changes in zirconia in static contact with molten flux are nearly identical to those following an electrolysis experiment. This indicated that the primary mechanism of degradation is not related to the passage of ionic current through zirconia.

Based on these results, MOxST concluded that membrane degradation is primarily due to dissolution of YSZ in the flux and the passage of electronic current through the SOM. Therefore, inexpensive static exposure experiments can provide the information necessary to assess corrosion behavior of YSZ. Toward that end, the next section gives the details of those static experiments.

MOxST and Boston University performed static experiments varying the immersion duration of SOM and using a flux additive to reduce yttria leaching. **Figure 6** compares as-received SOM from the vendor with the SOM after exposure to flux for different durations. The membranes exposed to flux for 100 hours and 500 hours show some degradation, but SOM exposed for 32 hrs shows little to no degradation under static or electrolysis conditions.

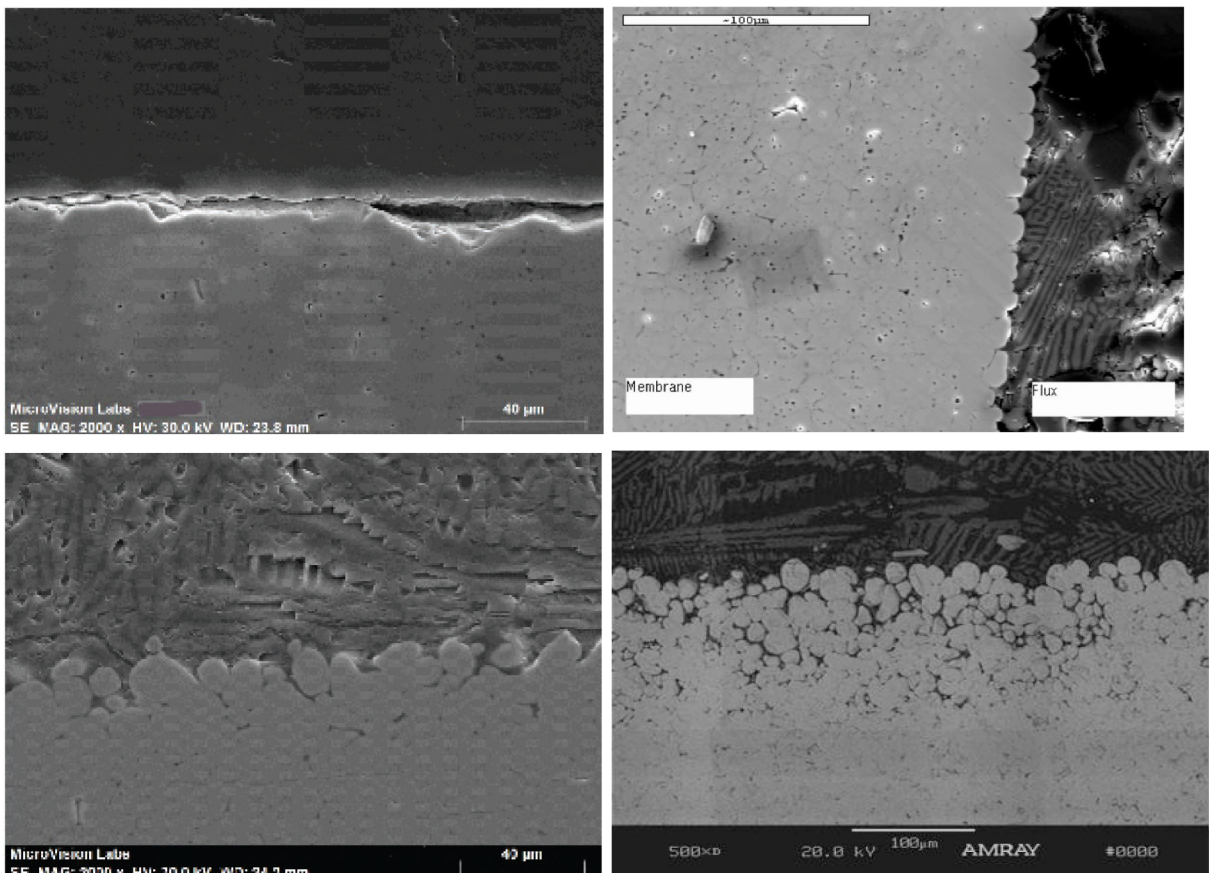


Figure 6. SEM micrograph of the SOM-flux interface: as-received (top-left), 32-hour exposure (top-right), 100 hour exposure (bottom-left), 500-hour exposure (bottom-right).

To date, MOxST has used off-the-shelf tubes for both static and SOM electrolysis experiments. MOxST believes it is possible to engineer the zirconia composition and processing method to improve its life time for this application. To test this, we performed static experiments on a zirconia compact made in house at MOxST. **Figure 7** compares micrographs of the vendor-SOM and MOxST-SOM exposed to molten salt for 100 hrs. The vendor-SOM sample shows internal cracking, while the MOxST-SOM is in considerably better condition with no internal cracks.

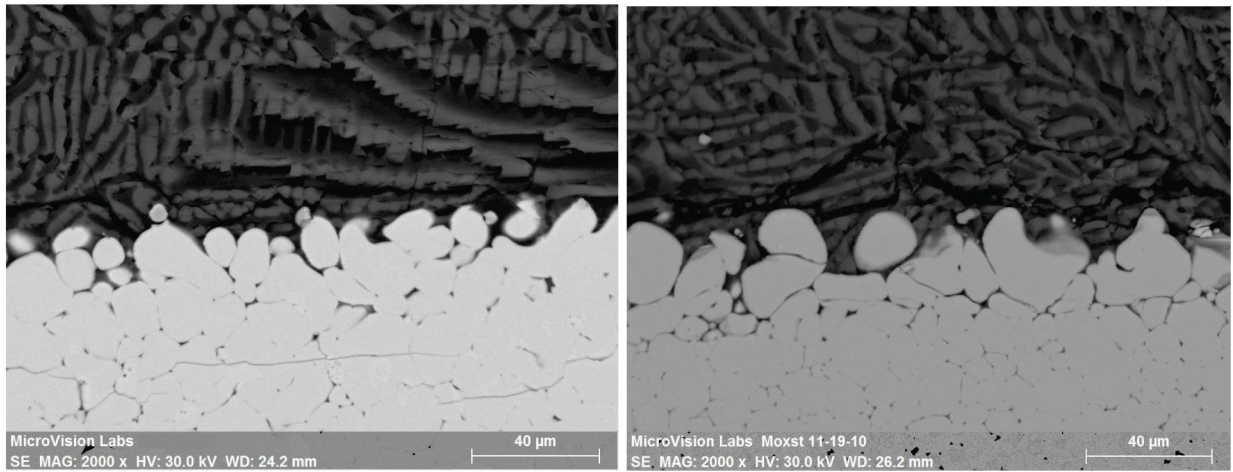


Figure 7. Vendor SOM (left) and MOxST-SOM (right) samples after 100 hours in molten salt.

SOM Robustness with Impurities in Flux

This section presents our work to understand the effect of impurities on the zirconia SOM. The key impurities for this section are:

- CaO because it is the most prevalent impurity;
- SiO₂ as the second-most prevalent impurity;
- Na₂O as the second-most prevalent impurity with lower electronegativity than MgO.

The static experiments showed that neither 5.0 wt% CaO nor 2.0 wt% Na₂O has a negative impact on membrane stability. However, with 2.0 wt% SiO₂ in the flux, the membrane developed porosity. That said, the much higher electronegativity of silicon than Mg (the dissociation potentials of SiO₂ and MgO are around 1.7 V and 2.4 V respectively at 1150° C) will cause it to deposit rapidly on the stainless steel cathode. The amount of SiO₂ in the molten salt should thus be insignificant, and it should not affect SOM durability.

Mathematical modeling and design of electrolysis cells

The goals of mathematical modeling in this project are to understand the working of the process, to assess performance and feasibility, and to develop tools for design of experimental and industrial SOM Electrolysis equipment. As such, design activity goes hand-in-hand with modeling and we present them together in this section.

This project's modeling and design activity consists of three components:

- Thermal analysis and energy budgeting for a self-heating cell;
- Mathematical modeling of transport and electrochemistry in the molten salt;
- Preliminary design and physical and cost modeling of an industrial-scale electrolysis cell.

Thermal analysis and energy budgeting

To determine the required voltage and thus the energy cost for a self-heated cell whose electrical resistance provides enough heat to sustain the crucible temperature at the desired reaction rate, we begin with the Nernst equation, which relates the reaction free energy ΔG to the minimum required voltage V :

$$\Delta G = -nFV. \quad (1)$$

Voltage and free energy are equivalent but use different units: free energy is the energy per mole of reaction extent and voltage is the energy per coulomb of charge passed.

At the 1150°C process temperature, the free energy for the reaction $\text{MgO} \rightarrow \text{Mg} + \frac{1}{2}\text{O}_2$ is 4.99 kWh/kg, corresponding to 2.27 V. If the applied voltage is higher than this, then the excess voltage provides the resistive and other overpotentials in the cell, such as the charge transfer overpotential. For high-temperature processes, the charge transfer overpotential is very small. These sum to the total voltage applied to the cell.

In addition to this energy budget, a second energy budget consists of all of the heating power provided to the cell. The enthalpy of Mg reduction to its vapor ΔH is 8.41 kWh/kg, corresponding to 3.81 V, and consumes most of the heat. If one supplies sufficient free energy but not sufficient enthalpy, then the reaction proceeds but cools the cell and shuts it down. Resistance in the cell or an external heater provides this heat and excess heat beyond the enthalpy leaves the cell through the cell leads and furnace walls.

For a self-heated cell (heated entirely by internal resistance), the total of the two electrical and thermal energies is the same. Figure 8 shows that total and the approximate composition of each energy budget.

The electrical energy budget consists of the following components:

- Cathode & anode resistances are based on minimum possible energy loss through leads.¹
- The value of 1.5 V for the zirconia SOM tube is based on 1 A/cm² current density through a 3 mm thick YSZ tube with conductivity 0.2 S/cm.
- The molten salt has 20 times the conductivity of YSZ, but the anode-cathode distance is roughly 20 times the SOM thickness (6 cm), effective area is roughly twice that of the SOM, making for half the resistance and voltage.
- The oxygen ion mass transfer number is based on its concentration (roughly 1/10 of the anions) and boundary layer thickness (roughly 1/12 of the anode-cathode distance), making it about 70-80% of the molten salt resistance.
- The Mg oxide dissociation potential is $\Delta G/nF$ as mentioned above.

The thermal energy budget consists of the following:

- Losses through cell leads mentioned above.
- Furnace vessel walls, which we estimate will lose about as much heat as the total through the electrical leads.
- Enthalpy of Mg oxide dissociation ΔH as mentioned above.

This thermal budget results in overall energy efficiency ($\Delta H/\text{input energy}$) between 63% and 76%, and even with no heat recovery in the condenser, liquid Mg energy efficiency between 52% and 63%. Because it indicates that sustaining the reaction and driving heat through the leads require a lot of energy, this reduces the motivation for using a thin YSZ solid electrolyte which would reduce the heat produced in the cell. This and other considerations such as mechanical and chemical stability lead us to conclude that a 2-3 mm YSZ tube may be better than one with a significantly thinner zirconia layer.

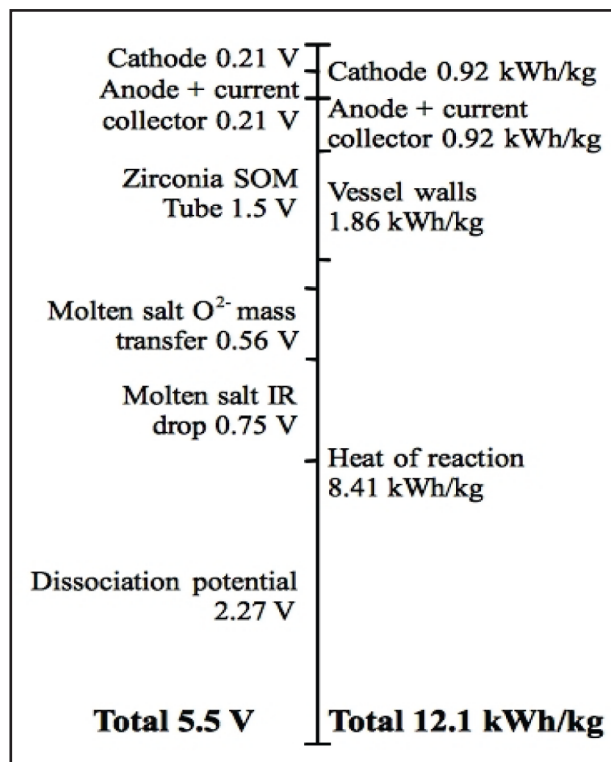


Figure 8. Electrical and thermal energy budgets for SOM Electrolysis of Mg.

¹ The wiedmann-Franz law indicates that good electrical conductors are also good thermal conductors, so low-resistance leads lose a lot of heat and vice versa. As a result, there is an unavoidable minimum heat loss through the leads. At the Mg electrolysis temperature, this minimum corresponds to at most 0.21 V in resistance losses, plus an additional 0.21 V (0.46 kWh/kg) of heat conducted from the crucible into and through each lead.

Mathematical Modeling of Transport in the Crucible

The most physically complex aspect of the SOM electrolysis process is transport in the crucible. The goal of this finite element (FE) model is to understand the physics of the scaled up electrolysis cell, particularly the thermal stresses and molten salt mixing. Toward those ends, MOxST developed a validated model of the molten salt component of the process which includes fully-coupled fluid flow driven by argon bubbling and natural convection, heat transfer with Joule heating, and static current conduction to assess process resistance energy losses, thermal stresses, and raw material mixing.

Model Geometries and Results

- MOxST extended the prior axisymmetric model by preparing 3-D solid geometries and meshes for the flux usable for anticipated model runs, including:
- One-tube shallow-immersion experiments using half of the geometry to take advantage of crucible symmetry;
- Three-tube deep-immersion experiments using a 1/6 wedge of the geometry;
- “Unit cells” which repeat to form scaled-up industrial systems with 30 or more tubes;
- A 1/6 wedge approach to the large hexagonal arrays of SOM tubes, generated by the FreeCAD cell design script described in the next section.

MOxST wrote a new Nernst-Planck electromigration term for the Elmer Finite Element Analysis (FEA) suite. We tested its electromigration simulation capability by running a one-tube simulation without electromigration as a driving force for oxygen flux and one with it. **Figure 9** shows the integrated oxygen flux over the SOM tube outer area with and without electromigration. Oxygen flux at the anode is higher with than without electromigration for two reasons: the electric field drives stronger flux and the thinner boundary layer leads to a stronger concentration gradient in the chemical diffusion term. This second effect is more pronounced at longer times.

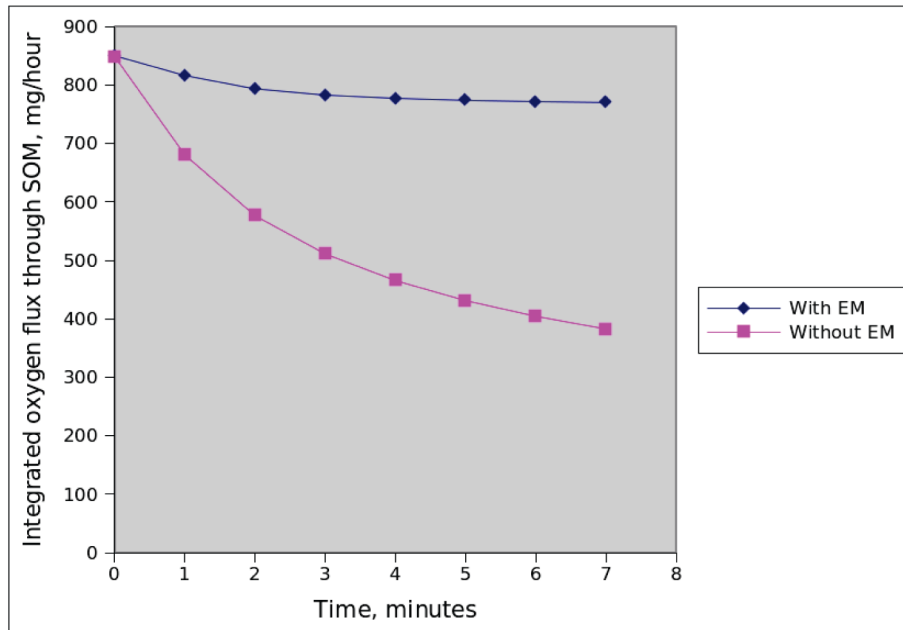


Figure 9. Calculated decline in oxygen ionic current with and without electromigration effects at the start of an experiment.

For a large multi-tube scale-up cell, there are two simulation approaches. The first is to take a hexagonal array of tubes as a series of unit cells, in order to study the temperature, flow field, and solute transport around a single tube. This approach is efficient, but loses the “edge effects” around the outside of the crucible, such as the sidewall natural convection boundary layer.

Figure 10 shows the unit cell in the context of a 37-tube array and the 3-D cell geometry and finite element mesh. Simulation results again show an upward-flowing natural convection velocity boundary layer around Figure 10 shows the hot SOM tubes, with downward flow between them.

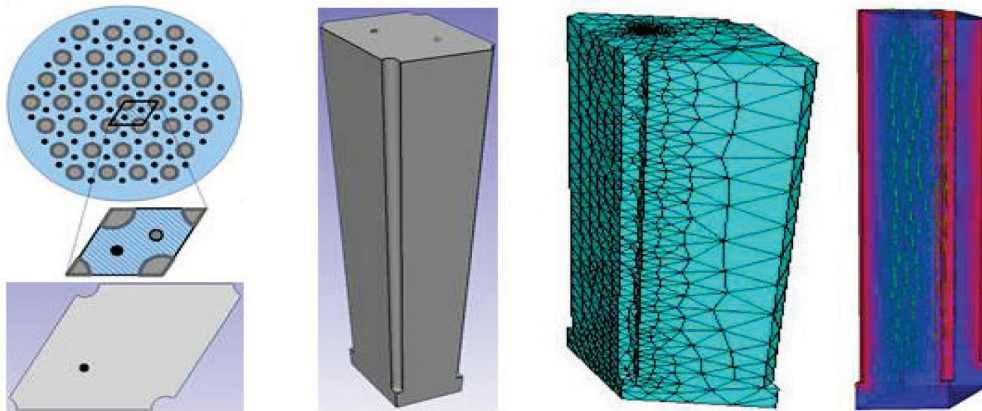


Figure 10. 60° repeat unit for a hexagonal array of SOM tubes and cathodes in a large electrolysis cell, flux domain geometry, FEA mesh, and FEA velocity and temperature results showing boundary layers near the SOM tubes

The other approach shown in Figure 11 represents the tube array using a 60° wedge simulation domain with symmetry planes at the faces. With a much larger domain, this must use a coarser finite element mesh for the simulation to run in a comparable time on the same hardware or a finer mesh with longer run time and/or more computational resources. MOxST ran several FEA simulations of flux transport in the crucible using a 1/6 wedge of a 37-tube geometry, as generated by the parametric scale-up cell design. These simulations included all of the physics in previous runs: electric current, heat transfer between SOM anodes and other system components with Joule heating, and fluid flow driven by thermal buoyancy and argon bubbling.

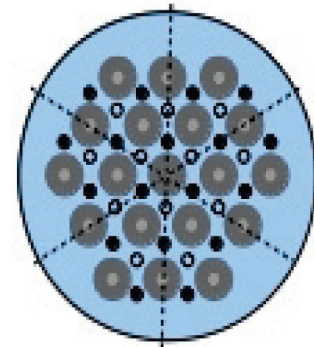


Figure 11. 19-tube SOM anode, cathode, and MgO feed layout with symmetry planes.

Figure 12 shows results mostly shared by these calculations. The 570,000-element mesh is well-resolved in each section, including boundary layers around the anodes and cathodes. A four-core machine runs the simulation, hence the partitioning shown here. Potential is not coupled with other phenomena, so it is the same in all of these simulations. And temperature is affected by strong flow, which is not the case here.

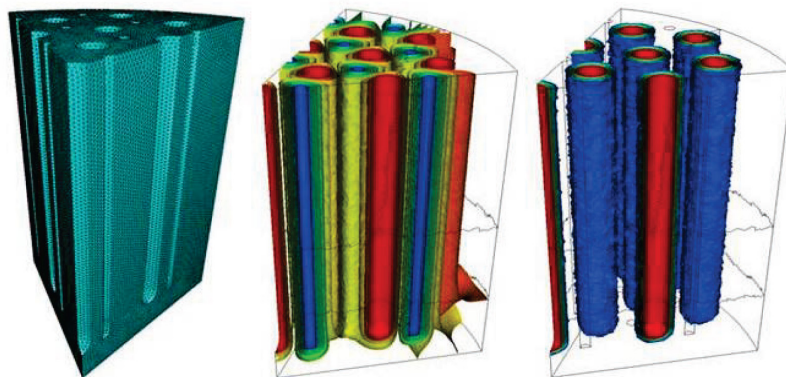


Figure 12. Mesh, potential, and temperature for 37-tube 1/6 wedge simulations.

Industrial-Scale Cell Design

MOxST has begun parametric design of an industrial-scale SOM Electrolysis cell. The goals of this design are to visualize various layouts of the cell and identify any potential design issues and to serve as a platform for reduced-order modeling. It is built on the Python scripting interface of the FreeCAD open source design tool. This automates much of the design work; e.g. for a hexagonal array of SOM tubes, one merely sets the number of tubes on the edge and tube dimensions and a loop creates all of the tubes. Similarly, the capacity of the liquid Mg holding tank is a parameter and the script sizes the tank height to meet this design goal.

Figure 13 shows a perspective view and a top view of the current state of the design. Working counter-clockwise from the bottom left in the top view, they show the following design features:

- Crucible with hexagonal array layout of SOM tubes and start-up heater;
- Primary condenser tubes in two rows from crucible to Mg holding tank;
- Mg holding tank (roughly cubic shape) with liquid Mg tap;
- Argon recycling tubes, pump and return tube;
- Flux withdrawal tank with siphon tube;
- Insulation around the crucible, Mg tank, and flux withdrawal tank (clear yellow).

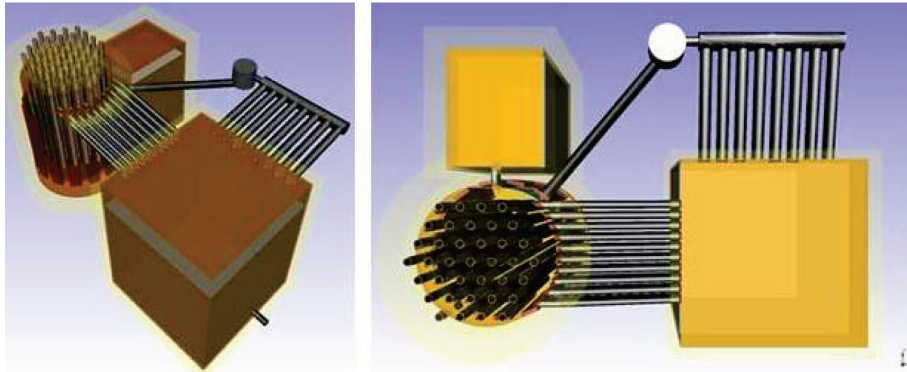


Figure 13. Perspective and top views of the industrial-scale magnesium electrolysis cell design.

The overall bounding box is 79×54×46 inches, which fits into a 7'×5'×4.5' furnace enclosure. Finally, the script exports a STEP format geometry of a 1/6 wedge of the flux in the crucible, which Elmer can directly import and mesh for FEA calculations. Indeed, the simulation shown in Figure 12 used this FreeCAD script to generate its geometry.

Scale-Up Experiments

In order to produce tens of tons of Mg per year, electrolysis cells must scale up by increasing both the number of SOM tubes and the immersion depth of each tube in the molten salt. MOxST conducted four 3-tube, deep-immersion Mg electrolysis experiments with better insulation between the top two and bottom two furnace zones. The details of the deep immersion 3-tube experiments are given below:

- 10" ID four-zone tube furnace, made by ATS, with each zone capable of reaching 1540° C; each zone has a separate controller to maintain the temperature independently.
- Three-tube, stainless steel reaction vessel (crucible-condenser assembly).
- Liquid silver anodes inside the YSZ tubes.
- 1/16" NiCr 60 wire current collector, attached to 1/8" alumel to provide for good electrical contact with power supply.

- Three 1/4" OD stainless tubes which bubble argon through the liquid flux to stir it.
- Flux weighing 3.2 kg, composed of 47% CaF₂, 41% MgF₂, 10% MgO, and 2% additive.
- Top and bottom plates machined of aluminum.
- PF-3350 powder feeder containing 320 g of MgO.

Over 14 total hours of electrolysis were done at 5V over the course of two days, in runs of 3 and 11 hours, with voltage set to zero overnight between runs. As is typical, the current decreased during the first few hours, from 4.5A to 4.2A, before reaching an asymptote. The currents through the two anodes, shown in Figure 14, mapped very closely with one another and remained stable, except for a sharp decrease at 4 p.m. on the second day. This was traced to a decrease in argon flow through the stirrer tubes. Once flow was reestablished, the current increased within a minute to or near its previous values.

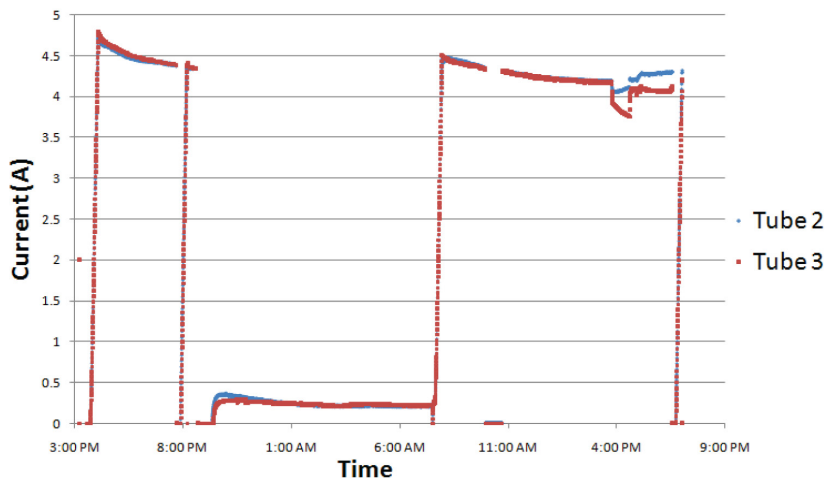


Figure 14. Current through two anode tubes during a two-day electrolysis run at 5 V.

Nine and one-half hours into the second run, MgO was introduced into the crucible through the powder feeder. This correlated with an increase in the current because of the higher MgO concentration in the flux. The cell passed a total of ~480 kC of charge, corresponding to about 60g of Mg.

High-current experiments

The last two experiments used 8.0 kg of flux each, which immersed the SOM tubes 8" deep. This resulted in very low resistance and enabled high current. All but the last experiment used HP 6630A power supplies limited to 30 A, with one power supply for each tube. The final experiment used a high-current HP 6881 power supply, which can provide up to 580 A. That experiment reached a total current of 205 A. The 100 A current in a single tube exceeded the prior maximum current for all three tubes, and opens the door to self-heated cell operation.

Mg Condenser and Use of Condensation Energy

The challenge in designing a liquid Mg condenser is that it has the highest vapor pressure of all metals at its melting point: 2 torr. And to prevent reaction with zirconia, the Mg vapor pressure in the crucible must be below 0.16 atm at 1150° C, which increases the difficulty of condensing it as a liquid. To our knowledge, only Mintek has built a working liquid Mg condenser² and that condenser requires 0.7-1.2 atm Mg partial pressure to be effective. MOxST has designed a proprietary condenser which produces liquid Mg from an atmospheric pressure Ar-Mg mixture with 0.1 atm Mg.

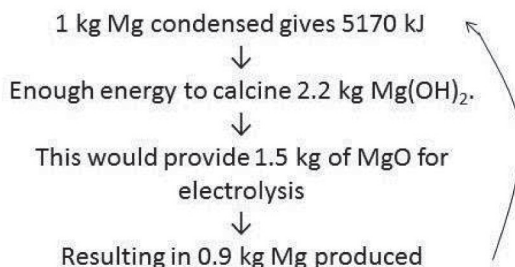
Using condenser waste heat for raw material calcination

Condensing Mg will release considerable excess heat, which one might use for calcination of either Mg hydroxide, Mg(OH)₂, or Mg carbonate, MgCO₃.

² Albert Schoukens et al., Metal Vapour Condensation and Liquid Metal Withdrawal, U.S. Patent 7,641,711 January 5, 2010 (PCT application filed Jan 24, 2006).

The energy required to calcine 1 kg of MgCO_3 , which dissociates at about 750°C is approximately 2415 kJ. For a 55% Mg(OH)_2 solid filter cake, which dissociates at 350°C , the energy is 2412 kJ, almost identical to that of MgCO_3 but nearly half of which is the vaporization of the excess water. For each kilogram, the MgCO_3 yields 0.48 kg of MgO , while 55% Mg(OH)_2 yields 0.38 kg MgO . Pure Mg hydroxide yields 0.69 kg MgO per kilogram.

Incorporating these energies into our model, we compared these heats to those present in the condensation process. Notably, with all processes being 100% efficient in a closed system, pure Mg(OH)_2 stock, which also has a calcining energy of about 2400 kJ/kg, could provide nearly all the MgO needed for Mg production, calcining at 600°C .



That is, 90% of the MgO could be provided by calcining Mg(OH)_2 with waste heat. In practice, obtaining 40-50% of the MgO supply from MgCO_3 or Mg(OH)_2 could reduce raw material costs considerably. Due to its lower temperature of decomposition, environmentally friendly byproduct (water cf. CO_2) and higher potential yield, Mg(OH)_2 would be the favorable choice.

MgO impurities in SOM electrolysis

- The composition of industrial Mg oxide from a likely MOxST supplier are in Table 1. Figure 15 shows the flows of impurities quantitatively per metric ton of Mg product. Impurities are of five types which the SOM Electrolysis process will handle in different ways:
- Calcium oxide: the most prevalent impurity in industrial MgO , MOxST will neutralize it by adding MgF_2 to the raw material, as shown in Figure 12. The additional flux will build up until removed, helping to flush out less electronegative metal oxides (below).
- Less electronegative metal oxides: oxides of potassium, barium and other less electronegative metals will accumulate in the flux over time. New flux from the above reaction (calcium oxide) will flush these out as old flux continuously exits the cell.
- More electronegative metal oxides: oxides of silicon, iron, aluminum, and other more electronegative metals will dissolve in the flux and form a solid metal deposit at the cathode and pure oxygen at the anode. The process will periodically replace the cathodes, removing these impurities. The iron cathodes with iron/silicon/aluminum deposit will be useful to the steel industry for reducing the oxygen content of liquid steel.
- Oxides of more electronegative volatile metals: oxides of zinc, cadmium and mercury, if present, exhibit lower free energy of formation than Mg , and form metal vapor at the cathode, and either remain in the circulating argon until removed by a cold trap, or a small amount may enter the magnesium product. Zinc is listed Table 1, but should be well below alloy limits (typically 0.2 wt% for alloys which do not specify it, such as AM60), so it should not pose a problem.
- Halides: chlorides (and bromides if any) have boiling points in the range of $1350\text{-}1450^\circ\text{C}$, and will slowly evaporate out and join the Mg in the condenser, then settle out due to higher melting point and density than Mg .

Table 1. Chemical composition of industrial MgO .

Chemical analysis, light-burned magnesia	
$\text{MgO}\%$	98.31 wt%
$\text{CaO}\%$	0.97%
$\text{SiO}_2\%$	0.28%
$\text{Fe}_2\text{O}_3\%$	0.15%
$\text{Al}_2\text{O}_3\%$	0.08%
$\text{Cl}\%$	0.21%
$\text{SO}_3\%$	0.01%
$\text{F}\%$	0.04%
K_2O	31 ppm
ZnO	13 ppm
L.O.I.%	1.12

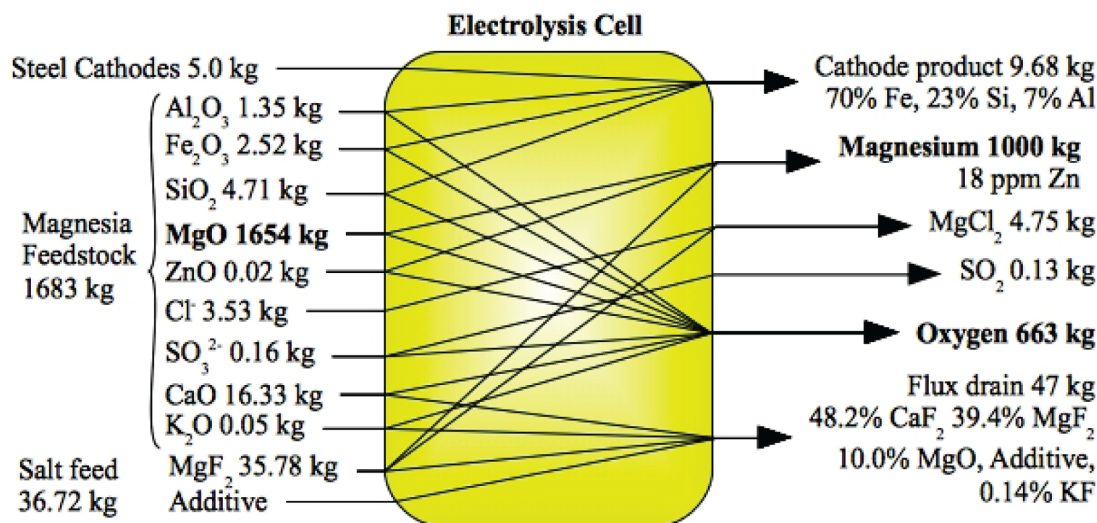


Figure 15. Mass balance of magnesia raw material and its impurities in the electrolysis cell.

SOM Electrolysis thus deals with all of the impurities present in raw material, and inline replacement of cathodes and flux minimizes the disruption.

Conclusions

MOxST has completed a one-year research project with several tasks which de-risked the SOM Electrolysis technology toward scale-up. During this time, the process ran more than twice as long as it has previously, at seven times higher current than previously reported. The project generated new data on zirconia stability for this purpose, and confirmed its fitness, while suggesting avenues for future improvement of the material composition and microstructure. Mathematical models at various scales have answered many questions about scale-up and paved the way for detailed engineering of pilot and full-scale electrolysis cells.

The economic opportunity presented by SOM Electrolysis is very compelling. At this point, there are no foreseeable technical or economic barriers that would prevent MOxST from scaling this process to a large plant. This would meet an important motor vehicle industry need for low-cost Mg from a zero-emissions process.

Presentations/Publications/Patents

E. Gratz, S. Pati, J. Milshtein, A. Powell, U. Pal, “Efficiency and Stability of Solid Oxide Membrane Electrolyzers for Magnesium Production,” Magnesium 2011 (Sillikens, Agnew, Neelameggham & Mathaudhu, eds.), presented at the TMS Annual Meeting, February 28, 2011.

References

Source: United States Automotive Materials Partnership (USAMP), Magnesium Vision 2020: A North American Automotive Strategic Vision for Magnesium, Technical Report, USCAR, Nov. 2006.

Source: Liming Peng, “Recent Developments in the Chinese Magnesium Industry,” Presentation at TMS Annual Meeting Magnesium Technology 2009 February 16, 2009; likely refers to the Chongqing National Engineering Research Center for Magnesium Alloys, <http://ccmg.cqu.edu.cn/>.

U.S. Patents 5,976,345 “Method and Apparatus for Metal Extraction...” and 6,299,742 “Apparatus for Metal Extraction”.

Source: Sujit Das, “Primary Magnesium Production Costs for Automotive Applications,” JOM 60(11):63-69, Nov. 2008.

D. Modeling and Computational Materials

Oak Ridge National Laboratory

Field Technical Monitor: C. David Warren
Oak Ridge National Laboratory
1 Bethel Valley Road; Oak Ridge, TN 37831
(865) 574-9693; e-mail: warrencd@ornl.gov

Technology Area Development Manager: William Joost
U.S. Department of Energy
1000 Independence Ave., S.W.; Washington, DC 20585
(202) 287-6020; e-mail: william.joost@ee.doe.gov

Contractor: Oak Ridge National Laboratory (ORNL)
Contract No.: DE-AC05-00OR22725

Executive Summary

Typical magnesium (Mg) alloys are brittle during vehicle crash events and difficult to form without elevated temperature processing. While several current efforts are aimed at understanding the crashworthiness and formability of current alloys, the long term solution is to develop new, more ductile alloys. A key component of new alloy development will be to have a comprehensive understanding of the diffusion of elements within the alloy. This project is aimed at developing that understanding.

Activity and Developments

High Throughput Isotopic Diffusion Databases for Magnesium Integrated Computational Materials Engineering

Principal Investigator: Nagraj Kulkarni, ORNL
(865) 576-0592; e-mail: kulkarnins@ornl.gov

Industrial Partner: U.S. Automotive Materials Partnership Integrated Computational Materials Engineering (ICME) Team, Magnesium Electron North America

Collaborators: Bruce Warmack, Balasubramaniam Radhakrishnan, Peter Todd, ORNL; Jerry Hunter, Virginia Tech; Yongho Sohn, Kevin Coffey, University of Central Florida; Graeme Murch, Irina Belova, University of Newcastle, Australia

Accomplishments

- Obtained Mg self-diffusivities in pure polycrystalline Mg samples using our secondary ion mass spectrometry (SIMS) - based thin-film stable-isotope technique, validating and extending historic radiotracer measurements to lower temperatures.
- Synthesized a matrix of Mg alloy compositions in the Mg-aluminum (Al)-zinc (Zn) system for tracer diffusion and interdiffusion studies and confirmed their composition uniformity across representative cross-sections. Mg and Zn tracer diffusion measurements for select compositions within this matrix are in progress.

- Developed a superior annealing system and procedure based on the Shewmon-Rhines approach that (a) minimizes Mg and Zn vapor phase loss during diffusion annealing of Mg alloy samples and (b) allows measurement of precise sample temperatures to enable full numerical corrections associated with heat-up and cooldown times during diffusion annealing.
- Applied molecular dynamics (MD) simulations for determining grain boundary diffusivities for select bicrystal grain boundaries in Mg.
- Conducted interdiffusion studies in the Mg-Zn system using solid-to-solid diffusion couples that were annealed at various temperatures and times.

Future Direction

- Measure Mg and Zn tracer diffusivities in the Mg-Al-manganese (Mn) and Mg-Al-Zn-Mn systems, similar to measurements carried out in Mg-Al-Zn. Using diffusion couples, determine interdiffusion coefficients in these systems and use diffusion theory to extract the tracer diffusivities of Al and Mn in these alloys.
- Obtain tracer diffusivities of Mg and X [X = rare earths: neodymium (Nd), cerium (Ce)] as a function of composition and temperature in Mg-Al-X rare earth systems at various temperatures (150°C–400°C) below liquidus.
- Synthesize Mg-Al-X (X = Nd, Ce) rare earth thick-film “compounds” using a vapor deposition technique (magnetron cosputtering), and obtain tracer diffusivities of Mg and X in these compounds as a function of temperature (150°C–400°C) using the SIMS-based thin-film tracer diffusion technique.

Technology Assessment

- Target: Enable rapid development of new Mg alloys using an ICME approach by providing critical Mg-Al-Mn-Zn diffusion and mobility data.
- Gap: Very little diffusion data for Mg alloys exist that can be used to construct a diffusion database. It is essential to have tracer diffusion data as the foundation of robust diffusion databases because such data are based on diffusion measurements in homogeneous alloys and are independent of thermodynamics.
- Gap: Elements such as Al and Mn that are important constituents of Mg alloys are monoisotopic. Hence there are no enriched stable isotopes of these elements that can be used in our approach. Additionally, the radioactive isotope for Al is not available at the present time.

Introduction

The objective of this project is to create an isotopic (tracer) diffusion database in the Mg-rich phase of the Mg-Al-Zn-Mn system. This database and a thermodynamic database that is being continuously updated will be provided to participants involved in various tasks in the Mg-ICME (Allison et al., 2006) program.

Approach

The approach for measuring the tracer diffusion coefficient is based on the thin-film approach (Shewmon, 1989). The procedure first requires the preparation of homogeneous single phase alloy samples in the desired Mg-Al-Zn-Mn system. This is followed by deposition of stable isotopes or radioisotopes of these elements in the form of thin films on the sample surfaces. After diffusion annealing at various temperatures below the melting temperatures of these alloy samples, the isotopic diffusion depth profiles in these samples are measured using SIMS. Analysis of the diffusion depth profile data using the thin-film solution (Shewmon and Rhines, 1954) provides the tracer diffusivity for the selected sample composition at the annealing temperature. At higher temperatures, the tracer diffusion in polycrystalline alloy samples is likely to be dominated by volume diffusion, while at lower temperatures, there will likely be an additional contribution from grain boundary diffusion. The SIMS diffusion data will be analyzed to extract both types of diffusion contributions, though in this fiscal year we have focused on volume diffusion measurements in large-grained samples. By repeating such measurements for different

compositions and temperatures, a significant amount of tracer diffusion data for Mg and Zn in the single phase Mg-Al-Mn-Zn system is obtained. Because Al and Mn are monoisotopic elements, their tracer diffusivities will be computed indirectly using diffusion theory (Darken-Manning relations) that connects interdiffusion coefficients (obtained from diffusion couples) with tracer diffusion coefficients and thermodynamics. The collection of tracer diffusion data for all the components in the Mg-Al-Zn-Mn system will then be fitted using suitable functions to generate the tracer diffusion database.

Results and Discussion

Our primary objectives in this fiscal year were to confirm that the SIMS-based thin-film stable-isotope technique for pure polycrystalline Mg would give us consistent self-diffusion coefficients such as those published in the literature that were based on the use of radioactive isotopes (Shewmon and Rhines, 1954) and to use this technique to measure the tracer diffusion coefficients of Mg and Zn in Mg-Al-Zn alloys. Following significant improvements in the diffusion annealing and SIMS measurement procedures based on the experimental effort conducted in the first quarter of FY 2011, we were successful in achieving our first objective in the final quarter of FY 2011. We expect to complete the measurement of the tracer diffusivities in Mg-Al-Zn alloy samples by the first quarter of FY 2012 using the matrix of compositions that have already been synthesized and characterized. We also conducted interdiffusion measurements in Mg-Al and Mg-Zn systems using diffusion couples to enable the computation of the tracer diffusivities of the monoisotopic elements (Al, Mn) using diffusion theory. Finally, we initiated MD simulations in pure Mg to obtain the grain boundary diffusivities for select grain boundaries in polycrystalline Mg.

Tracer Diffusion Studies in Pure Polycrystalline Magnesium

Tracer diffusion measurements in polycrystalline Mg samples that were carried out in the first quarter of FY 2011 showed significantly higher self-diffusivities in comparison to those in the literature based on radioactive tracers. This discrepancy was attributed to measurement errors caused by sputter-induced roughening during SIMS depth profiling that resulted in broadening of the SIMS diffusion depth profiles [Figure 1(a)]. A primary cause of this roughening is the rather broad grain size distribution (small average grain size of 10 μm) of the polycrystalline Mg extruded rod samples used in our studies. Using the improved annealing technique described in the next section, we were able to obtain a very large grain size that significantly minimized the roughening during SIMS depth profiling [Figure 1(b)]. The resulting tracer diffusion results based on measurements at three diffusion annealing temperatures (300°C, 350°C, and 400°C) showed an excellent match with those based on radioactive tracers when extrapolated down to the lower temperatures used in this work, as seen in the Arrhenius plot (Figure 2).

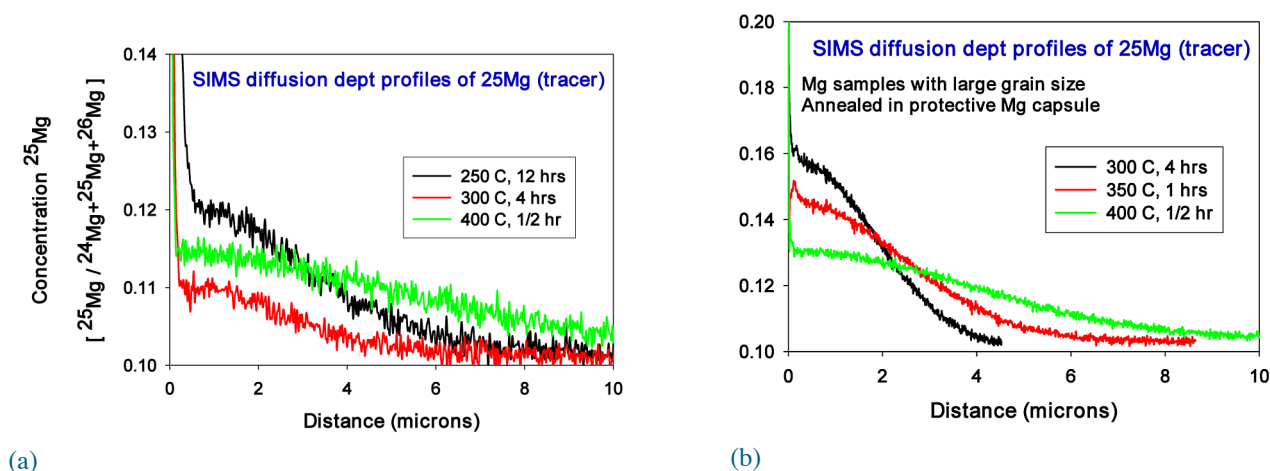


Figure 1. SIMS diffusion depth profiles of the stable isotope (tracer) ^{25}Mg in pure Mg polycrystalline samples: (a) extruded samples having a broad grain size distribution and a small average grain size ($\sim 10 \mu\text{m}$) and (b) extruded preannealed samples having an average grain size in the hundreds of microns. An improved annealing technique and a significantly larger grain size resulted in more reliable SIMS profiles with less scatter due to minimal sputter-induced roughening.

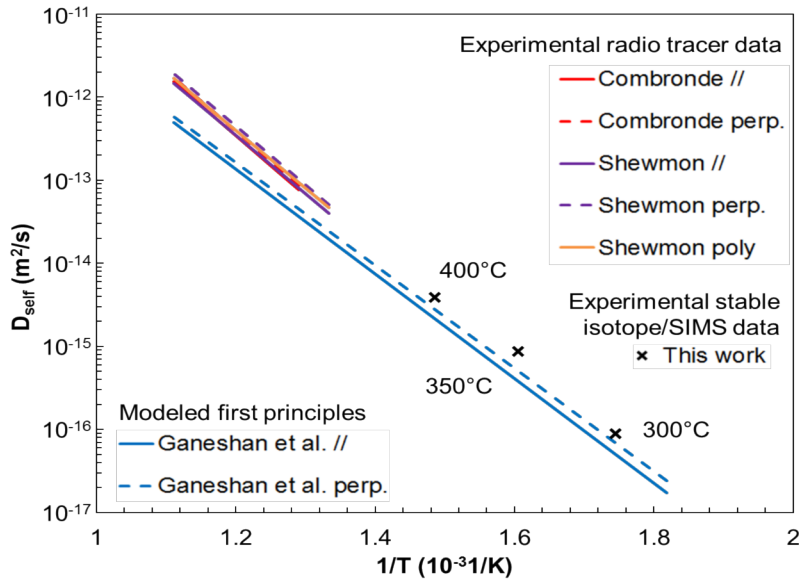


Figure 2. Arrhenius plot of the self-diffusion coefficients in pure Mg from this work using the SIMS-based stable isotope thin-film technique. Comparison with an extrapolation of the published self-diffusion radioactive tracer data at high temperatures (>400°C) shows excellent agreement.

Tracer Diffusion Studies in Mg-Al-Zn Alloys

Tracer diffusion measurements in polycrystalline Mg samples will be conducted from the matrix of alloy compositions (Table 1) that have been synthesized by Magnesium Elektron in the form of extruded rods (9 mm diameter). A total of 8–10 compositions from this matrix will be used for measuring the tracer diffusivities of Mg and Zn. Energy dispersive spectroscopic analysis carried out across the cross sections of these samples confirmed the homogeneity and nominal compositions specified.

Table 1. Matrix of Mg-Al-Zn alloys with nominal and measured compositions.

Alloy	Phase	Nominal composition (weight %)			Chemical analysis (weight %)						
		Mg	Al	Zn	Al	Zn	Mn	Ca	Pb	Si	Fe
MA1	α	99	1	0	0.97	0.0049	0.0054	0.0026	0.0021	0.0031	0.003
MA3	α	97	3	0	2.81	0.0035	0.0054	0.0036	0.0001	0.0043	0.0053
MA6	α	94	6	0	6.73	0.0056	0.0056	0.002	-	0.0029	0.0021
MA9	α	91	9	0	9.59	0.016	0.0054	0.0023	-	0.0025	0.0021
MA15*	$\alpha + \gamma$	85	15	0	14.4	0.01	0.0049	0.002	-	0.0019	0.0023
MZ0.5	α	99.5	0	0.5	0.0065	0.49	0.0052	0.0022	0.0039	0.0037	0.0019
MZ1	α	99	0	1	-	0.84	0.0054	0.004	0.0038	0.0032	0.0022
MZ3	α	97	0	3	-	2.62	0.0052	0.0018	0.0033	0.0032	0.0029
MZ6	α	94	0	6	0.01	6.23	0.0052	0.0027	0.0029	0.0053	0.0021
MZ9*	$\alpha + \delta$	91	0	9	0.22	9.5	0.0053	0.0014	0.0026	0.0062	0.0021
MA3Z1	α	96	3	1	2.92	0.96	0.0055	0.0035	0.002	0.0047	0.0056
MA5Z2	α	93	5	2	5.12	1.96	0.0054	0.0027	-	0.0032	0.0022
MA1Z3	α	96	1	3	0.97	2.99	0.0052	0.0019	0.0021	0.0039	0.002
MA3Z3	α	94	3	3	2.95	2.96	0.0055	0.003	0.0002	0.0051	0.0057
MA1Z1	α	98	1	1	0.99	0.9	0.0054	0.0036	0.002	0.0035	0.0033

α : hcp (hexagonal close packed); γ : Mg₁₇Al₁₂; δ : MgZn

Notes: Other elements detected in trace amounts are Cu (<20 ppm), Sn (<20 ppm), Ni (<5 ppm), Zr (<10 ppm) (ppm = parts per million).

Diffusion Annealing Technique for Magnesium

At the higher annealing temperatures (500°C–600°C) necessary for grain growth, the vapor pressure and oxidation rate of Mg is extremely high. Hence, based on a technique developed by Shewmon and Rhines (1954), we constructed a Mg capsule to contain the Mg vapors and also prevent oxidation during annealing. This Mg capsule was sealed in a partial atmosphere of



Figure 3. Diffusion annealing apparatus for Mg samples based on the Shewmon and Rhines technique (Shewmon and Rhines, 1954).

Ar-H₂ in a quartz enclosure and placed in a copper block inside a 2 in. diameter tube furnace (Figure 3). Annealing treatments at 545°C for 14.5 h and 595°C for 9 h showed roughly similar grain growth with grain sizes in the hundreds of microns in comparison to the grain size (~10 μm) prior to the annealing treatment (Figure 4). A similar design for encapsulation was used for tracer diffusion annealing. Sample slices of the above preannealed Mg rods were coated with the stable isotope (²⁵Mg), loaded inside a small Mg capsule, and enclosed in a quartz tube. Temperature cycles of an equivalent dummy sample showed that small samples inside the large copper block minimize the time to reach temperature equilibrium, though corrections for heat up and cooldown were applied for all anneal cycles. Calibrated thermometers (resistance temperature detectors) monitored the diffusion temperature to better than ±0.5°C.

Atomic Simulations of Grain Boundary Diffusion in Magnesium

The present effort focused on computing the grain boundary diffusivity in Mg bicrystals containing [10 0] tilt boundaries that are known to be present in high proportions. We specifically investigated three types of tilt boundaries—an asymmetric 34.2° boundary [Figure 5(a)], a general 40.3° tilt boundary [Figure 5(b)], and a 34.2° symmetric tilt boundary [Figure 5(c)]. The Sandia MD code LAMMPS, which had been previously validated by Sandia, was used for the simulations. The grain boundary diffusion coefficient was calculated from the slope of the mean square displacement (MSD) of atoms in the vicinity of the grain boundary versus time shown in Figure 2. The activation energy for grain boundary diffusion was calculated from an Arrhenius plot of the diffusion coefficient versus 1/T; the results are shown in Table 2. The symmetric 34.2° boundary did not show any appreciable MSD at the highest temperature studied. Both the asymmetric 34.2° boundary and the general 40.3° boundary showed measurable MSD in the temperature range of investigation, which was limited to 750 K. At higher temperatures, the boundaries were not stable and showed lateral migration and new facet formation. At low temperatures (600 K), the boundaries again showed facet formation and the MSD measurements are not reliable. Therefore, the 600 K measurements were not included in the MSD measurements. The simulated diffusion coefficients for the two tilt boundaries were roughly the same (5.0×10^{-7} cm²/s) at 750 K and were at least three orders of magnitude higher than the value for volume diffusion in polycrystalline Mg at 741 K experimentally measured by Shewmon and Rhines (1954).

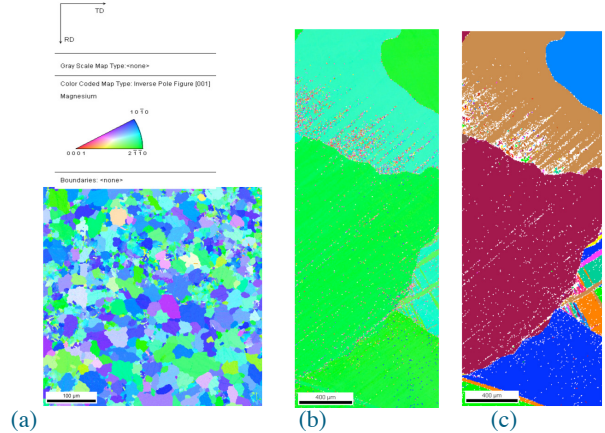


Figure 4. Electron backscatter diffraction map (inverse pole figure) of grain orientations in a pure polycrystalline Mg rod before (a), after an annealing treatment at 545°C for 14.5 h (b), and the identical grain structure map with enhanced contrast (c).

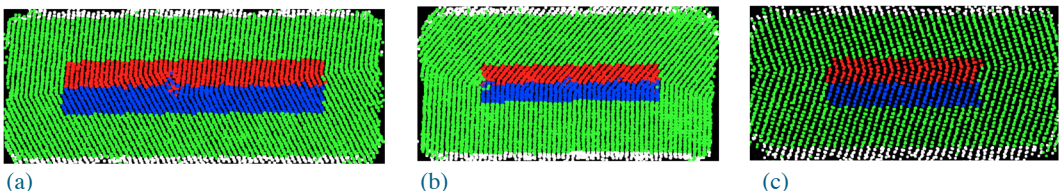


Figure 5. Atomic structures of the 34.2° asymmetric tilt (a), 40.3° general (b), and 34.2° symmetric (c) boundaries after expansion and equilibration at 750 K. The red and blue atoms correspond to the ones used for measuring MSD. The white atoms at the free surface are constrained to move parallel to grain boundary.

Table 2. Calculated diffusion coefficients and activation energies for the selected boundaries.

Grain boundary type	Activation energy (Cal/mole)	D at 750 K (cm ² /s)
34.2 asymmetric	11,680	4.97×10^{-7}
40.3 general	13,480	5.0×10^{-7}
34.2 symmetric ^a	-----	-----

^aThe symmetric tilt boundary did not show any measurable MSD at the highest temperature investigated.

Interdiffusion Studies

Zn is a common alloying element in commercial Mg alloys, typically added for solid solution and precipitation strengthening. However, little information is available regarding the phase layer growth and interdiffusion behavior in the Mg-Zn binary system. Intermetallic phase formation and growth in the Mg-Zn binary system was studied using the solid diffusion couple technique at 295°C, 315°C, and 325°C for 384, 168, and 120 h, respectively. The MgZn₂, Mg₂Zn₃, and Mg₂Zn₁₁ phases were identified in all three couples and the Mg₅₁Zn₂₀ phase in the 325°C couple (Figure 6). Parabolic growth constants were determined for each phase at each temperature, with MgZn₂ having the highest growth rates followed by the Mg₂Zn₃ phase and the Mg₂Zn₁₁ phase. The activation energy for growth was calculated to be 105 kJ/mole for the Mg₂Zn₃ phase and 207 kJ/mole for the MgZn₂ phase.

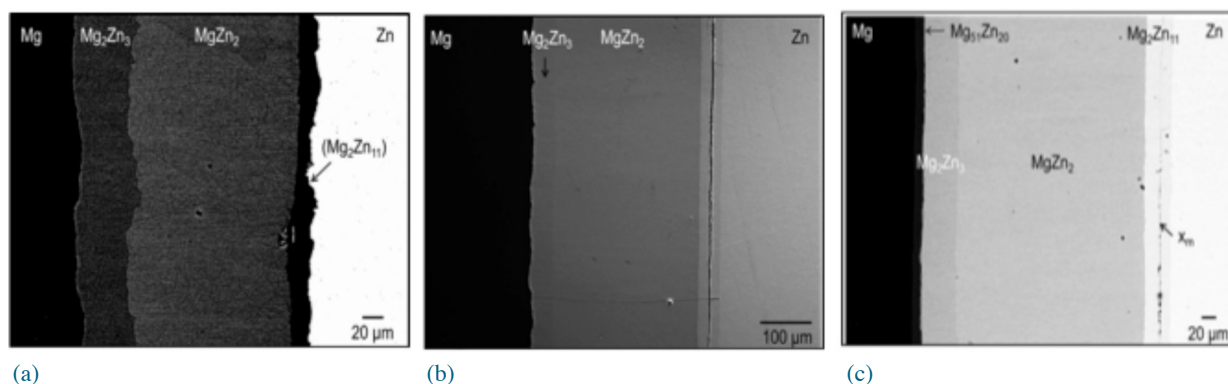


Figure 6. Representative backscatter electron images of Mg vs Zn diffusion microstructures at (a) 295°C for 384 h, (b) 315°C for 168 h, and (c) 325°C for 120 h. X_m is the marker plane. [Note: Mg₂Zn₁₁ in (a) is largely pulled out from the diffusion couple.]

Conclusions

We have confirmed the reported Mg self-diffusion coefficients based on radiotracer measurements in pure polycrystalline Mg samples at various temperatures using the SIMS-based stable-isotope thin-film diffusion technique. High-fidelity SIMS diffusion depth profiles were obtained as a result of significant improvements in the annealing technique based on the Shewmon-Rhines approach. Mg-Al-Zn alloy compositions were synthesized and characterized for tracer diffusion and interdiffusion measurements. Binary Mg-Zn interdiffusion studies were conducted for computing interdiffusion coefficients. Atomistic simulations of select grain boundary diffusivities in polycrystalline Mg revealed that these were about three orders of magnitude larger than the volume diffusivities.

Conclusions

The work to develop a fundamental understanding of diffusion in Mg is progressing on schedule. This work is part of the larger, nationwide ICME.

Presentations/Publications/Patents

Belova, I. V.; Allnatt, A. R.; Sohn, Y. H.; Kulkarni, N. S.; Brennan, S. T.; Murch, G. E. Development of a Theory of Solute Diffusion Enhancement for Analyzing Interdiffusion Experiments. Presented at the 2011 TMS Annual Meeting & Exhibition: Hume-Rothery Symposium Thermodynamics and Diffusion Coupling in Alloys—Application Driven Science in honor of Prof. John Agren, San Diego, California, February 27–March 3, 2011.

Brennan, S.; Bermudez, K.; Kulkarni, N.; Sohn, Y. H. Growth Kinetics of γ -Al₁₂Mg₁₇ and β -Al₃Mg₂ Intermetallic Phases in Mg vs. Al Diffusion. Presented at the 2011 TMS Annual Meeting & Exhibition: Symposium on Magnesium Technology 2011, San Diego, February 27–March 3, 2011.

Brennan, S.; Bermudez, K.; Kulkarni, N.; Sohn, Y. H. Growth Kinetics of γ -Al₁₂Mg₁₇ and β -Al₃Mg₂ Intermetallic Phases in Mg vs. Al Diffusion Couple. In *Magnesium Technology 2011*; Sillekens, W. H.; Agnew, S. R.; Neelameggham, N. R.; Mathaudhu, S. N., Eds.; TMS: Warrendale, Pennsylvania, 2011; pp. 549–552.

Brennan, S.; Bermudez, K.; Kulkarni, N.; Sohn, Y. H. Interdiffusion and Intrinsic Diffusion in Mg-Al System. *Metall. and Mater. Trans. A*, submitted for publication.

Brennan, S.; Warren, A. P.; Coffey, K. R.; Klimov, M.; Kulkarni, N.; Todd, P.; Sohn, Y. H. Aluminum Impurity Diffusion in Magnesium. *J. Phase Equilib. Diffus.*, submitted for publication.

Hunter, J.; Kulkarni, N.; Todd, P.; Radhakrishnan, B.; Sohn, Y. H.; Brennan, S.; Coffey, K.; Klimov, M.; Murch, G. E.; Belova, I. Self-Diffusion Studies in Magnesium Using Secondary Ion Mass Spectroscopy. Presented at the Symposium on Phase Stability, Diffusion, Kinetics and Their Applications (PSDK-V), Materials Science & Technology 2010 (MS&T2010), Houston, Texas, October 17–21, 2010.

Kulkarni, N. S.; Sohn, Y.; Hunter, J. L.; Brennan, S.; Coffey, K. R.; Todd, P. J.; Radhakrishnan, B.; Murch, G. E.; Belova, I. V. Tracer Diffusion Database for Mg-ICME. Keynote presentation at the 7th International Conference on Diffusion in Solids and Liquids: Symposium on Chemical Diffusion and Reaction in Engineering Alloys, DSL-2011, Algarve, Portugal, June 26–30, 2011.

Kulkarni, N. S.; Todd, P. J.; Radhakrishnan, B.; Sohn, Y.; Brennan, S.; Coffey, K. R.; Hunter, J. Tracer Diffusion Databases for ICME. Poster presentation at the 1st World Congress on Integrated Computational Materials Engineering, Seven Springs, Pennsylvania, July 10–14, 2011.

Radhakrishnan, B.; Kulkarni, N.; Parish, C. Atomistic Simulations of Grain Boundary Diffusion in Magnesium. Poster presentation at the 1st World Congress on Integrated Computational Materials Engineering, Seven Springs, Pennsylvania, July 10–14, 2011.

Radhakrishnan, B.; Kulkarni, N.; Sohn, Y. H.; Hunter, J.; Parish, C. Modeling of Tracer Diffusion in Magnesium Polycrystals. Presented at the 1st World Congress on Integrated Computational Materials Engineering, Seven Springs, Pennsylvania, July 10–14, 2011.

References

Allison, J.; Backman, D.; Christodoulou, L. Integrated Computational Materials Engineering: A New Paradigm for the Global Materials Profession. *J. Met.* 2006, 58, 25–27.

Combronde, J.; Brebec, G. Anisotropy for Self-Diffusion in Magnesium. *Acta Metall.* 1971, 19, 1393–1399.

Ganeshan, S.; Hector, L. G., Jr.; Liu, Z.-K. First-Principles Study of Self-Diffusion in HCP Mg and Zn. *Comput. Mater.s Sci.* 2010, 50, 301–307.

Shewmon, P.; Rhines, F. Rate of Self-Diffusion in Polycrystalline Magnesium. *Transactions AIME* 1954, 200, 1021–1025.

Shewmon, P. *Diffusion in Solids*, 2nd ed.; The Minerals, Metals & Materials Society: Warrendale, Pennsylvania, 1989; pp. 15–19.

E. Modeling and Computational Materials Science

Pacific Northwest National Laboratory

Field Technical Monitor: Dean Paxton
Pacific Northwest National Laboratory
902 Battelle Boulevard; P.O. Box 999; Richland, WA 99352
(509)375-2620; e-mail: dean.paxton@pnnl.gov

Technology Area Development Manager: William Joost
U.S. Department of Energy
1000 Independence Ave., S.W.; Washington, DC 20585
(202) 287-6020; e-mail: william.joost@ee.doe.gov

Contractor: Pacific Northwest National Laboratory (PNNL)
Contract No.: DE-AC05-00OR22725 & DE-AC06-76RL01830

Executive Summary

The Modeling and Computational Materials Science (CMS) project is targeted at developing techniques and methods for predicting and describing the structure, property, and processing relationships in light-weight materials with specific application to the automotive industry. This project currently includes two tasks entitled “Mechanistic-based Ductility Prediction for Complex Magnesium Castings” and “Materials Informatics for the Integrated Computational Materials Engineering Cyberinfrastructure.”

The use of modeling and CMS can greatly accelerate the introduction of lightweight materials and improve properties of existing materials. Greater implementation of modeling and CMS can guide experimental work and process modifications that improve material properties and performance and make such information more available to system designers. The current and future research conducted in this project is targeted at developing and validating modeling and computational materials science techniques for light-weight materials. The objective of this research is to demonstrate methods for predicting and describing the structure/processing/properties relationship in lightweight materials through the length scale continuum.

The following sections outline specific task work conducted by PNNL in the area of modeling and computational materials science disciplines. Each task supports one or more goals within the Modeling and Computational Materials Science Agreement.

Mechanistic-based Ductility Prediction for Complex Magnesium Castings

Principal Investigator: Xin Sun, PNNL
(509) 372-6489; e-mail: xin.sun@pnnl.gov

Key Contributors:
Kyoo Sil Choi, PNNL
(509) 372-6967; e-mail: kyoosil.choi@pnnl.gov

Dongsheng Li, PNNL
(509) 375-2406; e-mail: Dongsheng.Li@pnnl.gov

Erin Barker, PNNL
(509) 372-4727; e-mail: Erin.Barker@pnnl.gov

Industry Partners:
Mei Li, Ford Motor Company
(313) 206-4219; e-mail: mli9@ford.com

Allen Schroeder, MagTech Industries
(517) 789-8505; e-mail: allen@mag-teccasting.com

John Allison, University of Michigan
(734) 615-5150; e-mail: johnea@umich.edu

Accomplishments

- Performed microstructure analyses on AM50 casting samples using optical microscope and X-ray tomography to characterize the microstructure and defect features (i.e., the porosity percentage/density and largest pore size). Performed static tensile tests on the AM50 samples.
- Performed two-dimensional finite element (FE) analyses based on synthetic microstructures of magnesium (Mg) castings to investigate the effects of porosity, pore size, and distribution on the ductility.

Future Directions

- Investigate mesh size effects on ductility prediction of porous materials to determine the reasonable mesh size and representative volume element (RVE).
- Extend the modeling regime to include other porosities up to 10% and maximum pore size up to 500 μ m.
- Quantify the skin effects on the predicted ductility with various thicknesses of pore-free zone at the sample skin.
- Examine the crack path and fracture surface of tested samples.
- Perform FE analysis based on actual microstructures obtained from X-ray tomography and/or microscopy of Mg castings to examine the extent of interactions and competitions between the pores and the brittle eutectic β phase.

Technology Assessment

- Target: To develop a ductility prediction method for high-pressure die casting that has the potential for error of less than 25%.
- Gap: Conventional computational techniques (i.e., homogenization, continuum damage mechanics, crystal plasticity) and some phenomenological approaches have no (or quite limited) ductility predictive capability. As ductility is a macroscopic exhibition of microstructure level material deformation behavior, microstructure-level mechanistic-based modeling techniques are critical to ductility prediction.

Introduction

Mg castings have found increasing applications in lightweight vehicles because Mg and its alloys are the lightest metallic structure materials. However, a critical technical challenge hindering the wider applications of Mg castings in vehicle applications is its limited ductility. It is well established that among various factors, microstructure features such as properties and distributions of porosity, brittle eutectic phases, and grain size can significantly influence the ductility of Mg castings. However, these microstructure features vary from specific alloy to alloy, different casting processes, and different locations on a single casting. Although some commercial casting software packages or material models are available for Mg castings, their predictive capability typically stops short of predicting the location dependent stress versus strain behavior, particularly ductility. The purpose of this project is to develop an empirical casting process simulation tool and a mechanistic-based ductility predictive capability to provide a modeling framework that can be used in the future alloy design and casting process optimization.

Approach

In fiscal year (FY) 2011, AM50 castings (Mg–4.9wt.%Al–0.39wt.%Mn–0.2wt.%Zn) were acquired in the cylindrical dog-bone shape for tensile tests. A small portion was cut from the end of each sample for microstructural analysis. Optical microscopic pictures were taken from these cut samples and then porosity analysis in skin and center regions was performed to determine the areal porosity percentage, porosity distribution, and largest pore size. The high-resolution X-ray tomography technique was also adopted to generate three-dimensional images of the tensile samples with the porosity distributions inside. The information obtained from these structure and image analyses will help researchers determine a feasible correlation between the microstructure and defect features and the fracture behaviors of Mg castings. Static tensile tests ($\epsilon = 10^{-3} / \text{sec}$) were completed for all tensile samples, and the fracture surfaces are planned to be examined to determine the fracture paths.

As the porosity is one of the dominant ductility limiting factors for Mg castings, synthetic two dimensional microstructures of Mg castings were first generated such that they have various feasible pore sizes/volume fractions (i.e., pore size 4~40 μm , pore volume fraction 1~4%). FE models were built based on these synthetic microstructures and then stress versus strain curves, ultimate tensile strength (UTS) and strain at UTS (i.e., ductility) were obtained and compared with each other. For the modeling works, the effects of larger pore sizes/volume fractions will be examined together with the mesh size effects. Development of FE model based on the actual microstructure of Mg castings will also be considered.

Technology Transfer Path

This task is mainly focused on the development of a casting process simulation tool and a mechanistic-based ductility predictive capability to provide a modeling framework that can be used in future alloy design and casting process optimization to maximize ductility. This project has active industrial participation and the results of this project will be transferred to the OEM participants and casting producers through periodic project review meetings, as well as project reports including methods/software releases. The modeling methodology and modeling results will also be published in peer-reviewed technical journals so they are widely disseminated to a broader engineering community.

Results and Discussion

Figures 1(a), 1(b), and 1(c) show some optical microscopic pictures of the cross-sections of the AM50 casting samples. Due to the different solidification rate between the surface and center regions, all samples exhibit different microstructures between these two regions as shown in Figures 1(a) and 1(b). The center regions also have different microstructures (i.e., porosity distribution) for different samples as shown in Figures 1(b) and 1(c). Porosity analysis has been performed on the cross-section micrographs to determine the areal porosity and largest pore size of each sample.

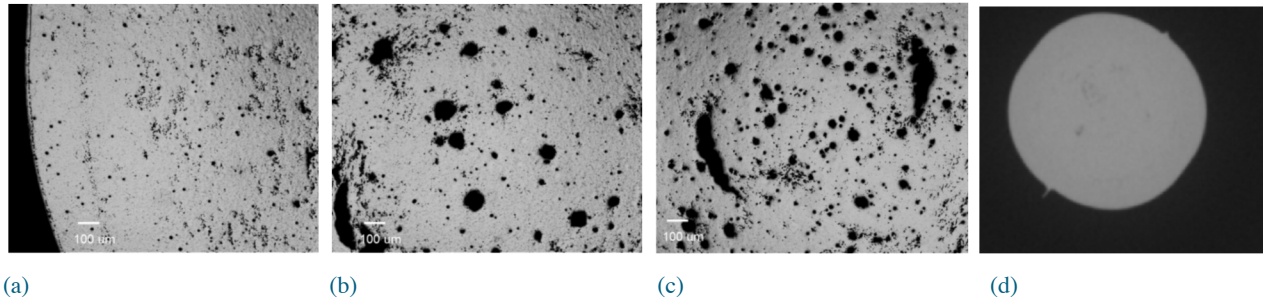


Figure 1. Cross-section micrographs of the tested AM50 casting samples: (a) skin area of sample#3, (b) center area of sample #3, (c) center area of sample #5, and (d) cross-section micrograph of sample #8 from reconstructed computerized tomography (CT).

Figure 2 shows the stress-strain curves of the tested samples. These casting samples show the similar yield strengths and hardening rates during the initial loading process. However, their fracture strains are quite different from each other, which is due to different microstructural features. According to the porosity analysis of the cross-section micrographs, sample #8 is expected to show quite low ductility due to its high-porosity contents and large pore sizes. For this project, the high-resolution X-ray tomography technique was also employed before the tensile test to generate the three-dimensional image of the samples and its porosity distribution. For example, Figure 1(d) shows the X-ray image of a cross-section of sample #8, captured during X-ray scanning. The results of X-ray tomography are being post-processed and the generated three-dimensional images will be used to investigate the fracture behaviors of the AM50 samples.

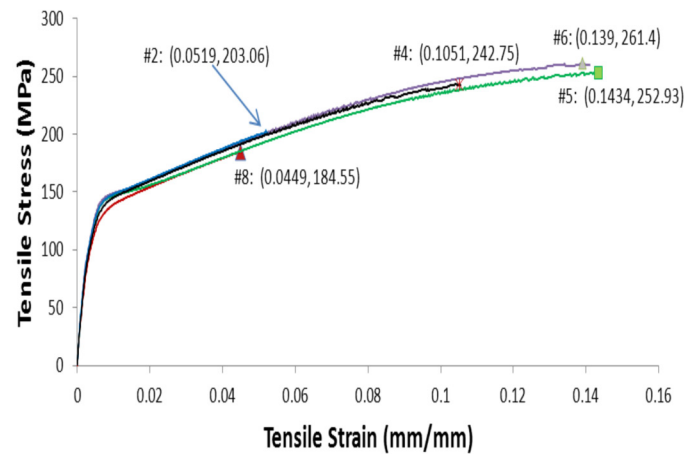


Figure 2. Stress-strain curves for the AM50 casting samples

Figure 3 shows some synthetic microstructures of Mg castings developed to investigate the effects of pore structure on the ductility. The $1 \times 1\text{-mm}^2$ FE models were generated based on these microstructures. Various models are generated such that three different pore volume fractions (i.e., 1, 2, 4%), five different pore sizes (i.e., 4, 12, 20, 28, $40\mu\text{m}$ in diameter), and two different pore size distributions (i.e., uniform and linear pore size distribution) are considered in this investigation.

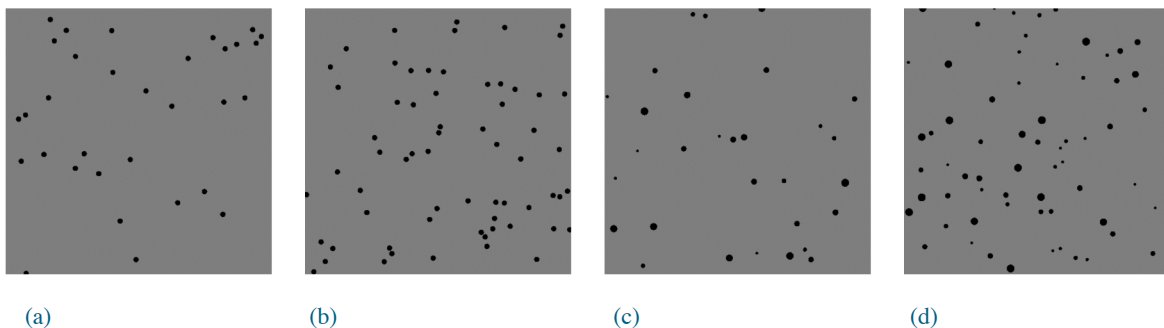


Figure 3. Examples of synthetic microstructure of Mg castings: (a) pore size $10\mu\text{m}$ and volume fraction 1%, (b) pore size $10\mu\text{m}$ and volume fraction 2%, (c) average pore size $10\mu\text{m}$ and volume fraction 1%, and (d) average pore size $10\mu\text{m}$ and volume fraction 2%

Figure 4 shows some simulation results based on the synthetic microstructures. Figure 4(a) shows the predicted stress-strain curves for the models with 1% pore volume fraction and uniform pore size. Six different cases were simulated for each pore size case to obtain statistically meaningful average and standard deviation for strength and ductility. As shown in Figure 4(a), the six different pore sizes generate different tensile curves. In general, the UTS and ductility decrease as the pore size increases. Figures 4(b) and 4(c) show the effects of pore size/volume fraction on the average ductility and its deviation based on the models with linear pore size distribution. As shown in the figures, generally, ductility decreases as pore size and volume fraction increase. This is consistent with many reported experimental findings for relatively small pore sizes. However, this is not necessarily the case for large pore size as shown in the case of $40\mu\text{m}$ pore size in Figure 4(c). For this different behavior, the mean distance between the pores begins to influence the strain distribution inside the model and thus the material ductility in this relatively large pore size and volume fraction region. Further investigations are underway on this observation. Regarding the modeling work, mesh size effects on the predicted ductility will be quantified and larger pore size (up to $500\mu\text{m}$) and porosity (i.e., up to 10%) will also be examined.

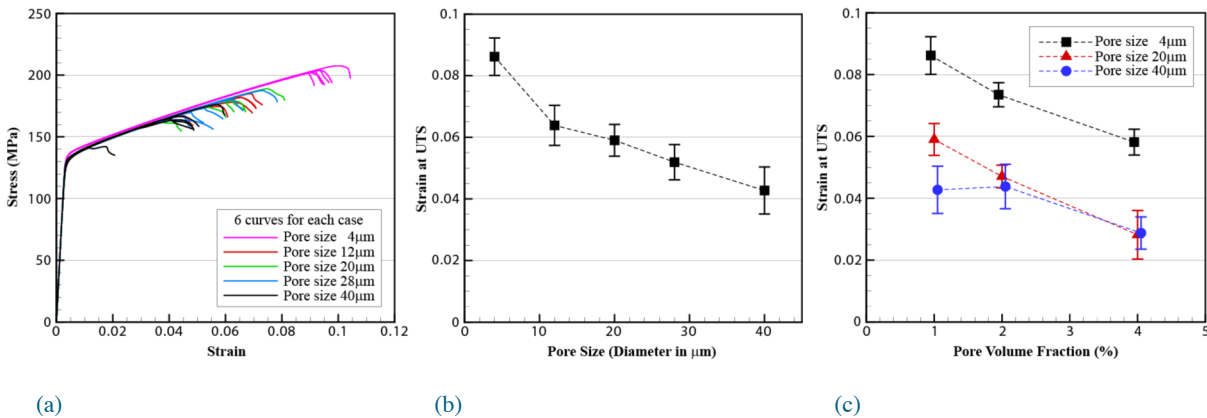


Figure 4. Some simulation results based on synthetic microstructures: (a) stress-strain curves for pore volume fraction of 1%, (b) effects of pore size on the predicted strain at UTS for pore volume fraction of 1%, and (c) effects of pore volume fraction on the strain at UTS.

Conclusions

AM50 casting samples were acquired for the tensile test. Microstructure analysis using an optical microscope was performed on the local areas cut from the ends of the samples. The X-ray tomography technique was also used to generate three-dimensional images of the tensile samples with the porosity distributions in it before the static tensile tests were performed. The results of X-ray tomography are currently being processed to provide information in finding a possible correlation between the porosity distribution and the fracture behaviors (i.e., ductility) of Mg castings. Two-dimensional FE analyses have been conducted based on synthetic microstructures with different pore sizes, volume fractions, and distributions. It was observed that, in general, the ductility decreases as the pore size and volume fractions increases. In some range of pore size and volume fraction, the mean distance between pores has some substantial influence on the predicted ductility, which needs further investigation. Mesh size effects, larger pore sizes, and volume fractions are among the many factors to be examined next.

Materials Informatics for the Integrated Computational Materials Engineering Cyberinfrastructure

Principal Investigator: Kim Ferris, PNNL
(509) 375-3754; e-mail: kim.ferris@pnnl.gov

Principal Investigator: Dumont Jones, Proximate Technologies, LLC
(614) 258-8835; e-mail: dumont.jones@prxt.com

Accomplishments

- Developed a toolkit for the analysis of multi-repository data on Mg alloys; used materials physics component to resolve system definitions in unresolved data reporting to augment knowledge content.
- Applied tools to four recognized materials repositories (MetalsBank, ASM Materials Handbooks, MatWeb, Center for Advanced Vehicular Systems (CAVS)) as individuals and collectively.

Future Directions

- Identify information weaknesses in data resources; recommend new repository data or updates to improve reliability of data for model validation and experimental verification.
- Update informatic tools for multi-repository analysis of property data consistency and knowledge content, provide new versions to ASM, Kent State Center for Informatics, and CAVS.
- Provide informatic framework for information-based design that leverages existing data resources (repositories, individual collections) and current results.

Technology Assessment

Targets

- Assess the current state of Mg-alloy repositories to perform information-driven design of new materials and validation of parameterized models;
- Determine the scope of what to store to support information-based design and model validation in materials repositories;
- Compare the efficiency and inherent limitations of current approaches to global collection of materials information: consolidation versus federation;
- Evaluate repositories and assess their ability to address validation and verification concerns. Assure new materials information is consistent with supporting design.

Gap: Current materials design approaches do not take sufficient advantage of materials data resources. To develop predictive capabilities for new lightweight alloy development and joining capabilities, future efforts will need to leverage current and past experimental and modeling results. Models for materials properties tend to be validated against a limited data set (“data shopping”), experimental measurements need more robust verification points consistent with the behavioral properties of materials classes. Frameworks for materials design tend to focus on single property estimation rather than a system-level, performance basis. Current approaches lose knowledge content through ineffectual formats for property storage.

Introduction

Repositories of alloy information should be evaluated for their suitability as platforms for multiscale alloy design. In principle, joining the information content of multiple property repositories should further increase researcher's ability to verify and validate model development and support design aspects. However, more information does not guarantee better property modeling information. The key metric for repository development is its ability to provide data support, both alone and in combination with other data collections. Project milestones for FY 2011 were to establish metrics for evaluating property data consistency and completeness in a repository for information-driven design, model validation, and experimental verification, and to present these results to the U.S. Department of Energy (DOE) and Integrated Computational Materials Engineering (ICME) teams. Team results indicate that current repositories have design utility but also have significant data inconsistencies and completeness gaps.

Approach

The project team examined the Mg-alloy contents of four material repositories individually and in combination; the CAVS repository associated with Mississippi State University; the ASM Handbook published by ASM International; MatWeb, an Internet-available reference source; and the publicly available portion of the Metals Bank repository, associated with the Korea Institute of Metals. Informatic tools have been developed to resolve several database features needed for data support: 1) signatures indicating that system or property definitions are resolved within the context of the design problem; 2) gaps in data support with respect to systems or properties; and 3) potential associations between data. Correlations help define true completeness requirements, have intrinsic value to informatics models, and offer suggestions for repository augmentation. The limitations in data coverage and completeness detected by these metrics identify critical weaknesses in the data support needed for model development and suggest a strategy to address data augmentation in a repository. The CAVS repository has limited content and continues to be in an early stage of development. Its current system definitions (alloy designation only) do not hold sufficient information to resolve properties for design purposes. After careful comparisons, it was determined that MatWeb largely reproduced the content of the ASM Handbooks. Therefore, the following discussion on multiple repositories focuses on the ASM and MetalsBank repositories.

Technology Transfer Path

Informatic tools provide capabilities for data joining and analysis for the specific alloy property problems of the lightweight materials group and multiple data resources like the MetalsBank, ASM Handbook, and CAVS. This project has had active industrial and data society participation, and the results of this project will be transferred to the OEM participants and data society groups. The first-generation toolkit was deposited at the CAVS and is generally available to ICME interested parties. The current developmental version of the toolkit is available at https://spteamsl.pnl.gov/sites/mat_informatics/default.aspx. Updated informatic tools for multi-repository analysis of property data consistency and knowledge content will be provided at the end of the project to ASM, Kent State Center for Informatics, and CAVS.

Results and Discussion

While it is possible to construct purely analytic measures of data coverage, a visual summary often suffices to illustrate data coverage. In Figure 5, a coverage map for the combined content from the ASM and MetalsBank data repositories is shown. The number of reported data values is color coded. This graphical display illustrates the data strength areas of each repository, and the potential data support over a broader range of properties than covered by an individual repository.

Delving deeper into the data support, Figure 6 illustrates the data density from the MetalsBank for its Mg alloy content. The number of measures is color coded; red shows areas of one measurement; yellow and green areas show concentrations of multiple measurements per allowed system. Other repositories differ in details of the coverage map, but the overall features showing a preponderance of measurements clustered on the AZ systems generally prevails.

While crude measurement clustering of this type does not preclude informatics studies, it does indicate that data-based tasks relating AZ series behavior with that of other systems will present a challenge. The pattern of existing measurements also indicates interesting, if tentative, associations that can drive hypothesis generation and focus data acquisition. For example, AZ61 is not as well characterized in tensile strength measurements as its relatives AZ31, AZ61A, and AZ91. Procuring data for this single system and examining property differences compared with similar systems, might produce a useful property association or even a structure-property relation. The fact that antimony, silver, strontium, and yttrium are not reported in these alloys is very likely misleading; these less common elements are not natural impurities and are generally added deliberately.

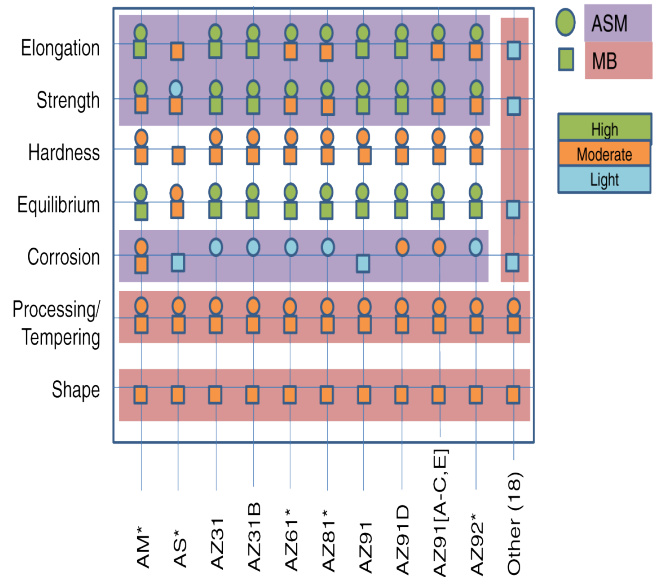


Figure 5. Coverage mapping for ASM (ASM) and MetalsBank (MB) repositories

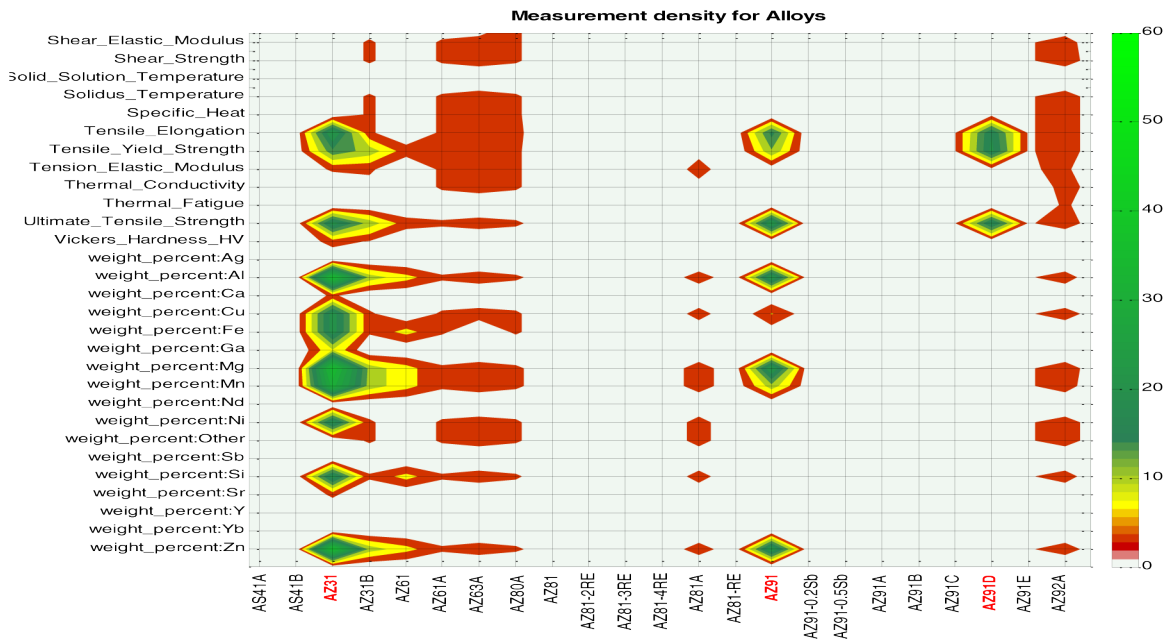


Figure 6. Data coverage map (partial view) for the Metals Bank repository

The job of a system definition is to resolve physically distinct systems. In addition, for informatics work the system definition must be formulaic, using any valid recipe known in advance of synthesis. Resolution implies there is a one-to-one mapping (perhaps a complex one) between system definitions and the system's set of physical properties. If a single definition shows a range of property values (within reasonable error), the system definition is said to be incomplete or partial.

To better understand system definition issues, the project team identified two tools. The first tool is a visual map like that shown in Figure 7, which shows incomplete current system definitions and the affected properties. This graphic illustrates deviations in property values as a response to be derived from system definitions of differing granularity. This figure illustrates that one system definition may be complete for some properties, but only partial for others. Tensile strength and

elongation properties show substantial variation even when some metrics of the alloy system, processing, post treatment, and shape are known. In regions of sparse data, the system definition map is not known but it is expected the findings will be relevant to new repository data.

A second assessment tool for system definition comes from a statistical analysis of how system definition components impact observed property error. For each property, the observed error was computed applying the 15 system definition types (alloy, alloy+processing, alloy+post treatment...). Principal components analysis (PCA) was then used to relate the presence of each system definition component (alloy, processing, post treatment, shape) to the observed error. The contribution of each component to reducing observed property error is shown in Figure 7.

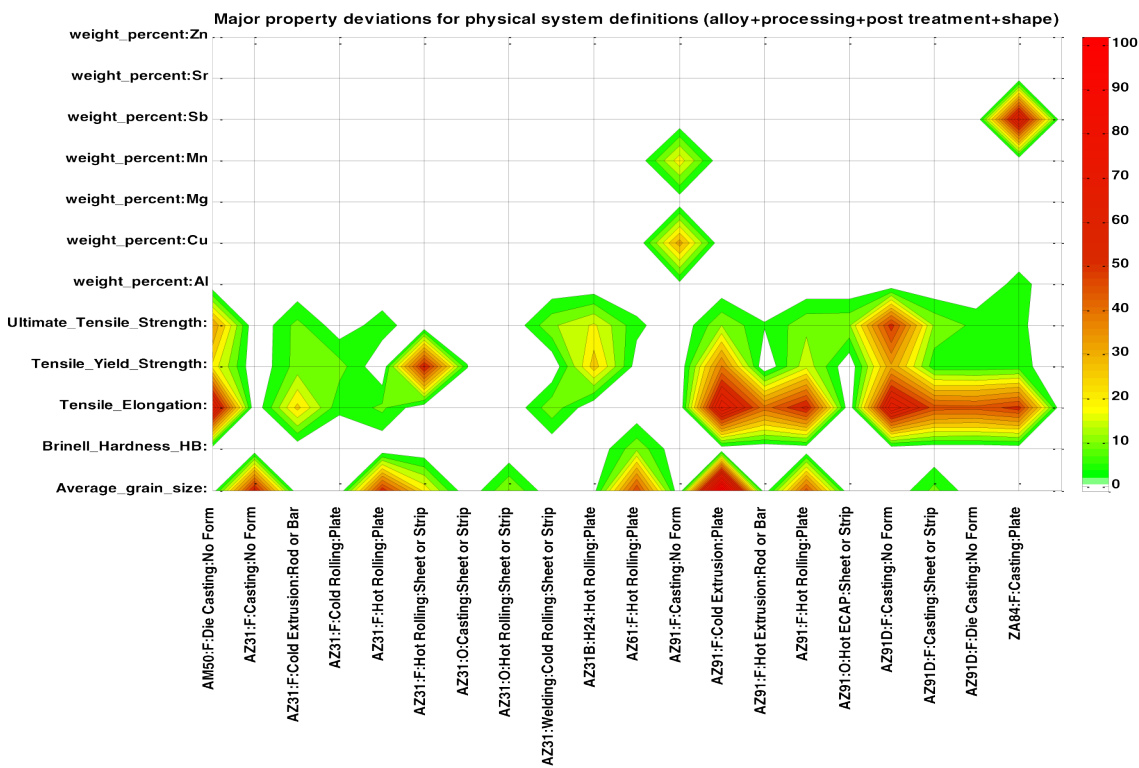


Figure 7. System definition map and property deviation mapping for common alloys in the MetalsBank

Specific to the target objectives, we offer the following comments:

- Information forms the basis for new material discoveries, and current practices tend to focus on diversifying information from current and past materials. For validation of models and verification of measurement techniques, repositories again serve as a knowledge reference. This places a heavy reliance on consistent and accurate storage of materials properties. The specific term “information-driven design” implies that information relating materials formulations and properties can be systematically extracted using data analysis techniques.
- The current state of repositories is encouraging but embryonic. In the current work, the team has evaluated data repositories of Mg alloy information, and while there is considerable data there, it is not always enough to support design work and act as a comparative reference source. Example: There is a specific data weakness (data is incomplete and not diverse) in the effects of trace elements on the tensile properties of Mg alloys.
- The mission of a materials repository should be to provide, in order of priority: 1) fidelity of data storage, 2) data completeness, and 3) simple data queries. This order is nearly inverted for current repositories, as many repositories store ambiguous information and only incompletely support design, validation, and verification tasks. Such repositories will have limited utility, but will not scale to new problems, support general information-based design, and add a degree of uncertainty for validation of new experimental measurement and modeling methods. Further work is needed to develop repositories that focus on accurate storage of materials data. Ease of general property querying is a specific concern because current repositories have been constructed with a particular problem in mind.

- Current repositories duplicate information and compete needlessly with one another. Federated repositories could combine best-of-breed data from independent member repositories and provide an appropriate contextual basis. A simple and effective method is needed to be able to contribute and retrieve information, and form a knowledge resource directly relevant to the design, validation, and verification tasks at hand.
- New methodologies are needed to help researchers assess what is new and valuable for a repository, and avoid accumulation of redundant data. A natural basis for joining information sources is needed for design problems, uncomplicated by incomplete system definitions and semantics. Informatics tools can be helpful in this regard: along with helping to establish appropriate system and property definition requirements, data analysis tools can establish the types of measurements that will refine or extend a model, and thus constitute true information for purposes of materials design.

Conclusions

The project team has developed analytic tools and metrics to examine the capability of materials data repositories (ASM, MetalsBank, MatWeb, CAVS) to support materials development as individual entities or in fusion from multiple data resources. These tools identify the presence of information gaps, frequently associated with details of alloy state definition, and suggest pathways to optimally closing these gaps. Analysis of Mg alloy data indicates there is a limited degree of data support for information-derived materials development (a combination of limited data diversity and number of resolved systems), model validation, and experimental verification. The most common deficiency in these repositories is that the system definition metadata does not consistently resolve property values. Refined system definitions and validation of design hypotheses resulting from property correlations methods suggest a directed method to enhance the design value of repositories like the CAVS and the Metals Bank.

Conclusions

The two tasks within the Modeling and Computational Materials Science project, namely “Mechanistic-Based Ductility Prediction for Magnesium Castings” and “Materials Informatics for the Integrated Computational Materials Engineering Infrastructure”, are developing methods and techniques to more accurately predict, describe, and interconnect information associated with structure, property, and processing data and relationships for lightweight materials.

Presentations/Publications/Patents

Jones, D.M.; Ferris, K.F. Towards Informatics Tools and Information Assessments for the Development of Lightweight Mg-Alloys. Presented at Materials Science & Technology 2010 Conference, Houston Texas.

Jones, D.M.; Ferris, K.F. Materials Informatics for the ICME CyberInfrastructure. USAMP ICME for Mg Program Workshop, August 2010, Ann Arbor, Michigan.

Jones, D.M.; Ferris, K.F. Materials Informatics: Developing Tools for Knowledge Assessments of Data Resources in Lightweight Mg Alloys and Semiconductors. Presented at Oak Ridge National Laboratory, November 2010, Oak Ridge, Tennessee.

Jones, D.M.; Ferris, K.F. Assessing Data Completeness and the Predictive Potential in Mg Alloy Databases. Presented at TMS 2011 Annual Meeting & Exhibition, February 27-March 3, San Diego, California.

Jones, D.M.; Ferris, K.F. Informatic Tools for Assessment of Data Completeness for Model Development in Mg Alloy Databases. 1st World Congress on Integrated Computational Materials Engineering, July 10-14, 2011, Seven Springs, Pennsylvania.

Jones, D.M.; Ferris, K.F. Tools for Assessing Information-Based Design and Identifying Information Gaps in Mg Alloy Repositories. Materials Science & Technology 2011 Conference & Exhibition, October 16-20, 2011, Columbus, Ohio.